University of Alberta

Investigating the Performance of a Rectangular Secondary Clarifier

by

Saifuddin Molla 

A thesis submitted to the Faculty of Graduate Studies and Research
in partial fulfillment of the requirements for the degree of

Master of Science

in

Environmental Engineering

Department of Civil and Environmental Engineering

Edmonton, Alberta

Fall, 2008

Your file Votre référence
ISBN: 978-0-494-47369-6
Our file Notre référence
ISBN: 978-0-494-47369-6

ABSTRACT

A single rectangular horizontal flow secondary clarifier at Gold Bar Waste Water Treatment Plant was selected for study. Research was conducted to obtain a good understanding of the existing design and operation, in terms of activated sludge properties, sludge settling characteristics and hydrodynamics of the existing unit. Extensive literary study was conducted and based on the findings performance of the selected clarifier was evaluated. Clarifier operational problems like sludge rising and formation of density waterfall and density current were identified and appropriate recommendations were made. Attempt was made to establish seasonal trends on different physical properties and settle-ability of incoming sludge, return sludge and clarifier effluent. Different mathematical models, describing sludge settling velocity, were tested using batch settling data and the most accurate model response was reported. Existing design and flow distribution of the selected clarifier was studied and based on the acquired data a pilot-scale hydraulic model was designed and manufactured. The design of the pilot-scale unit was validated and the unit was prepared for further study and enhancement in design.

ACKNOWLEDGEMENTS

First of all, I would like to express my deepest gratitude to my supervisor Dr. M. Gamal El-Din for his continuous guidance and support. His brilliant ideas and invaluable suggestions helped me overcome all the frustrating setbacks I encountered during the course of this study. I learned most of what I know from his vast knowledge in different areas of research. I would also like to convey my sincere gratitude to Dr. M. S. A. Baawain for his outstanding cooperation. I immensely enjoyed working with him and I hope to work with him again in the future. I am also thankful to Dr. I. D. Buchanan for his contribution at the initial stage of this research.

Furthermore, I would like to thank Darryl Seehagel and Bilgin Buberoglu at Edmonton Waste Management Center of Excellence for their role in acquiring design data from Gold Bar Waste Water Treatment Plant. Their help in collaborating with Gold Bar operations made it possible for me to carry out all the sampling and on-site experiments. A very special thanks goes to Maria Demeter and Jody Yu for providing transportation and technical support throughout the course of the project. I would also like to thank PG Plastics for doing a wonderful job in manufacturing the pilot-scale model as per design specifications. Also, I am grateful to the very skilled and resourceful Nick Chernuka for his help in setting up the pilot-scale model.

I am eternally indebted to my parents for believing in me and being there for me when I needed them. I am what I am because of them. Finally, I would like to thank my beloved wife Afsana, for her extraordinary patience, unwavering support and outstanding teamwork. She remains my dearest friend, my finest colleague, my best adviser and my soul mate.

TABLE OF CONTENTS

LIST OF TABLES

LIST OF FIGURES

LIST OF ABBREVIATIONS

AVI	Aggregate Volume Index
BOD	Biochemical Oxygen Demand
BNR	Biological Nutrient Removal
CFD	Computational Fluid Dynamics
CSTR	Continuous-flow Stirred Tank Reactor
DI	De-Ionized
ENR	Endogenous Nitrate Respiration
EPT	Enhanced Primary Treatment
HRT	Hydraulic Retention Time
MLSS	Mixed Liquor Suspended Solids
NTU	Nephelometric Turbidity Unit
PIV	Particle Image Velocimetry
PLIF	Planar Laser Induced Fluorescence
PFR	Plug Flow Reactor
PMMA	Polymethyl-Methacrylate
RTD	Residence Time Distribution
RAS	Return Activated Sludge
SQI	Sludge Quality Index
SRT	Sludge Retention Time
SSI	Sludge Stability Index
SVI	Sludge Volume Index
SSVI	Stirred Sludge Volume Index
TDS	Total Dissolved Solids
TS	Total Solids
TSS	Total Suspended Solids
UV	Ultraviolet
VFA's	Volatile Fatty Acids
WAS	Waste Activated Sludge
WWTP	Waste Water Treatment Plant
ZSV	Zone Settling Velocity

1.0. Introduction

The role of a secondary or final clarifier is crucial in the biological wastewater treatment process. Often the efficiency of these clarifiers are greatly reduced due to poor flow distribution and sometimes the efficiency of such units may need to be optimized in view of a more stringent discharge regulation or a growing population.

This thesis represents the initiation of a larger research project aimed at optimizing the performance of secondary clarifiers at Gold Bar Waste Water Treatment Plant (WWTP). The project is intended to investigate the design of the operational rectangular secondary clarifiers and ways of improving their performance with the use of Computational Fluid Dynamics (CFD) modeling. Although the secondary clarifiers at Gold Bar were operating adequately, the project was started in order to plan for any future upgrades. The introductory chapter of the thesis provides a background for this research including a brief sketch of the biological treatment process at Gold Bar.

1.1. Gold Bar Wastewater Treatment Plant

Gold Bar WWTP is an Advanced/tertiary WWTP owned and operated by the City of Edmonton. It provides primary, secondary and tertiary treatment to effectively treat all of the wastewater and combined sewer flow generated in the Edmonton area, serving a population of about 700,000. The plant is located on the eastern outskirts of Edmonton, Alberta along the south shores of the North Saskatchewan River. The plant was initially constructed in 1957 and underwent two major expansions in 1966 and 1981 in order to increase the average daily flow capacity. In 1996, Biological Nutrient Removal (BNR) was introduced by installing two new bioreactors along with two new secondary clarifiers

with the existing eight treatment trains. Finally, with the installation of an Ultraviolet (UV) disinfection facility in 1997 followed by the conversion of all existing aeration tanks into bioreactors, the plant became a Tertiary WWTP by 2002. A new bioreactor coupled with a new secondary clarifier went into operation in 2004 and the plant initiated the installation of an Enhanced Primary Treatment (EPT) system in 2006. Currently the plant is rated for treating an average daily flow of 340 ML/d and a peak daily flow of about 550 ML/d.

Although the City of Edmonton has individual sanitary sewers that carry wastewater produced by the residents and storm sewers that carry storm-water and snowmelt runoff, about 20% of the total length of sewers in the city is combined sewers. This combined sewer system generates larger amounts of diluted sewage which requires rigorous treatment at the Gold Bar WWTP. The volume of wastewater in the combined sewer system can increase alarmingly during severe wet weather conditions, posing a greater challenge on the plant operation. The treatment process at Gold Bar is briefly described in the following paragraphs with greater emphasis on the BNR system as the Secondary/Final Clarifiers are an integral part of it.

As a pre-treatment, the wastewater arriving at Gold Bar WWTP flows into aerated grit tanks. As the grit settles, lighter organic particles remain suspended by the aeration and leave the grit tanks with the effluent. The effluent from the grit tanks passes through bar screens and moves on to primary treatment facilities. The plant has seven grit tanks and all of the tanks are in operation during peak flows. The primary treatment consists of eight large rectangular settling tanks (primary clarifiers). In these clarifiers, the heavier

organic matter suspended in the wastewater slowly settles to the bottom while the lighter scum rises to the top under quiescent condition. Both sludge and scum are removed using mechanical scrapers and piped away for anaerobic digestion, while the effluent travels on to the secondary and tertiary treatment stages. Approximately 55% of the Total Suspended Solids (TSS) and 45% of the Biochemical Oxygen Demand (BOD) in the wastewater is removed during the four hours of primary treatment.

The primary effluent is then distributed among the eleven aeration batteries designated as Bioreactors #1 through #11. Each bioreactor has four passes (Figure 1.1) and operates in suspended growth BNR mode to remove nutrients (phosphorus and ammonia nitrogen) from the wastewater. The bioreactors employ a pre-anoxic single sludge process for the removal of biological nitrogen. The first pass of each bioreactor has baffles placed inside to create three distinct zones. The first zone is a pre-anoxic zone where oxygen is only available in nitrate (NO_3) form. Return Activated Sludge (RAS) from the secondary clarifier is fed into this zone. The RAS provides the bioreactor with necessary microbial population to carry out the BNR process. The second zone is an anaerobic zone where biological activity occurs entirely in the absence of oxygen. Supernatant from the fermentation reactor, rich in Volatile Fatty Acids (VFA's), is fed into this zone in order to enhance biological phosphorus removal. The third zone is a full anoxic zone where recycled mixed liquor from the fourth pass of the bioreactor is fed. The following three passes of the bioreactor have a uniform aerobic zone where aeration is provided with a fine bubble aeration system.

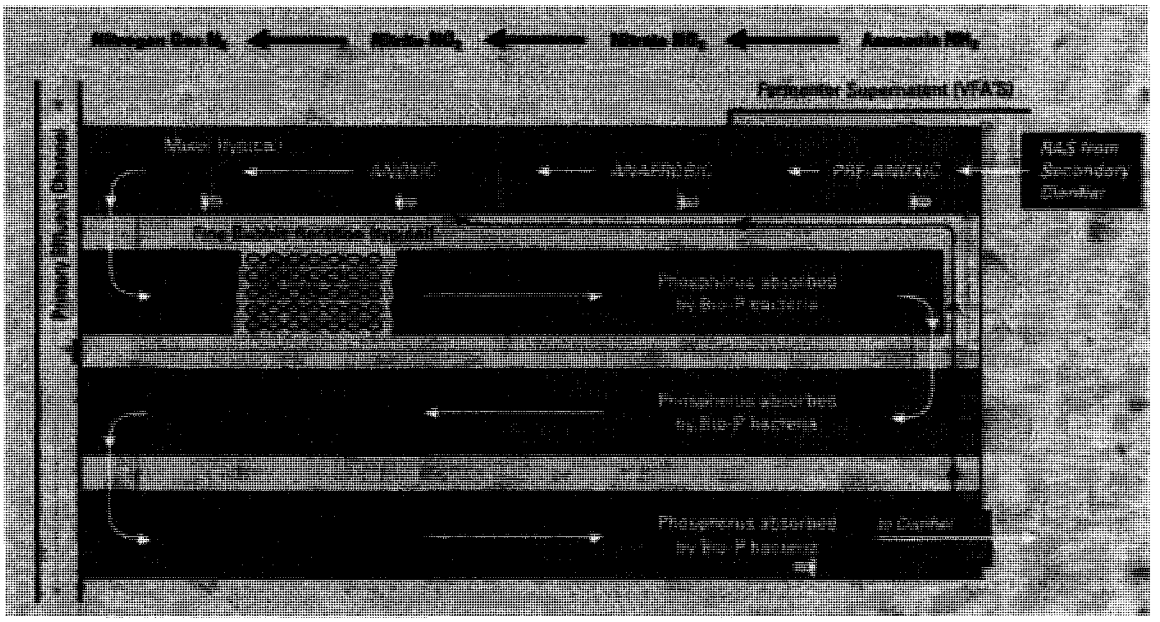

Figure 1.1: Biological Nutrient Removal System at Gold Bar

In the aerobic environment of the last three passes (Figure 1.1), the ammonia present in the wastewater is oxidized into nitrate by two groups of aerobic autotrophic bacteria. These nitrifying bacteria have much slower growth rates than heterotrophic bacteria. Thus, the aerobic zone designed for the biological nitrification process constitutes of three among the four passes of each bioreactor, providing longer hydraulic and solids retention times. By the time the wastewater reaches the end of the fourth pass, most of the ammonia is converted into nitrates. This nitrate rich wastewater is recycled back to the anoxic zone of the first pass where the nitrate is biologically reduced to nitrogen gas and released into the atmosphere by heterotrophic denitrifying bacteria. This phenomenon is referred to as the biological denitrification process.

The total amount of wastewater flowing through the bioreactor is recycled back to the anoxic zone approximately two to three times before entering the secondary clarifier. The primary purpose of this internal recycle is to maintain low nitrate concentration in the

mixed liquor leaving the bioreactor in order to prevent denitrification in the secondary clarifier. In addition, the denitrifying bacteria use organic carbon for growth and therefore are responsible for removing carbonaceous BOD from incoming and recycled wastewater. This action by the denitrifying bacteria in the pre-anoxic and anoxic zone reduces the oxygen demand of the wastewater thereby lowering the oxygen requirement in the subsequent aerobic zone. This in turn lowers the required aeration rate and saves power.

Biological phosphorus removal is initiated in the anaerobic zone of the first pass where VFA's are taken up by a group of heterotrophic bacteria and converted to carbon storage products that provide energy and growth in the subsequent anoxic and aerobic zones. These bacteria store large quantities of phosphorus in the form of polyphosphate within their cells in excess of their growth requirements. In Gold Bar, these bacteria are selectively enriched in the bacterial community within the activated sludge by employing a form of 'shock treatment'. First the bacteria are deliberately starved in the anoxic and anaerobic zones and then they are feasted on oxygen in the aerobic zone. This treatment conditions these bacteria to grow and multiply, thereby absorbing more phosphorus.

After several hours of biological treatment the effluent from the fourth pass of each bioreactor flows into a mixed liquor distribution channel which feeds across the influent end of the secondary clarifiers. In Gold Bar, each bioreactor is followed by a rectangular clarifier for gravity separation and thickening of the activated sludge. The eleven clarifiers are designated as Clarifiers #1 through #11 in accordance with their preceding bioreactor. Approximately 90% of the activated sludge from the secondary clarifiers is returned to the bioreactors as Return Activated Sludge (RAS) and the remaining 10% is

pumped to the Waste Activated Sludge (WAS) thickeners and then to the anaerobic digesters. A detailed description of the design and operation of the final clarifiers at Gold Bar is provided in Chapter 5 of this thesis. Treated wastewater from the final clarifiers flows through the high intensity UV disinfection facility before being discharged to the North Saskatchewan River.

In order to proceed with the research, a specific clarifier among the eleven units was selected by the Gold Bar operations on the basis of performance and solids removal efficiency. This unit (Clarifier #1) was used for all study and analyses mentioned within this thesis.

1.2. Scope and Objective of Thesis

The objective of this research is to prepare groundwork for optimizing the performance of the selected secondary clarifier at Gold Bar WWTP. In order to optimize the performance of an existing secondary clarifier, good understanding must be obtained in terms of activated sludge properties, sludge settling characteristics and the existing hydrodynamics of the unit.

The scope of this thesis started with the investigation into available literature in order to find out about the key characteristics of activated sludge, modeling of activated sludge settling velocity and typical operational problems of secondary clarifier. In addition, the properties and settle-ability of incoming sludge, return sludge and clarifier effluent were evaluated by using gravimetric solids analyses and particle size distribution study. Also, different settling tests were performed, using samples from the operational clarifier, to

investigate the sludge settling characteristics. To better understand the complex hydrodynamics of the secondary clarifier, a pilot-scale reproduction was designed and manufactured based on the present design and flow distribution of the chosen full-scale unit. Finally, the design of the pilot-scale unit was validated and the unit was prepared for further study and enhancement in design.

2.0. Literature Review

This chapter consists of a comprehensive review of the available literature in the area of activated sludge settling characteristics and its effect on the design and operation of secondary clarifiers. The review deals with the background theory of basic sedimentation followed by its application in advanced wastewater treatment. Some typical properties, used to characterize activated sludge, have been discussed along with their relation to sludge settle-ability. A brief overview of the solids flux theory has been presented in addition to some proposed mathematical models describing the sludge settling in secondary clarifiers. Finally, the review deals with the typical operational problems in an activated sludge system associated with sludge settling properties, hydraulic regimes and design criteria. Details of the microbiological and kinetic aspects of the system are beyond the scope of this thesis and hence have been overlooked in this review.

2.1. Background

2.1.1. Settling

Sedimentation or settling, in terms of water and wastewater treatment, is the removal of solid particles from a suspension under the influence of gravity. For a sedimentation tank, impurities that settle to the floor and into the hopper of the tank are called sludge while lighter impurities that float on the surface are called scum. Settling of suspended material inside a sedimentation tank depends on numerous factors including particle characteristics (size, shape and density), water temperature, internal hydrodynamics of the tank, presence of flocculation etc.

Usually, larger and denser particles settle out more easily than smaller and lighter particles. Presence of flocculation may aid in the settling of these small colloidal particles but the particles have to be flocculent in nature and the tank design must allow sufficient depth for flocculation. Particles with a round shape usually settle more readily than irregularly shaped particles, as spherical particles have lower drag coefficient. Viscosity of water increases with decreasing temperature and the viscous water poses more resistance towards the settling of suspended matter. Thus, settling is deteriorated at lower temperatures. Presence of turbulence and short circuiting within the tank negatively affects the settling efficiency. Density currents and other hydrodynamic factors also affect settling. Sometimes the presence of these currents promotes flocculation but the overall efficiency is reduced because of uneven settling.

Three common types of settling tanks, in terms of design, are currently in practice. They are rectangular horizontal flow, circular radial flow and up-flow tanks. The selected clarifier at Gold Bar WWTP is a rectangular horizontal flow type tank. Such a tank is considered to be divided into four zones: inlet zone, settling zone, sludge zone and the outlet zone (Larsen, 1977). The inlet zone of the tank is designed to distribute the flow uniformly across the width of the tank. Usual practice includes an inlet baffle that dissipates the momentum of the inlet flow. The settling zone is the largest portion of the basin and suspended particles settle in this zone under quiescent conditions. The settled impurities are collected and stored in the sludge zone until they are removed from the tank through the hopper. The outlet zone consists of decanting launders through which the clarified effluent leaves the tank. The overall operation of the tank depends on the proper function of each of these individual zones.

2.1.2. Classification of Settling Behavior

Based on the nature and concentration of suspended matter, the settling behavior of a suspension can be classified into four types: Discrete or Unhindered Settling (Type I), Flocculent Settling (Type II), Zone or Hindered Settling (Type III) and Compression Settling (Type IV).

Discrete or Unhindered Settling refers to the settling of discrete particles *i.e.* particles that remain separate from each other in a suspension. The concentration of suspended solids is very low in such cases and so each particle settles freely without interference from adjacent particles. A discrete particle, settling in a suspension, accelerates under gravity until the resisting drag force equals the effective submerged weight of the particle. Beyond this point, the particle settles at a constant velocity, which is referred to as the terminal settling velocity. The terminal settling velocity (v_t) is characteristic of discrete settling and is given by the formula (American Water Works Association, 1999):

$$v_t = \sqrt{\frac{4gd(\rho_s - \rho)}{3C_D\rho}} \qquad (2.1)$$

where, g is the gravitational acceleration (m/s^2); d is the diameter of the particle (m); ρ_s is the density of the particle (kg/m^3); ρ is the fluid density (kg/m^3) and C_D is the drag coefficient. By substituting the value of C_D with the appropriate Reynold's number expression, the above formula yields the Stokes' equation for laminar flow conditions. According to this relationship, the settling of discrete particles is independent of the depth of the tank or the suspended solids concentration.

With higher concentration of suspended solids, particles start to collide with each other and start to form larger flocs, provided the suspension is of a flocculent nature. This inter-particle collision promotes settling, as the larger flocs settle more easily than the individual particles. This type of settling is referred to as Flocculent Settling. Larger flocs settle out faster than discrete particles and hence have higher velocities than the terminal settling velocity. The settling velocity, in this case, becomes a function of the depth of the tank because a greater depth allows longer retention time for particle growth. Usually, the rectangular settling tanks are built with a long and shallow configuration, which allows the horizontal flow to provide a greater opportunity for inter-particle collision.

With further increase in suspended solids concentration, a point is reached where inter-particle space becomes so small that the particles can no longer settle independently of one another. Also, the liquid displaced by the settling particles generates a net upward flow. Thus, the settling of a particle is hindered by the adjacent particles and the displaced liquid motion, which results in a reduced settling velocity. This effect is known as Hindered Settling. When particle concentration is sufficiently high, the whole suspension settles as a blanket and distinct zones within the suspension can be identified, separated by concentration differences. This type of settling is referred to as Zone Settling. When such a suspension is left to stand in a settling column, a clear interface, separating the sludge blanket from the clarified supernatant, is formed near the top of the column. This interface moves downwards as the suspension settles. Similarly, there is an interface which exists between the portion of the sludge that has hit the bottom and the portion that is still suspended. This interface slowly moves upwards until it meets the upper interface, at which point the zone settling ends and compaction of the settled

sludge begins. If the upper interface height is plotted against time, the slope of the settling curve gives the Zone Settling Velocity (ZSV) of the suspension, before compression begins. This parameter is used in designing secondary clarifiers for activated sludge systems. The ZSV is a function of the sludge concentration and settle-ability, among many other factors. The relationship between ZSV and the volumetric concentration of particles in a suspension has not yet been determined analytically. However, many empirical equations for this relationship have been proposed. This is discussed further in later parts of this chapter.

When the settling particles approach the floor of the sedimentation tank, very high particle concentrations arise and Compression Settling takes over. In this settling regime, consolidation of the sludge occurs as the settled solids are compressed under the weight of overlying solids. The void spaces in between the particles are gradually diminished and water is squeezed out of the matrix. Thus, in this zone, adjacent settling particles actually come in contact as they approach the floor and further settling can only take place by adjustments within the matrix. Consequently, settling takes place at a far more reduced rate. For a suspension, the point at which zone settling ends and compression settling begins, is known as the compression or inflection point. Beyond the inflection point, the settling curve flattens out gradually indicating lower settling rate. Compression settling is the governing settling regime in gravity thickening processes. It is also significant in secondary clarifiers, where some degree of activated sludge thickening takes place.

2.2. Settling in Advanced Wastewater Treatment

Advanced Wastewater Treatment involves biological nutrient removal, which integrates the conventional activate sludge process with the manipulation of activated sludge microbial population, for the removal of nutrients. The conventional activated sludge process was originally developed in England by Arden and Lockett in 1914 (Metcalf and Eddy Inc., 2002) and over the years, the process has undergone many improvements. The process consists of a bioreactor, where a suspension of mixed bacterial cultures carries out the desired biological conversion of contaminants in the wastewater. The suspension is then forwarded to the secondary clarifier, where the activated sludge is removed from the effluent by means of gravity settling.

2.2.1. Secondary Clarifier

Secondary or final clarifiers play a vital role in the performance of an activated sludge system. The unit acts as a clarifier to produce clarified effluent, as a thickener to thicken the return activated sludge up to the desired concentration and as a storage tank to store the thickened sludge before returning or disposal. The quality of the effluent is to a large extent dependent on the performance of the final clarifier in terms of these three functions. The factors that influence the performance of a final clarifier may be classified into two general categories: design features of the clarifier (surface area, depth, inlet and outlet configuration, hydraulic regimes and disturbances) and sludge characteristics or settle-ability. To accurately predict and evaluate the performance of a secondary clarifier, both these factors need to be carefully examined.

The optimal design and performance of an activated sludge system depends on the relationship between the bioreactor design and the clarifier design. The performance of the clarifier varies with the quality of the mixed liquor coming from the bioreactor or aeration tank, while the performance of the aeration tank is affected by the sludge returning from the clarifier. Thus both the clarification and thickening function must be considered in the design of a secondary clarifier. Although, the clarification function of the unit is critical for producing an overall plant effluent that meets the discharge criteria but when the hydraulic loading is steady, the thickening or solids handling criterion becomes the governing function of the clarifier (Laquidara and Keinath, 1983).

Traditionally, the surface loading rate is used as the main parameter for designing settling tanks with clarification purposes. This parameter was established for an ideal horizontal flow model developed by Hazen (1904) and is applicable for discrete settling. Camp (1953) later made a modification to Hazen's model and demonstrated that the slowest settling particle to be completely removed has a settling velocity equal to the overflow or surface loading rate of the tank. Assuming, that the solids concentration is sufficiently low in the upper portions of the clarifier, this theory can be extended in determining the unit's clarification efficiency. But owing to the flocculent nature of the particles in an activated sludge suspension, the depth of the tank and the particle characteristics come into play.

In terms of solids removal in secondary clarifiers, Fitch (1957) first suggested that the Hydraulic Retention Time (HRT) is the governing criterion rather than the overflow rate. It was later proposed by him (Fitch, 1979) that clarification of a flocculent suspension is a two-step process consisting of flocculation followed by settling. He suggested that if the

flocculation was rapid or the suspension was pre-flocculated then the settling velocity would be constant over the entire settling period and the tank and overflow rate would then govern the solids removal. But if the flocculation was slow then the HRT or the tank depth would be the governing factor. In his research, Pflanz (1969) found out that the effluent clarity is affected by the overflow rate, the operating temperature, the sludge concentration and the sludge settle-ability in terms of Sludge Volume Index (SVI). He proposed the Mixed Liquor Suspended Solids (MLSS) concentration as a key design parameter for secondary clarifiers in addition to the hydraulic loading or overflow rate. As a summary, it can be said that the factors influencing the clarification function of a secondary clarifier include the design of the tank (overflow rate, depth, HRT etc.), internal hydrodynamics of the tank (Ekama *et al.*, 1997) (flow disturbances, short circuiting, turbulence etc.) and nature of the activated sludge (MLSS concentration or solids loading, sludge settle-ability, flocculated state etc.).

2.2.2. Thickening in Secondary Clarifier

Usually in municipal wastewater treatment, thickening is thought of as a special treatment for the settled sludge before its further treatment or disposal. Nonetheless, any secondary clarifier in an activated sludge process performs the thickening function together with clarification. The satisfactory performance of a secondary clarifier depends on the production of a clarified overflow as well as a concentrated underflow. Thus, both these functions must be taken into consideration while designing the required surface area and depth of the proper settling basin. Thickening occurs in two distinct steps inside the

sludge zone of a clarifier: zone settling followed by compression settling. These settling regimes were described in the previous section of this chapter.

Dick (1971)first realized the importance of the thickening function in terms of final clarifier operation. He proposed that each layer of sludge that might exist in the clarifier has a specific capacity for transmitting solids to the bottom of the tank (Dick, 1972). This capacity depends on the sludge settle-ability and the removal rate of sludge from the bottom of the tank. When a sludge layer exceeds its capacity for transmitting solids to the bottom, it acts as a limiting layer and solids that cannot pass through the limiting layer start to accumulate on top of it. This approach is based on the Flux Theory which is described in later parts of this chapter. Based on this approach, the solids loading rate was established as a critical factor in the performance of final clarifiers (Dick, 1976). Thus, sludge settle-ability greatly affects the thickening function and the overall performance of the final clarifier. A specific measure of the sludge settle-ability was later incorporated in a design procedure, based on the flux theory, for predicting the maximum solids handling capacity of settling tanks (White, 1975). Full scale research was carried out to indicate that the procedure predicts within 20% the maximum solids handling capacity of a settling tank based on the Stirred Sludge Volume Index (SSVI) as the sludge settle-ability measure (Ekama and Marais, 1986). Application to full scale secondary clarifiers also indicated that the flux procedure over-predicts the maximum allowable solids loading by about 25% (Gohle *et al.*, 1996).

According to Ekama *et al.* (1997), the design of secondary clarifiers is currently done in two stages. In the first stage, specification of a required surface area and depth is made by applying the zone settling and thickening considerations. Although proper design

features for clarification has to be incorporated but the specification of required surface area is governed by the zone settling and thickening criteria. In the next stage, the clarification efficiency of the tank is optimized by allowing for the detailed design of features such as: inlet-outlet arrangement, baffling, control of short circuiting and turbulence, sludge transport and collection capacity etc.

2.2.3. Solids Flux Theory

The solid-flux theory has been developed and applied successfully, throughout the years, in designing full scale activated sludge secondary clarifiers and predicting their thickening performance. The importance of solids flux theory in the design and operation of settling tanks and thickeners was first established by the early works of Coe and Clevenger (1916) and Kynch (1952), using non-flocculent suspensions. Later, it was shown that the mass flux concept can also be applied to the flocculent activated sludge suspensions (Dick, 1971; 1972). The theory provides a rational basis for the selection of surface area and underflow rates, in designing activated sludge secondary clarifiers.

According to the solids flux theory, the thickening capacity of a secondary clarifier is a function of the MLSS and return sludge concentration as well as the sludge settling characteristics. The total solids flux inside the unit is a sum of the solids flux due to settling and the solids flux due to bulk flow (representing sludge removal or underflow). Each flux value is represented by the sludge concentration multiplied by the corresponding velocity. At a sufficiently high solids load the thickening capacity of the clarifier is restricted by the limiting solids flux. If the applied flux or solids loading is greater than the limiting flux then the sludge blanket will increase resulting in thickening

failure and solids carry over. According to this theory, the design of a secondary clarifier is based on the estimation of required surface area corresponding to the limiting solids flux. This concept that the limiting flux governs the ultimate transport of solids was later confirmed by George and Keinath (1978) in their research.

According to Kynch's theory, based on the results of a single batch settling test, the settling velocity of a particle in the flow field is a function of the local concentration only. Talmage's method (Talmage and Fitch, 1955) was developed based on Kynch's model assuming that the limiting solids handling capacity can be determined from a single settling curve, as opposed to Coe and Clevenger's model based on multiple batch settling tests. This technique has received considerable attention because of its simplicity. However, it has been reported by many authors later on, including Fitch (1962), that better results can be obtained from multiple batch settling tests. According to Dixon (1982), Coe and Clevenger's method is preferable to Talmage's method, with respect to the effect of compression resistance of the suspension.

Application of the mass flux theory to the settling behavior of activated sludge was particularly assisted by the graphical method proposed by Yoshioka *et al.* (1957). This method was developed by obtaining the settling velocity as a function of sludge concentration using multiple batch settling tests. The solids flux can then be calculated and plotted against each corresponding sludge concentration. According to this method, the limiting flux can be determined by drawing a tangent from the desired underflow concentration to the underside of the flux curve. The limiting solids flux is given by the intercept of this line at the Y-axis. In order to use this method, settling curve needs to be

constructed to estimate the settling velocity for each concentration. For this reason, despite developments (Hassett, 1964) in the graphical solids flux theory, the procedure remains rather tedious. Another experimental procedure for determining the solids flux curve was presented by Waters and Galvin (1991). The authors used a semi-continuous sedimentation test and measured the concentration at various heights of the settled solids bed. The solids flux curve was determined at different feed flux demonstrating the dependence of the flux curve on the system feed flux.

Investigators have argued that the existing thickening theories, described in earlier works, cannot be applied to activated sludge, because in those theories, considerations have been made for gravity and viscous fluid drag while the significance of inter-particle or compressive forces have been ignored. Based on the flux theory, Michaels and Bolger (1962) first developed a model of compressive batch thickening. They also observed the formation of channels in sedimentation. Fitch (1966) later proposed a mechanism in order to explain this phenomenon. Further elaboration on the Michaels and Bolger model was done by Vaccari and Uchrin (1989). Owing to the difficulty of their application, these methods have not been used extensively. According to Dick and Ewing (1967), in case of thickening under steady-state conditions, inter-particle forces may account for the deviation from ideal behavior, as described in Kynch's theory. Shannon and Tory (1965) and Fitch (1962) also reported similar results. They found that for flocculent suspensions, settling velocity changed with the conditions under which aggregates were formed. Javaheri and Dick (1969) determined the variation in aggregate particle size and the nature of liquid displacement as consolidation takes place during sludge thickening. The authors introduced the Aggregate Volume Index (AVI) as a ratio of volume occupied by

aggregate particles to the volume occupied by dry sludge solids. They found that good settling characteristics of an activated sludge sample are associated with low AVI and high porosity values. Strong correlation between SVI and AVI was shown in a later study (Knocke, 1986), by conducting lab and full scale experiments. In later studies (Takacs *et al.*, 1991; Dupont and Henze, 1992; Dupont and Dahl, 1995; Ekama *et al.*, 1997), attempts were made to extend the flux theory to the discrete setting conditions in the upper effluent region of the clarifier. These researchers proposed some models by modifying the solids flux theory for lower concentrations and their work improved the accuracy of dynamic model prediction for effluent suspended solids concentration.

Numerous studies have been performed on the process of secondary clarification and thickening, using the solids-flux theory. Over the years, researchers have tried to develop reliable models for the activated sludge settling properties, but no universally accepted solution has yet been established. According to Giokas *et al.* (2003), this is mostly because of the different experimental conditions, sludge types and instrumentations employed for these studies.

2.3. Characterization of Activated Sludge

As mentioned in the previous sections, the performance of a secondary clarifier and the overall biological treatment process greatly depends on the characteristics and settle-ability of the activated sludge. Due to the presence of microbial population, activated sludge flocs have a very complex structure. The characteristics and settle-ability of the activated sludge can be described by a number of different parameters. Urbain *et al.* (1993) made a summary of the most common methods for describing the characteristics

of activated sludge flocs. According to the authors, the activated sludge characteristics are most often described by the amount of filamentous microorganisms, specific surface area, and surface charge, floc size, strength and density, amount of extra-cellular polymers and sludge hydrophobicity. A previous study (Barber and Veenstra, 1986) indicated filament length to be the single most important factor in defining the sludge characteristics. Some of the relevant characteristic factors of the activated sludge are discussed in detail within this section.

2.3.1. Particle/Floc Size

Suspended solids, within the secondary treatment system, undergo physicochemical and biochemical flocculation to form activated sludge flocs containing different groups of microorganisms. The flocs are fragile, irregularly shaped and biological in nature and have high water content. Among the many physical characteristics of activated sludge flocs, reported in the literature, only floc size, filament length, floc settling velocity and density can be measured directly.

In earlier works, activated sludge flocs were considered as particles with diameters larger then 20μm (Finstein and Heukelekian, 1967). A distinction was made between flocs and aggregates by Javaheri and Dick (1969), who defined a floc as a group of particles containing liquid and an aggregate as a cluster of flocs with the liquid between them. Owing to the irregular shapes of the activated sludge flocs, many different ways have been reported to express their size. The floc size has been described by the floc length or maximum dimensions (Ganczarczyk, 1970; Sezgin *et al.*, 1978) as well as the floc perimeter and circumference or breadth (Mueller *et al.*, 1967).

According to researchers, the range of activated sludge floc sizes varies between 0.5 and 1000 μm (Knudson *et al.*, 1982), although less than 20% of the flocs have sizes larger than 100 μm (Li and Ganczarczyk, 1988). The results of another study (Li and Ganczarczyk, 1991) showed that, while flocs smaller than 5 μm were dominant in number, those larger than 50 μm were the major sources for surface area, volume, and mass of activated sludge. A later study (Andreadakis, 1993) reported that more than 85% of activated sludge flocs have sizes in the range of 10 to 70 μm.

Snidaro *et al.* (1997) investigated the activated sludge floc structure and reported that it consists of three basic elements. According to the authors, predominating microflocs (125 μm) are formed from aggregates (13 μm) of individual particles, which in turn are made up of smaller particles or living bacteria cells (2.5 μm). However, in their research using lab-scale activated sludge units, Sezgin *et al.* (1979) found that the mean floc size varied from day to day. According to a number of studies (Li and Ganczarczyk, 1990; Barbusinski and Koscielniak, 1995; Wilen and Balmer, 1999), floc size can be affected by the basin scale, sludge age, nature of substrate, presence of microorganisms, dissolved oxygen, particle concentration, organic loading, sampling procedure and agitation. Ganczarczyk *et al.* (1992) recommended an improved technique for the physical stabilization of microbial aggregates, to retain the specific size distribution and the geometric properties of the floc.

Along with the many factors, results of particle sizing for activated sludge may also vary depending on the sizing technique. Realistic sizing is very difficult to achieve because most of the sizing techniques assume a spherical shape of the particles. The first

method accepted for floc size measurement was by direct observation using a microscope (Sezgin *et al.*, 1978). Photographic technique for floc size measurements was first used in 1955 (Mueller *et al.*, 1967). This technique was later used by many researchers (Magara *et al.*, 1976; Tambo and Watanabe, 1979) for measuring activated sludge and inorganic floc sizes. This technique was useful because it allowed floc size measurement without directly touching the samples. Li and Ganczarczyk (1987) later modified the technique by introducing a multi-exposure photographic method. The authors measured the size and the settling velocity of activated sludge flocs and found that the settling velocity has a linear relationship with the floc size. In later works (Li and Ganczarczyk, 1992), the settling velocity of microbiological aggregates was reported to be a function of their density and porosity as well as their geometrical parameters. Additional studies have linked particle size distribution with the sludge volume index (Barbusinski, 2000) and sedimentation properties (Hilligardt and Hoffmann, 1997) of the activated sludge. Other particle measurement techniques reported by various authors include image analyzing system (Zahid and Ganczarczyk, 1990), coulter counter or electrical sensing zone method (Andreadakis, 1993) and laser beam diffraction method (Jorand *et al.*, 1998). Govoreanu *et al.* (2004) presented a review of different measurement techniques including electron and optical microscopy methods, electrical sensing zone methods and light scattering and light obscuration methods.

2.3.2. Sludge Volume Index

Because of the thickening functions of the secondary clarifier, its design is usually based on the results of thickening tests carried out in batch. The purpose of these tests is

to determine the settle-ability of the activated sludge. Different test methods and corresponding parameters have been established to obtain a quantitative measurement of the sludge settle-ability. The Mohlman sludge index better known as the Sludge Volume Index (SVI) is perhaps the most widely used among these parameters. The SVI of a sludge sample is determined by finding out the volume of the sludge occupied in a 1 L graduated cylinder after 30 minutes of setting. The test is usually performed without stirring, although stirring is recommended by the Standard Methods (American Public Health Association, 1999). The test can be performed very easily and thus it has a widespread use in the routine control and monitoring of activated sludge processes.

Relationships between the organic loading and the SVI of activated sludge have been investigated by many authors (Ford and Eckenfelder, 1967; Ganczarczyk, 1970; Rensink, 1974). According to their study the sludge settle-ability is reduced at both low and high organic loadings. In his study, Pipes (1979) reported that for an activated sludge sample, higher values of SVI are usually caused by the presence of filamentous microorganisms in the sludge. The production of filamentous bacteria within the activated sludge, which affects the SVI values, was later linked to the concentration and nutritional conditions of the sludge (Wagner, 1983). Many other studies (Forster, 1968; Forster and Dallas-Newton, 1980; Wu *et al.*, 1982; Clarke and Forster, 1983) also reported that sludge settle-ability, in terms of SVI, depends on the level of nutrients within the sludge and the solids loading rate. These studies were later verified (Forster, 1985a, 1985b) by carrying out an investigation to find out the relationship between activated sludge settling characteristics and the main nutrients (carbon, nitrogen, phosphorus), using full scale plant data.

After the Sludge Index was first introduced in 1934 by Mohlman, its shortcomings were discussed by Finch and Ives (1950), who argued that the sludge index does not have any theoretical support. For poorly settling sludge samples, the values of the SVI depend largely on the initial sludge concentration. Fitch and Kos (1976) proposed a modified index called the Sludge Quality Index (SQI), in order to overcome the influence of initial concentration. The SVI values may also vary depending on the testing method, type of settling vessel used and volume of sludge used. If stirring is used, the test may produce different results than an unstirred test. The volume of sludge used for the test and the initial interface height is proven to affect the outcome of the test (Dick and Ewing, 1967). The authors also suggested that for short cylinders the settling velocity may be retarded owing to the build-up of solids at the bottom of the vessel. According to Vesilind (1968), the diameter of the sedimentation vessel may affect the settling velocity and consequently the SVI value. His study showed that a suspension with high suspended solids concentration may settle more slowly in a small cylinder than in a large one, and vice versa, because of wall effect and quicker solids build-up.

Dick and Vesilind (1969) showed that SVI does not relate to such parameters as sludge yield strength, plastic viscosity, and an initial settling velocity. It has been shown that two different sludge samples with different sedimentation and dewatering properties may have the same SVI value (Renko, 1996). These variations make it difficult to compare the SVI values between different plants. To evaluate the effects of different variables on SVI results Bye and Dold (1998) presented a simple model that predicts settling behavior in a column settling test. Although many authors have indicated that the SVI is not a very good measurement for monitoring sludge settle-ability, but in spite of

these weaknesses the SVI is used successfully in wastewater treatment plants on a daily basis. Methods of on line SVI measurements, in full scale plants, have also been proposed (Sekine *et al.*, 1989; Sadar and Molina, 2003).

2.3.3. Settling Curve and Zone Settling Velocity

Owing to the unpredictable nature of the sludge volume index, various attempts were made to predict the sludge settling characteristics with alternate parameters. One such parameter is the Zone Settling Velocity (ZSV) of the activated sludge. This parameter is obtained by constructing an interface depth vs. time plot from batch settling data and is given by the slope of the linear region of the curve. The value of ZSV decreases with increasing solids concentration. The ZSV has a limitation in describing the sludge settle-ability because it ignores the end of the settling curve once it goes into compression. Unlike the SVI, the ZSV is not used in monitoring and evaluation of activated sludge process on a daily basis, because of the strenuous measurement technique.

The notion of using batch settling data for design purposes was first introduced by Coe and Clevenger (1916), but no underlying theory for sedimentation was presented. Later, a kinematical theory of sedimentation was proposed by Kynch (1952), based on the propagation of concentration waves in ideal suspensions. The settling curve proposed by Kynch had two stages: a constant rate period representing the ZSV and a falling rate period with velocities less than the ZSV. According to this idealized concept of batch thickening, each concentration within the flow field propagates at a characteristic upward velocity and eventually intercepts the solid-liquid interface at which point the interface assumes a settling velocity which is characteristic of that concentration. When the

maximum concentration reaches the interface, no further settling is possible. Following the theory proposed by Kynch, Talmage and Fitch (1955) recognized that in the settling plot, the water-suspension interface slope gives the settling velocity of the suspension and thus the slopes at different times represent the settling velocity at different concentrations. They used this information in conjunction with Coe and Clevenger's technique to devise their method for the design of continuous thickeners.

Many researchers have later indicated that the batch settling curve is more complicated than initially suggested by Kynch. While investigating the settling of a less idealized sludge, Fitch (1975) found an induction period preceding the linear settling portion. He also suggested the presence of a compression phase at the end of the falling rate period. Later studies verified this compression phase in terms of compressive stress and the resulting flow resistance (Kos, 1977; Dixon, 1978). Tiller (1981), Fitch (1983) and Font (1988) later tried to modify Kynch's theory to account for the compressive effects within the settling curve but each of them had deficiencies derived from unrealistic assumptions. In a later study, pure chemical sludge was used to examine the interfacial settling behavior at varying concentrations (Vesilind and Jones, 1990). The authors found that at lower sludge concentrations, an increasing interface velocity period is located between the first and the second decreasing rate periods. This region was explained by the upward propagation of lower concentrations, similar to Kynch's theory, created by the removal of liquid from within the compression region. Chen *et al.* (1996) conducted a similar study with low sludge concentrations and identified a period with interface velocity higher than the ZSV, preceding the compression region. This was explained by the formation of large aggregates at lower concentrations by means of

flocculation. Renko (1996) treated the several separate parts of the entire settling curve as a whole and developed a model for describing sludge blanket interface settling in a batch reactor.

2.4. Modeling of Activated Sludge Settling

Throughout the years, attempts have been made to develop predictive models that describe the activated sludge settling in the secondary clarifier. Because of the complexity in the modeling process, research is still under progress in this field. Many models have already been proposed by numerous researchers, and at present a range of models exist starting from very simple empirical ones to very complicated ones. Some of the models describe the whole activated sludge process combining the operations of both the bioreactor and the clarifier, while others simply attempt to predict the settling and thickening part in the secondary clarifier. This section provides a review of the research done so far in the modeling of settling velocity within the activated sludge secondary clarifier.

2.4.1. Settling Velocity Models

Because of the complexity associated with the graphical representation of solids flux theory, studies have been conducted over the years to find an empirical relationship between the settling velocity and sludge concentration. Consequently, many relationships (Kalinske, 1948; Richardson and Zaki, 1954; Bond, 1961; Vesilind, 1968; Dick and Young, 1972; Cho *et al.*, 1993; Zhang *et al.*, 2006) have been proposed to facilitate the direct analysis of settling tank behavior. Employing different formulas, suggested by different authors, with the flux theory leads to significant differences in the

interpretations of settling behavior. The most prominent and useful ones among these relationships will be discussed within this section.

One of the earliest and most accepted among these relationships is given by the Richardson-Zaki equation (Richardson and Zaki, 1954). According to the authors, the initial settling velocity for a suspension containing uniform spherical particles, settling under viscous (laminar) flow conditions, can be expressed as:

$$V_s = V_o \varepsilon^{4.65} \qquad (2.2)$$

where, V_s = the settling velocity (m/hr), V_o = the terminal settling velocity (m/hr) given by Stokes' equation and ε = the sludge porosity (the fraction of total volume not occupied by flocs). From the above relation, it is evident that for 100% sludge porosity (discrete particles), the settling occurs at the terminal settling velocity.

Apart from the Richardson-Zaki equation, the two most widely accepted formulas are given by Vesilind (1968)and Dick and Young (1972). The Vesilind formula is given as:

$$V_s = V_o e^{-nXo} \qquad (2.3)$$

While, the Dick and Young formula is given as:

$$V_s = V_o X_o^{-n} \qquad (2.4)$$

where, X_o = MLSS concentration (g/m^3). The constant parameter (n) and the terminal velocity (V_o) in the formulas are usually referred to as Vesilind model parameters and can be obtained by carrying out batch settling experiments with different initial sludge concentrations. None of the aforementioned settling velocity models account for the compression and channeling within the sludge blanket. Nonetheless, these models are established to provide better results than most of the later models.

Smollen and Ekama (1984) conducted a study to compare the predictions of the Vesilind and the Dick and Young formula. The authors found that the Vesilind formula produced better correlation when fitted with different sets of experimental data. Researchers (Hultman *et al.*, 1991; Xu and Hultman, 1996) have recommended the use of these two settling velocity formulas above others because they are widely used, which facilitates the comparison of obtained coefficients (V_o and n) with other experimental studies. A recent study (Zhang *et al.*, 2006) indicated that the Vesilind function is capable of describing compression settling velocity, upon the correct estimation of appropriate parameters. The authors concluded that, dividing the complete activated sludge settling process into zone and compression settling stages, and describing them by the Vesilind function with different parameter sets was more appropriate.

Cho *et al.* (1993) presented another model to determine the activated sludge settling velocity based on the solids flux theory. The model is developed from the Carmen-Kozeny equation for flow through porous media and is presented as:

$$V_s = V_o e^{-nX_o} / X_o \qquad (2.5)$$

In recent studies, Zhang *et al.* (2006) reported that due to the poor ability of the Vesilind function in describing the transition settling, between zone and compression stage, the Cho function is more suited to describe complete batch settling curves.

Although some of the aforementioned models are able to provide good estimation of activated sludge settling velocities, but these models have some setbacks in terms of everyday use. Because these models utilize the solids flux theory, they require the experimental development of a settling flux curve to determine the model parameters,

which being both time consuming and labor intensive, is not widely practiced. Moreover, the extensive period of settling required may lead to denitrification within the sludge, severely affecting the zone settling velocities. In view of this issue, several investigators (Forster, 1982; Daigger and Roper, 1985; Pitman, 1985; Ekama and Marais, 1986; Wahlberg and Keinath, 1988; Hartel and Popel, 1992; Akca *et al.*, 1993; Daigger, 1995; Ozinsky and Ekama, 1995; Wahlberg and Keinath, 1995; Renko, 1998; Mines *et al.*, 2001; Giokas *et al.*, 2003) have developed empirical relations to determine the Vesilind model parameters using several sludge settling factor (SVI or modified SVI). These models attempt to predict sludge settling velocity in terms of initial sludge concentration and sludge indices. Some of the recognized and well practiced models are briefly described below.

One of the earlier among these models was developed by Forster (1982) using Stirred Sludge Volume Index (SSVI). The model replaces the Vesilind parameters as:

$$V_o = 5 \text{ m/hr} \qquad (2.6)$$

$$n = 0.2498\, e^{0.0046 \times SSVI} \qquad (2.7)$$

In his research Pitman (1985) studied the settling properties of activated sludge from four biological nutrient removal plants and found out that well settling sludge samples have high values of V_o with low values of n and vice versa. He developed his model based on the correlation of SSVI with V_o/n. The model is given as:

$$V_o/n = 67.9\, e^{-[0.016\,(SSVI)]} \qquad (2.8)$$

Ekama and Marais (1986) compared the model developed by Pitman with data reported in the literature to show a significant close correlation. The authors then came up with a

relationship to define V_o and n individually from the expression V_o/n, obtained from Pitman's model.

$$n = 0.88 - 0.393 \log(V_o/n) \quad (2.9)$$

Daigger and Roper (1985) developed an empirical relation between the SVI of an activated sludge and the Vesilind parameter n, within SVI values of 13 ml/g to 402 ml/g. They found that the parameter V_o was independent of SVI with a mean value of 7.8 m/h.

$$V_s = 7.8\, e^{-[0.148 + 0.00210\,(SVI)]Xo} \quad (2.10)$$

In their research, Wahlberg and Keinath (1988) reported that there is a linear relationship between V_o and SSVI and a parabolic relationship between n and SSVI. They found that the traditional SVI can lead to very imprecise estimation. The model replaces the Vesilind parameters as:

$$V_o = 153 - 0.615\ SSVI \quad (2.11)$$

$$n = 0.426 - 0.00384\ SSVI + 5.43\times10^{-5}\ (SSVI)^2 \quad (2.12)$$

Keinath (1990) later developed a design and operation chart for use by design engineers and wastewater plant operators, using this concept. Hermanowicz (1998) also came up with another operating diagram based on this model in conjunction with the Daigger and Roper model.

Akca *et al.* (1993) investigated the relationship between SVI and sludge age. They determined the Vesilind parameters in terms of both the SVI and sludge age. Their model can be given as:

$$V_s = 28.1\ SVI^{-0.2667}\ e^{-(0.177 + 0.0014\ SVI)\ Xo} \quad (2.13)$$

In an attempt to establish the most representative secondary clarifier operating diagram, Daigger (1995) utilized the data collected in several preceding studies.

According to his findings, a single relationship could accurately describe a wide variety of data. His model is given as:

$$\ln V_s = 1.871 - (0.1646 + 0.00158\ SVI)\ X_o \qquad (2.14)$$

His research also aimed at comparing the predictive capabilities of three sludge settling indices and he found that the SSVI had more accurate predictions as compared to the other two indices, in terms of activated sludge settling.

2.5. Final Clarifier Operational Problems

One of the many parameters to estimate the overall performance of an activated sludge system is the suspended solids concentration in the final effluent. This is directly related to the performance of the secondary clarifier and can be affected by an array of different factors. These factors may include the biological activity of microorganisms within the activated sludge and hydraulic disturbances within the clarifier. These factors affect the activated sludge properties and its settle-ability thereby affecting the ability of the clarifier to separate and concentrate the activated sludge from the effluent.

According to Ekama *et al.* (1997), excessive solids in secondary clarifier effluents may occur because of hydraulic short-circuiting or high velocity currents causing re-suspension of solids from the surface of the sludge blanket, solids overload resulting in elevated sludge blanket, denitrification within the clarifier causing solids to float to the surface, flocculation problems due to either poor floc formation or floc breakup and finally poor performance of the sludge collection and removal system. Most of these factors are briefly discussed within this section.

2.5.1. Sludge Microbial Activity

The microbial activity within the sludge may create various problems leading to the poor performance of secondary clarifiers. It has been shown that the settling properties of the sludge are related to the biological activity within it (Clarke and Forster, 1983). Many factors may in turn influence the microbial activity. One of the factors that inhibit the growth and performance of microorganisms is the presence of toxic heavy metals in the sludge. Metals in the activated sludge may originate from industries such as metal finishing, hydrometallurgical refining, battery manufacturing, etc. Tyagi *et al.* (1991) made an attempt to develop a mathematical model describing the solids concentration, recycle ratio and sludge settling velocity in relation to metal inhibition. The toxic effects of heavy metals on the activated sludge have been studied by many authors (Battistoni *et al.*, 1993; Chua *et al.*, 1999; Sin *et al.*, 2000; Oviedo *et al.*, 2002; Sorour and Sayed-Ahmed, 2005; Ozbelge *et al.*, 2007) in the recent past.

Sludge activity that causes poor settling and leads to solids carryover in the secondary clarifier, may be classified into four categories: bulking sludge, rising sludge, dispersed sludge or pinpoint floc and floating sludge. Activated sludge with very poor settle-ability is usually referred to as bulking sludge. This is primarily caused by an excessive growth of filamentous microorganisms within the sludge (Forster, 1971; Pavoni *et al.*, 1972; Sezgin *et al.*, 1978; Jenkins *et al.*, 1983). Filamentous microorganisms can extend from the floc particles, thereby decreasing its settling rate. They can also deter the compaction and thickening process by physically holding the particles apart. Filamentous microorganisms, in the activated sludge, can grow in different forms and lead to different settling characteristics.

A procedure to classify the different types of filamentous bacteria was developed (Eikelboom, 1977) based on their size, morphology and response to standard staining technique. According to Jenkins and Richard (1985), identification of the predominant type of filamentous bacteria within the system can help to determine the cause of sludge bulking and lead to potential solutions. His research in addition to the results from several other research studies (Wagner, 1983; Foot, 1992) indicated that many factors influence the growth of filamentous bacteria including high or low oxygen concentration, high sulfide concentration, high carbohydrate and fatty acid concentration, high or low solids loading, lack of major nutrients, and the feed pattern. Consequently, extensive research (Rensink, 1974; Chudoba *et al.*, 1985; Pujol and Boutin, 1989; Novak *et al.*, 1993; Casey *et al.*, 1994; Foot *et al.*, 1994; Casey *et al.*, 1995; Kim *et al.*, 1998; Saayman *et al.*, 1998; Seka *et al.*, 2001; Hossain, 2004) has been performed towards the control of filamentous sludge bulking. Apart from causing sludge bulking, presence of filamentous bacteria has also been attributed to the floc forming process within activated sludge (Lau *et al.*, 1984). Although, non-filamentous sludge bulking, associated with the excess production of viscous exo-cellular polymers by certain strain of bacteria, has been observed (Heukelekian and Weisberg, 1956) and studied, this problem is not usually encountered in wastewater treatment plants.

The term sludge rising refers to the rising of the settled activated sludge, in the secondary clarifier, due to nitrogen gas produced by the denitrification process. The gas micro-bubbles produced within the settled sludge blanket, lowers the specific gravity of the sludge, resulting in sludge rising. This phenomenon was observed and reported in

early literature by Sawyer and Bradney (1945). Clayfield (1974) reported that the rate of Endogenous Nitrate Respiration (ENR) is the most important parameter in terms of sludge rising. He noted that a critical amount of N_2 gas must be produced through ENR for the settled activated sludge blanket to become unstable. He proposed a mathematical formula to determine this concentration as a function of sludge and water density, MLSS concentration and pressure.

In a later research, Henze *et al.* (1993) identified the factors influencing the concentration of N_2 gas at a specific depth within the settling tank. These factors include: solubility of nitrogen gas, depth below water level, N_2 concentration in the influent, N_2 production rate, O_2 concentration in the influent, hydraulic retention time of the tank and available nitrate in the influent. The authors indicated that the critical N_2 concentration at 20°C is about 6-8 g $N0_3$-N/m^3 and without pre-denitrification the nitrate concentration for all clarifier influent will be above this value. Clayfield (1974) indicated that the value of the critical N_2 concentration rises with depth but the rate of ENR increases with depth as well because of higher biomass concentration. In order to compare these two conflicting factors, Kim *et al.* (1994) proposed a Sludge Stability Index (SSI) to determine the stability of a particular sludge layer. The SSI was defined as the ratio of nitrate concentration utilized through ENR to the critical N_2 concentration for sludge rising and was given as gNO_3/gN_2. The researchers found that a particular sludge layer becomes unstable and rises to the surface at an SSI value above 1g/g. They also developed a comprehensive activated sludge settling model, based on the solids flux theory, to account for the denitrification. In advanced wastewater treatment plants, the rising sludge problem in the secondary clarifier can be encountered by employing denitrification in the

preceding biological treatment and also by increasing the sludge recirculation ratio (Ekama *et al.*, 1997).

Dispersed sludge refers to the presence of unflocculated biosolids within the effluent from the secondary clarifier, leading to turbid effluent with high Biochemical Oxygen Demand (BOD). The dispersed particles in the supernatant are either caused by poor flocculation properties of the sludge or by floc breakage. Floc breakage is usually caused by shearing effects within the settling tank induced by undesired turbulence and hydraulic currents. The poor flocculation of biosolids may be caused by low sludge retention time, high MLSS concentration, absence of oxygen, presence of sulphide etc. (Kjellerup *et al.*, 2001). Temporary deflocculation may also occur as a result of the sudden changes in temperature, dissolved oxygen, salinity and pH value (Pipes, 1969). These problems inhibit floc-forming microbial activity as a result of which the sludge becomes dispersed with poor settle-ability. The term pinpoint floc refers to the small flocs of particles present in the supernatant after the sludge has settled (Pipes, 1978; Sezgin *et al.*, 1978; Palm *et al.*, 1980). In this case, the effluent from the secondary clarifier contains higher than desired suspended solids but the effluent is clear (not turbid or cloudy) with individually visible flocs suspended within. This problem is a result of dispersed growth within the activated sludge at low organic loadings, although absence of filamentous bacteria is also suggested to be a possible reason (Barahona and Eckenfelder, 1984; Nguyen *et al.*, 2007). Permanent deflocculation leading to highly stable pinpoint flocs may also occur in the absence of proper nutrients and under the toxic effect of heavy metals in the activated sludge (Neufeld, 1976).

Floating or foaming sludge is attributed to the presence of filamentous microorganisms that create foam in the secondary clarifier. The activated sludge foaming was first linked to the activity of filamentous actinomycete bacteria *Nocardia amarae* (Lechevalier and Lechevalier, 1974). These bacteria produce a lipid material and excrete it into the mixed liquor, which then collects on the entrained air bubbles. These air bubbles mesh together to form larger bubbles containing *Nocardia* colonies and float to the surface to form scum (Pipes, 1978). If the floating foam has sufficient density then wind cannot blow it away. The bacterial colonies are able to survive and grow within the floating scum because they are resistant to dryness and can store polyphosphate to deal with starvation. Although floating or foaming sludge has been attributed to other genera of filamentous bacteria, but these foams are usually referred to as *Nocardia* foams because *Nocardia* was the first branching actinomycete isolated from activated sludge foams. Some of the other filamentous bacteria isolated from activated sludge foams may just be entrapped within the foam and have nothing to do with the actual foaming process.

Activated sludge foaming can also be influenced by the presence of surface active agents within the wastewater. Because of the ability of the surfactants to lower surface tension, they may help to stabilize the liquid film between air bubbles thereby stabilizing the *Nocardia* foam, if present within the system. It has been shown (Ho and Jenkins, 1991) that the presence of non-ionic surfactants may significantly enhance the activated sludge foaming, but in absence of *Nocardia* cells, the surfactants are unable to generate stable foam. Overdosing of polymer in sludge dewatering systems has also been indicated as a possible reason behind scum formation (Bradley and Kharkar, 1996).

Control of microbial foaming may be achieved by employing modifications of usual plant operation in terms of aeration within the bioreactor, recirculation and sludge withdrawal. Because *Nocardia* bacteria are slow growing microorganisms, they need to spend sufficient time within the system to compete for substrates in order to grow. Thus, the most successful method of preventing the *Nocardia* growth is lowering the Sludge Retention Time (SRT) within the bioreactor (Jenkins *et al.*, 1983). But this method is not applicable for plants with biological nutrient removal, thus it has been suggested that properly designed anoxic selectors are effective in controlling *Nocardia* growth (Pitt and Jenkins, 1990; Blackall *et al.*, 1991). Another method was proposed by Richards *et al.* (1990), in which increased aeration is employed in the bioreactor to strip the foaming organisms from the MLSS followed by selective wasting of the foam.

2.5.2. Hydrodynamic Problems

As previously mentioned, the initial theory of an ideal sedimentation tank was proposed by Hazen in 1904 and since then relentless efforts have been given by researchers to better understand and improve the flow conditions and hydrodynamics within the settling tank. Camp (1946) first suggested that the settling tank hydrodynamics may deviate from the ideal behavior proposed by Hazen. He indicated four major reasons for this deviation: flocculation, turbulence, short-circuiting and density currents. Short-circuiting within the settling tank refers to the phenomenon when a fraction of the fluid passes through the tank in a shorter time than the hydraulic retention time. On the other hand, density current refers to the presence of internal currents within the tank, caused by density differences among layers of fluid. According to Camp, all tanks experience short-

circuiting due to difference in velocity and length of stream paths. He believed that short-circuiting is accentuated by density currents while the density currents may be caused by differences in temperature, salt content or suspended solids concentration. Anderson (1945) also studied the existence of density current in secondary clarifier caused by density stratification. He investigated the effects of density current on different design parameters as well as the overall performance of the clarifier.

The most significant work in the study of flow patterns and hydrodynamics of secondary clarifiers was done by Larsen (1977). He investigated different hydrodynamic processes within rectangular horizontal flow clarifiers and studied the energy flux, energy dissipation, density currents, inlet considerations, jets etc. He introduced the concept of density waterfall, which is described as a phenomenon that causes the incoming suspension to sink to the bottom of the tank upon entrance. This is caused by the difference in density between the entering suspension and the suspension within the tank. The density difference might be the result of difference in temperature, suspended solids and dissolved solids concentration.

Larsen also introduced the concept of stream function and vorticity, which may be caused by internal density gradients. He divided the rectangular clarifier into inlet zone, settling zone, sludge zone and effluent zone, subsequently identifying the hydrodynamics within these different zones. In the inlet zone, the flow pattern is dependent on the momentum and energy carried by the influent suspension. He identified two different currents within the settling zone, separated by a roughly horizontal interface, a bottom density current initiated by the inflow and a buoyant density current or a return current in

the supernatant layer. The bottom density current may have a higher flow rate than the inflow because the return current provides additional flow to the bottom current. The sludge zone moves horizontally on the tank floor with the settled sludge, while in the effluent zone the flow pattern is governed by the design and placement of the effluent weirs. Lighter settled particles from the sludge zone may get entrained in the bottom density current and get carried off to the end wall of the tank where the density current rebounds at the wall resulting in high effluent suspended solids.

Larsen identified the major energy fluxes within the clarifier and discussed the corresponding effects. The influent to the tank carries kinetic energy, owing to the volumetric flow rate, which is mostly dissipated in the inlet zone. Because of higher density, the influent suspension also carries potential energy into the tank, which is partially dissipated at the inlet and partially converted to kinetic energy, forming a density current that flows along the bottom of the tank. Significant amount of energy may be transferred from the ambient into the upper layers of the tank by wind shear and surface heat exchange thereby enhancing turbulent mixing. According to Larsen, the energy leaving the system as kinetic energy of the overflow and potential energy of the effluent suspended solids is negligible. He suggested that any input of energy into the clarifier causes turbulence that may negatively affect the flow patterns and concentration gradient within the tank. Therefore, the quality of the effluent in terms of suspended solids concentration may vary depending on these energy inputs.

Considerable amount of research have been conducted by various authors to study the flow patterns and hydrodynamics within the clarifier. Undesired hydrodynamic phenomena within secondary clarifier like turbulent dispersion and mixing, density waterfall in the inlet mixing zone, entrainment of clarified supernatant into density waterfall increasing total flow, formation of bottom density current, rebound at the end wall, formation of buoyant density current, recirculation of excess flow, possible short-circuiting and other associated effects have been identified and extensively studied by many researchers (Price and Clements, 1974; Ostendorf, 1986; Lumley *et al.*, 1988; McCorquodale *et al.*, 1988; Bretscher *et al.*, 1992; Samstag *et al.*, 1992; Deininger *et al.*, 1996; Krebs *et al.*, 1998). Figure 2.1 shows some of the typical density associated effects in rectangular secondary clarifiers.

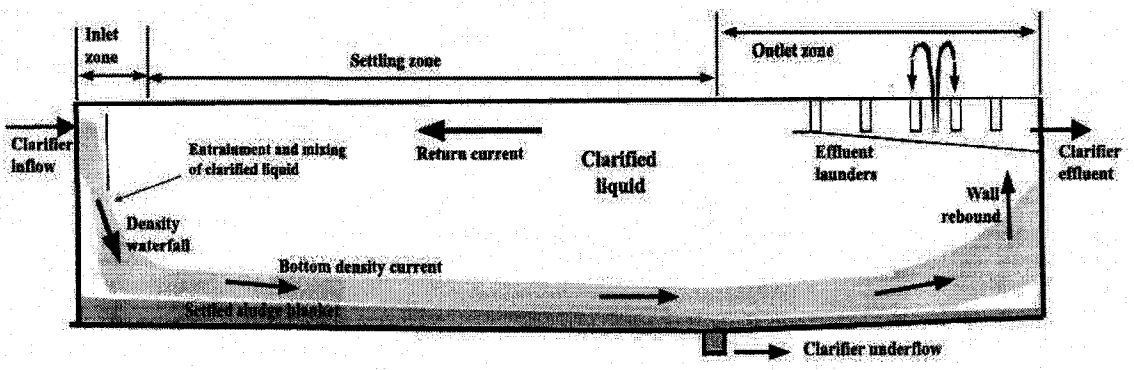

Figure 2.1: Typical Density Related Hydrodynamic Trends in Rectangular Secondary Clarifiers

Improvements in tank hydrodynamics by adding inlet baffles were experimentally demonstrated by Silveston *et al.* (1981). Imam *et al.* (1983) conducted a study to determine the effective baffle placement and proposed that a 30% submerged baffle may contribute towards optimum removal efficiencies for the clarifier. Extensive

investigations were conducted by Adams and Rodi (1990) on the clarifier inlet arrangements. Effect of unsteady inflow conditions was studied (McCorquodale *et al.*, 1991) on clarifier performance. The authors observed a strong bottom density current and increased flow recirculation, at high inlet concentrations, leading to higher solids concentration in the effluent. To reduce the intensity of density currents, Krebs (1991) investigated the use of inlet baffles. He suggested the use of densimetric Froude number, which relates the local convection to the local density differences without assuming tank averaged values. He suggested that the ratio of local kinetic and potential energy is given by the square of densimetric Froude number. In his study, the design of inlet baffle was optimized in terms of the densimetric Froude number and use of intermediate transverse baffles was suggested for clarifiers, in order to reduce the bottom density current effect. Other studies (Zhou and McCorquodale, 1992) also demonstrated the effectiveness of inlet baffles and the use of densimetric Froude number in their design.

Bretscher *et al.* (1992) conducted extensive experimental studies in order to find out ways of improving the settling characteristics of rectangular and circular tanks. The authors suggested that if the inlets of the tank are positioned too high, it introduces larger amount of potential energy in the tank thereby aiding the formation of bottom density currents. Thus they recommended the placement of tank inlets at increased depth. The authors also proposed that using a barrier wall, the basin should be divided in two, which will reduce the loading thereby increasing the depth of clear water in the effluent zone of the tank. According to them, the outlet weirs should be place at a position where the suspended solids concentration is the lowest. Use of perforated baffles was investigated by Krebs *et al.* (1992), to improve tank performance. Clarifier performance in terms of

varying hydraulic and solids loading was investigated by McCorquodale and Zhou (1993). The authors found strong relationship between clarifier performance and densimetric Froude number, for a specific solids loading. They suggested that the Reynolds number has a very small effect over clarifier performance and the bottom density current is insensitive to this parameter. They also found that the lowest effluent concentration can be achieved at an optimum value of the densimetric Froude number. Different inlet arrangements for the clarifier were investigated by Krebs *et al.* (1995). They also studied the effect of inlet baffle position and depth, deflection of inlet jets and inlet dissipating devices *e.g.* angled bars.

3.0. Analysis of Clarifier Influent, Effluent and RAS

As a first step towards understanding the final clarifier operation and possible operational problems, the properties of the incoming mixed liquor were investigated along with the properties of the effluent and the RAS. The properties that were analyzed include Total Solids, Total Suspended Solids, Turbidity and Particle Count. This chapter envelopes the methodology of the aforementioned analyses as well as the results obtained from them.

3.1. Sample Collection

The analyses were done with the intention of observing seasonal effect on the operation of the final clarifier. Thus collection of samples was carried out in three batches representing three different seasons of the year. The first batch of sampling was done on October 16, 2007, the second batch on February 28, 2008 and the third batch on April 28, 2008. The first two batches of sample represent the Fall and Winter operation of the final clarifiers respectively. While the last batch of sample was collected in Spring right after a heavy rainfall event, thus representing the clarifier operation during a storm-water runoff.

The sample collections were done manually using the grab sampling technique, as per section 1060B of Standard Methods (American Public Health Association, 1999), from the sampling rack of Secondary Clarifier #1 at Gold Bar WWTP (Figure 3.1). The sampling rack held sampling lines from the fourth pass of Bioreactor #1 - giving mixed liquor sample going into Clarifier #1, from effluent end of the clarifier - giving treated wastewater sample going into the disinfection facility and from the return activated sludge line - giving RAS sample going into the thickener. The composite sampling

technique was not used due to a limitation of proper time and resources. As such, the samples reflect performance only at the point in time when the samples were collected. For this reason, the Gold Bar operations were contacted beforehand to ensure steady plant operation at the time of sampling. It was made sure that the sampling line and the units in concern were recently maintained and inspected, thereby providing stable samples representative of the plant's normal operation at the time of year. Before collecting the samples, the sampling lines were flushed for at least one minute to clear away any residuals and contaminants. Samples were collected using either 500 or 1000 ml Nalgene® bottles and the bottles were rinsed before filling. At least two containers of sample were collected for each of the aforementioned wastewater stream. All of the samples were kept in coolers and the coolers were placed in temperature controlled rooms until the time of analysis. To minimize the changes caused by the growth of microorganisms, the samples were stored at below 4°C but above freezing.

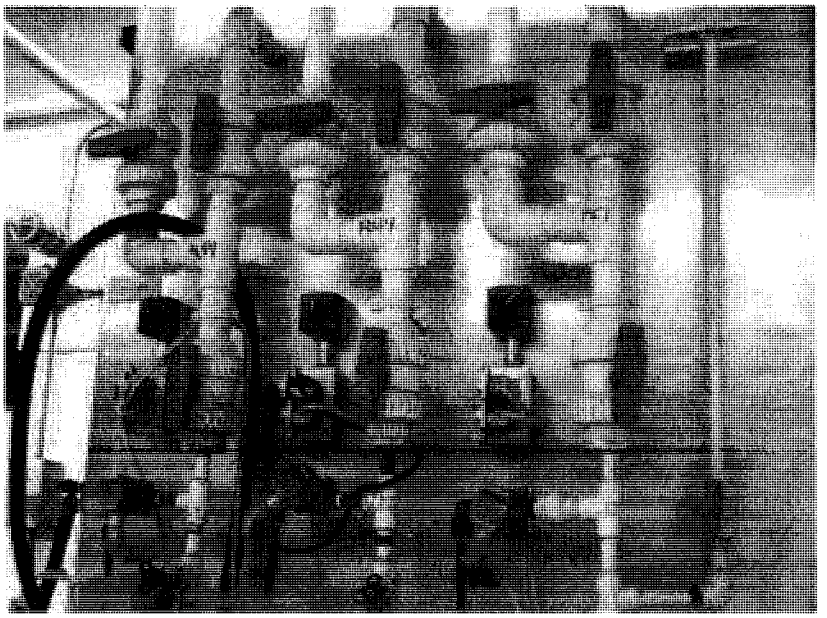

Figure 3.1: Clarifier #1 Sampling Port at Gold Bar WWTP

3.2. Analytical Procedures

3.2.1. Total Solids

The material residue left in a vessel after evaporation of a sample and its subsequent drying in an oven at a defined temperature is termed as Total Solids (TS). The TS value of a sample is expressed as the ratio of mass of solids per volume of sample (mg/L) (American Public Health Association, 1999).

For the TS measurements, clean evaporating dishes (Figure 3.2 a) of 100-mL capacity, made of porcelain, were heated to 103 to 105°C for 1 hour in a drying oven. The dishes were then stored and cooled in a desiccator for drying, before taking the initial weight in grams (W_{TSi}). Anhydrous Calcium Sulfate was used as desiccant for the drying. This pre-conditioning was done each time to ensure stable, constant weight before use. The dishes were labeled with permanent ID. To ensure homogeneous samples, the plastic bottles containing the wastewater were vigorously shaken before the samples were poured into a small graduated cylinder. The graduated cylinder was used to measure the predetermined volume (25 mL) of sample which was then transferred into the designated pre-weighed evaporating dish. The evaporating dishes were then carefully placed into the drying oven. The samples were kept in the oven overnight at 105°C. The dishes were then placed into the desiccator and cooled to ambient temperature before attempting to determine the final weight in grams (W_{TSf}). This was done in order to attain thermal equilibrium or to balance the temperature and weight of the dishes. Subsequent drying was done in the oven for 1 hour, if necessary. The cycle of drying, cooling, desiccating, and weighing was repeated until a constant weight was obtained. Duplicate measurements were taken for each sample.

The TS data were calculated as:

$$TS\ (mg/L) = [(W_{TSf} - W_{TSi})\ (g) / \text{Sample Volume (mL)}] \times (1000)^2 \qquad (3.1)$$

Although residues dried at 180°C lose almost all mechanically occluded water, the temperature of 105°C was chosen for the measurements. This is because at 180°C organic matter, though not completely destroyed, may be lost by volatilization from the samples. As the samples had very high organic content including large microbial population, 105°C was the appropriate temperature for drying without losing the quality of the samples. But at this temperature the removal of occluded water is marginal and hence the attainment of constant weight was slow. For this reason, the evaporation dishes were dried overnight in the first cycle.

The samples were stored at 4°C in order to prevent microbiological decomposition of the solids. Samples were brought to room temperature before analysis. The same Analytical Balance (Mettler AE-163) was used for all the measurements to minimize instrumental error. All weights were recorded to the fourth decimal place (0.1 mg). Dishes were always handled using forceps or rubber gloves to prevent transfer of moisture from the hand. Measurements were taken as per section 2540B of Standard Methods (American Public Health Association, 1999).

3.2.2. Total Suspended Solids

The portion of Total Solids retained by a filter of 2.0 μm (or smaller) nominal pore size is referred to as Total Suspended Solids (TSS), while Total Dissolved Solids (TDS) is the portion that passes through the filter (American Public Health Association, 1999).

For the TSS measurements, clean porcelain Gooch crucibles (Figure 3.2 b) of 40-mL capacity in combination with glass-fiber filters of 1 μm nominal pore size (Pall Corporation, Type A/E) were heated to 105°C for 1 hour in a drying oven. The crucibles, labeled with permanent ID, along with the filters were then stored and cooled in the desiccator before taking the initial weight in grams (W_{TSSi}). The pre-conditioned crucibles were then placed over the vacuum filtration apparatus (Figure 3.2 c).

After assembling the filtering apparatus, the vacuum pump was turned on to begin suction. The filter on each crucible was wetted with a small volume of De-ionized (DI) water to seat it. Sample bottles were vigorously shaken before the samples were poured into a small graduated cylinder. The graduated cylinder was used to measure the predetermined volume of sample which was then transferred into the designated pre-weighed Gooch Crucible. During filtering, each filter was washed successively with small volumes of DI water, allowing complete drainage between washings, to remove all traces of dissolved solids from the sample. The suction was continued for about three minutes after the filtration had completed allowing the filter to retain all of the suspended solids from the sample. The graduated cylinder was rinsed thoroughly using DI water so that no solids may remain adhered to the glassware. DI water was used as control samples to account for any solids carried by the water. The crucible and filter combination were then removed from the filtration apparatus and kept overnight in the drying oven at 105°C. After drying, the crucible-filter combinations were cooled to ambient temperature in the desiccator before measuring the final weight in grams (W_{TSSf}). Duplicate measurements were taken for each sample. The TSS data were calculated as:

$$TSS\ (mg/L) = [(W_{TSSf} - W_{TSSi})\ (g) / Sample\ Volume\ (mL)] \times (1000)^2 \qquad (3.2)$$

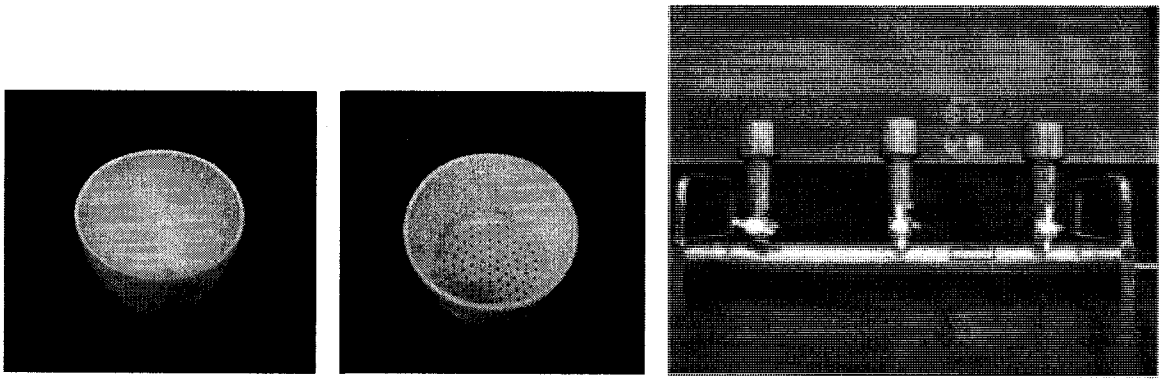

Figure 3.2: TS TSS Apparatus a) Evaporating Dish (left image), b) Gooch Crucible (middle image) and c) Vacuum Filtration Apparatus (right image)

Because excessive residue in the crucible may form a water-trapping crust over the filter, a very low sample volume (5 mL) was used for TSS measurements of clarifier influent and RAS. During the first runs in October, a higher volume of sample (20 mL) was used but for the subsequent runs in February and April the sample volume was maintained at around 5 mL for clarifier influent and RAS. This might have introduced some error in the TSS data for these samples in October. Also, lower volumes of sample were used for water with higher solids because they may cause clogging of the filter. Filter clogging leads to prolonged filtration times, which in turn may produce incorrect results owing to increased colloidal materials captured by the clogged filter. Measurements were taken as per section 2540D of Standard Methods (American Public Health Association, 1999).

3.2.3. Turbidity

Turbidity is one of the optical properties of a liquid that causes the scattering and absorption of incident light. Turbidity is caused by suspended and colloidal particulate matter such as clay, silt, fine organic and inorganic matters etc. It can also be caused by

particles that are in a different phase like immiscible liquid or microscopic gas bubbles. The size, shape, amount, color, density and refractive index of the particulates affect the light-scattering properties of the suspension. Turbidity is an inherently unstable property as it changes over time as the sample undergoes settling, dissolution, flocculation or degassing. Correlation exists between the turbidity and the TSS of the same liquid sample provided the samples are uniform and identical.

Turbidity of a sample of water is determined by an instrument called nephelometer or turbidimeter in which an intense collimated beam of white light is directed through the sample, contained in a vial, and the amount of scattered light is measured with a photometer located at 90^{o} to the beam. The amount of scattered light is directly proportional to turbidity for a given range. To account for any light scattered by the sample vial the readings must be referenced to a blank.

Turbidity is measured by Nephelometric Turbidity Unit (NTU), which is a measurement of the cloudiness of water. For this research, Orbeco-Hellige Model 965-10A (Figure 3.3) turbidimeter was used. The instrument had three different ranges (0-20, 0-200, and 0-1000 NTU). The calibration was done using a 40 NTU formazin standard on the 0-200 NTU range, and a 0 NTU blank solution on the 0-20 NTU range. The measurements of highly turbid samples cannot be done with confidence due to attenuation of the light beam. The solids content of the clarifier influent and RAS samples were too high to be measured by the turbidimeter and so turbidity measurements were done on clarifier effluent samples only.

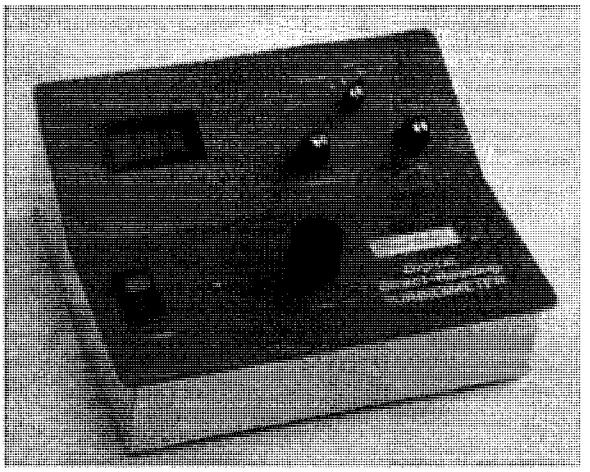

Figure 3.3: Orbeco-Hellige Model 965-10A Turbidimeter

Samples were stored at or below 4°C before analysis in order to prevent microbiological decomposition. Small cylindrical glass vials with plastic caps were used to hold the samples and the vials were kept clean, scratch free and dry. To reduce interference, samples were thoroughly mixed before transferring them into the vials and also it was made sure that there are no particles or bubbles adhered to the walls of the vials. Before filling the vials they were rinsed with the sample and before putting the vials in the instrument the outside walls were dried using Kleenex® Tissues. Each sample was measured in triplicate to ensure quality assurance. Measurements were taken as per section 2130B of Standard Methods (American Public Health Association, 1999).

3.2.4. Particle Size Distribution

Particle counting and size distribution analysis is an important physical property of any wastewater. It helps to determine the makeup of a particular treatment stream thereby providing an estimate of process or treatment efficiency. In this report, the term 'Particle

Size' refers to the Equivalent Spherical Diameter, while the Particle Size Distribution is expressed as the number concentration or particle count per mL of sample.

Methods for measuring particle size distribution of less than 500 μm usually depend on electronic measurement devices. Among the electronic particle-counting instruments three types are most common: electrical sensing zone instruments, light obscuration or blockage instruments, and light-scattering instruments. The particle counting apparatus used for this research, manufactured by Hach Ultra Analytics Inc., consists of three major components, the HIAC Model 8000A Particle Counter, The HIAC Model ABS-2 Automatic Bottle Sampler and the HIAC Model HRLD-400HC light obscuration liquid particle counting sensor. The system configuration is shown in Figure 3.4.

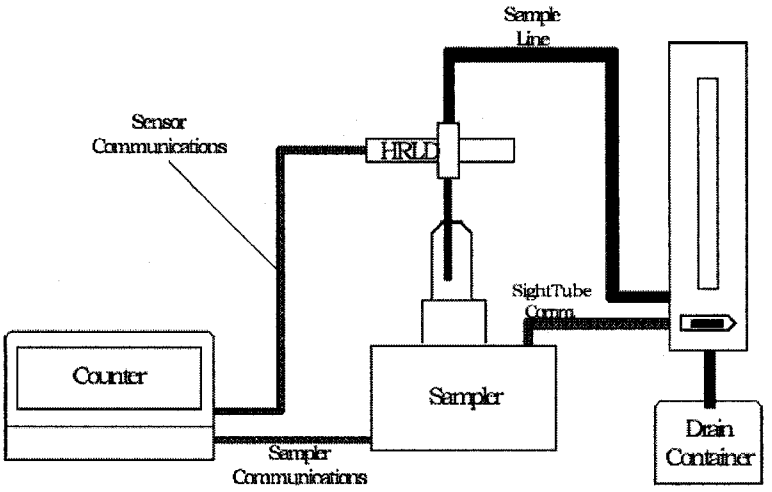

Figure 3.4: System Configuration of Particle Counting Apparatus

The particle counting sensor in this system is a self contained unit that uses a laser diode as the illumination source and a photodiode as the detector. The sensor utilizes the principles of light obscuration for particle detection. During a run, the liquid sample flows through the sensor micro-cell where a laser beam is directed at the sample through

a window. When the sample contains particles, they block the laser beam from the photo-detector. The light-extinction photodiode detects the loss of laser light intensity and generates an analog electronic pulse for each particle. These pulses are proportional to the light intensity which is a measure of the particle size. The photodiode pulses are then amplified and sent to the particle counter. The particle counter identifies the quantity and height of the analog pulses and sorts the pulses into bins with predefined pulse amplitude ranges. Particle counts with corresponding size ranges are then displayed by the counter.

The Model ABS-2 Automatic Bottle Sampler (Figure 3.5 a) is a pressure sampling device used for batch analysis of volatile or viscous liquid samples. A check valve is incorporated in the sample introduction line to eliminate backflow thereby minimizing sample cross-contamination. For flow control, a precision metering valve is located downstream of the sensor. The sampler has a built-in pressure/vacuum chamber which was interfaced directly to a pressure/vacuum pump for operation. The pressure operation is used for samples with high viscosity while the vacuum operation is used to degas samples which contain entrained air. The sample flow rate can alternatively be controlled by the pressure/vacuum regulator within the sampler.

The Model HRLD-400HC sensor (Figure 3.5 b) is designed to measure particles with equivalent spherical diameter ranging from 2.0 μm to 400 μm. It can measure liquid sample with particle number concentration of up to 18,000/mL. The standard calibrated flow rate of the sensor is 20 mL/min and it can handle flow rates from 10-50 mL/min. The pressure limit for the sensor is 69 bar (1000 psi) and the sample temperature limit is 65 °C (150 °F).

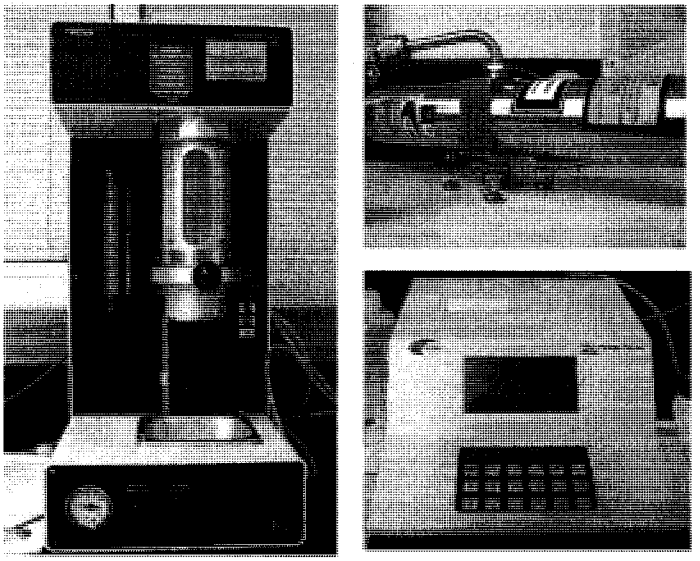

Figure 3.5: Particle Counting Apparatus a) Automatic Bottle Sampler (left), b) Particle Counting Sensor (top right) and c) Particle Counter (bottom right)

The Model 8000A Particle Counter (Figure 3.5 c) is used to process signal output from the sensor located within the sampler. It has eight selectable channels to measure particles in eight different size ranges. The particle counter acts as a display interface for the whole apparatus as all the factors and parameters of the measurement can be programmed into this device including sample name, sampling volume, particle size ranges to be measured, dilution factor used, background subtraction etc.

Samples were stored in a refrigerator at 4°C in order to prevent microbiological decomposition but were restored to room temperature before measurement. For each run, a sample volume of 10 mL was used for each measurement and triplicate readings were taken each time. 200 mL glass beakers were used to hold the samples inside the bottle sampler. It was made sure that the sampling line is submerged within the sample and is not in contact with the sides of the beaker.

No dilution water was used for the clarifier effluent samples, thus unit dilution factor and zero background was specified. For concentrated samples (clarifier influent and RAS) dilution was necessary. A process of trial and error was used to determine the appropriate dilution factor for these samples. After the first few runs the cumulative particle number concentration for each sample was checked against the maximum allowable number concentration. Thus, the required dilution factor was determined to be 55 for clarifier influent and RAS samples and distilled DI water was used for dilution. For each dilution, 162 mL of distilled DI water was first measured using a graduated cylinder and poured into the 200 mL glass beaker. The sample container was then vigorously shaken to re-suspend any deposited solids and to breakup unwanted flocs. Using a pipette, 3 mL sample was transferred to the glass beaker by submerging the pipette tip in the dilution water and releasing sample slowly. The beaker was then transferred to the sampler and using the built-in magnetic stirrer the sample was mixed with the dilution water. Measurements were made immediately after mixing. For these runs, distilled DI water was counted for particles to save background data and background subtraction was enabled from within the particle counter.

Interferences in particle size distribution measurements may be caused by sample cross-contamination, presence of gas bubbles, and electronic noise. As the instrument was new and recently calibrated it did not generate any noticeable electronic noise. To prevent sample cross-contamination, the sampler and sampling lines were cleaned using a 30% bleach solution in water, before each run and in between runs. Following the cleaning solution, the instrument was rinsed each time with distilled DI water and the upcoming sample in sequence. The sample was mixed constantly using the built-in

magnetic stirrer to avoid deposition of solids within the beaker. Also it was made sure that no gas bubbles are present within the sample and in the sampling line. Particle contamination from the air was avoided by minimizing time between taking the samples out of the containers and analyzing them. For each sample, multiple replicates were performed and the first results were always discarded. When the particle counter gave steady readings, triplicate measurements were done for each sample.

Using the flow control valve and the pressure regulator, the sample flow rate was maintained at the standard calibrated value of 20 mL/min for all the measurements. This means that for a sample volume of 10 mL approximately 30 sec time was allotted for each run. Readings at a flow rate grossly deviating from the standard calibrated value were discarded. Measurements were taken as per section 2560C of Standard Methods (American Public Health Association, 1999).

3.3. Results & Discussion

3.3.1. TS and TSS for Clarifier Influent and RAS

The TS results for clarifier influent, effluent and RAS are shown in Table 3.1 along with the TSS and Turbidity results. From the numbers it is evident that the influent TS data for fall and winter are close to each other but the fall RAS had much lower TS than the winter RAS. This indicates that although similar amount of solids were introduced into the clarifier at these two times, in winter there was a greater amount of solids present in the settled activated sludge as compared to fall. This can be explained by the comparison of TDS data for the influent as shown in Figure 3.7. As for the spring measurements both the influent and the RAS samples had much higher TS as compared

to the other two measurements. This can easily be explained by the rainfall event preceding the spring sampling. Thus the results confirm the introduction of large amount of solids into the clarifier during spring runoff.

From the TSS data presented in Table 3.1, it is evident that both the RAS and influent TSS show a gradually increasing trend from fall to winter and spring as shown in Figure 3.6. Although the influent TS had comparable values in fall and winter, the TSS values were larger in winter than in fall. This is explained in later paragraphs with Figure 3.7. Raw data for these analyses are presented within Appendices A-1 to A-6.

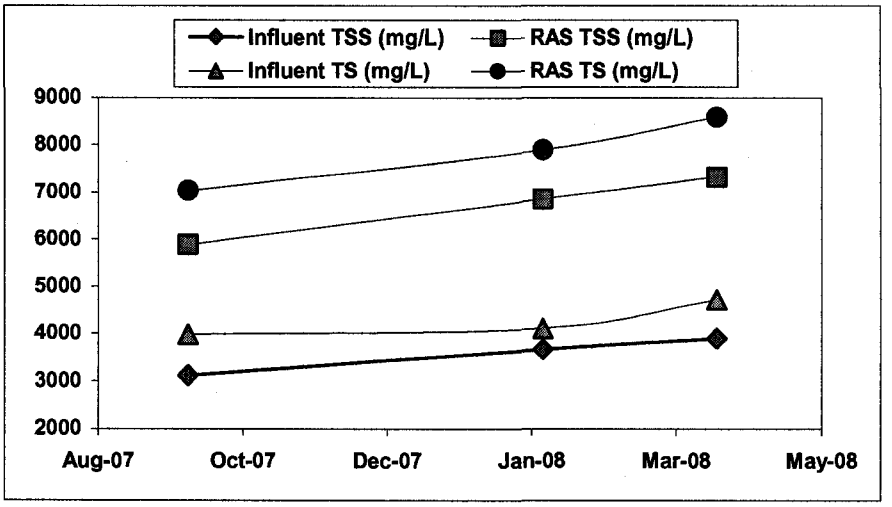

Figure 3.6: TS and TSS results for Clarifier Influent and RAS

Figure 3.6 shows the seasonal comparison of the TS and TSS results for clarifier influent and RAS. From the figure, it can be seen that the seasonal TS and TSS curves are almost parallel to each other for RAS samples, whereas some difference exists in case of the influent curves. Thus, seasonal effect is almost negligible on the fraction of suspended solids for RAS samples while for influent sludge, the fraction of suspended solids is higher in winter than in the other two seasons.

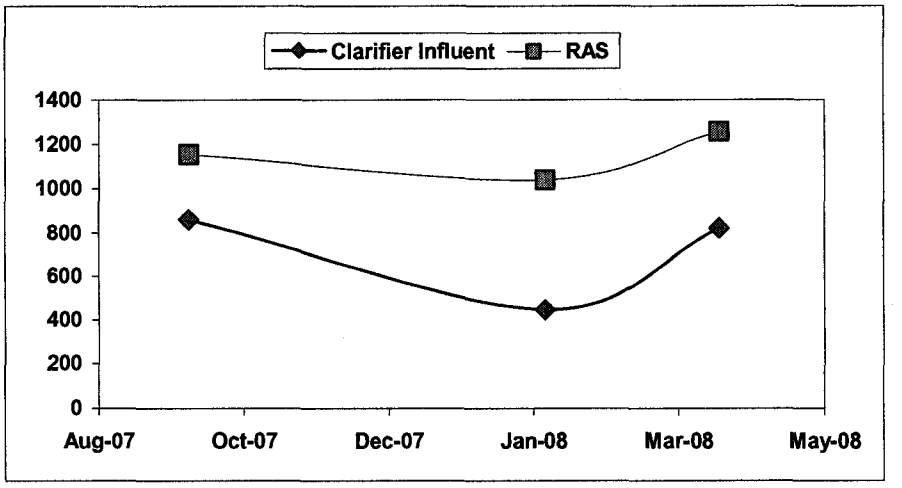

Figure 3.7: Total Dissolved Solids (mg/L) Results for Clarifier Influent and RAS

Figure 3.7 shows the TDS results for clarifier influent and RAS. The TDS values were obtained by subtracting TSS from TS. For both the influent and RAS, the lowest TDS occurred in case of winter samples while the values were comparable for the other two seasons. This is due to the low water solubility of most types of solids at lower temperatures. The collected samples had a temperature of 7°C in winter while the temperature was 15°C for fall samples and 19°C for spring samples. This low amount of dissolved solids or high amount of suspended solids in the clarifier influent provided the opportunity of greater amount of solids settling in winter, which in turn resulted in the high TS value of the winter RAS samples, as discussed in previous paragraphs.

Table 3.1: TS, TSS and Turbidity Data for Clarifier Influent, Effluent and RAS

	Clarifier Influent		RAS		Clarifier Effluent	
Month	Avg. TSS (mg/L)	Avg. TS (mg/L)	Avg. TSS (mg/L)	Avg. TS (mg/L)	Avg. TSS (mg/L)	Avg. Tub. (NTU)
Oct-07	3115.50	3976.00	5880.50	7034.00	16.00	4.20
Feb-08	3658.00	4104.00	6858.00	7896.00	18.00	3.60
Apr-08	3890.00	4710.00	7327.27	8584.00	21.60	6.20

3.3.2. TSS and Turbidity for Clarifier Effluent

Table 3.1 includes the TSS and turbidity results for clarifier effluent. These results are shown graphically in Figure 3.8. Raw data are presented in Appendices A-1, 2, 3 & 7.

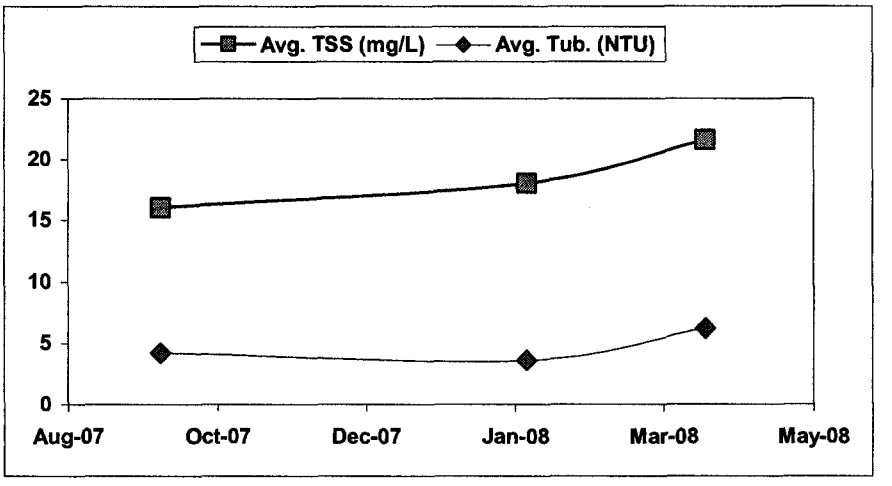

Figure 3.8: TSS and Turbidity results for Clarifier Effluent

Figure 3.8 shows the TSS and turbidity results for clarifier effluent. From the numbers given in the preceding table and the above figure, it is evident that the TSS and turbidity exhibited somewhat similar seasonal trends. In case of TSS, the results show that the effluent had comparable values in fall and winter but the spring samples had higher suspended solids than the other seasons. This can easily be explained as to be caused by the spring runoff event. If the TSS of the effluent is compared to that of the clarifier influent a measure of clarifier performance can be established in terms of percentage suspended solids removal. As such, the percentage suspended solids removal for Clarifier #1 at Gold Bar WWTP was found out to be 99.49% in fall, 99.51% in winter and 99.44% in spring. Although the seasonal differences are quite small, the reason for lower removal in spring may be awarded to higher flows caused by the runoff event. Fall operation gave slightly higher suspended solids removal than spring but the highest

removal among the three was during the winter operation. This is unlikely because during the winter season poor clarifier operation is expected which can be explained by the higher viscosity of water at lower temperatures providing higher resistance towards settling of solids. An attempt is made to clarify this and explain the anomaly in the following chapter by means of batch settling tests.

In Canada, for municipalities with population greater than 20,000, the best practicable technology standard for effluent TSS from a tertiary WWTP is currently 20 mg/L. (Chinniah, 2006). Although the effluent from the clarifier is not the final effluent from the plant, the TSS value corresponding to the spring runoff was slightly higher than the best practicable standard. This may be because of the higher flow rates caused by the runoff. The higher flow rates reduce the effective HRT and increase the overflow rate of the tank, thereby leading to reduced performance. Also, the samples collected for these analyses were grab samples while the standards are monthly average values established on the basis composite samples. Although the plant continuously analyzes and records these data on a daily basis but the efforts to obtain the corresponding data from the plant were unsuccessful due to a complicated and lengthy course of action. Hence, it was not possible to compare the results presented within this report with the actual plant data as analyzed and recorded by the plant itself.

3.3.3. Particle Size Distribution

The particle size distributions for clarifier influent obtained from three different seasonal samples are shown in Table 3.2. In case of RAS, no seasonal variation in particle size distribution was considered for observation. Therefore, RAS samples were collected and analyzed only in April, 2008 representing plant operation during a spring runoff. The corresponding results are tabulated along with the influent data in Table 3.2. The eight size ranges specified for the analysis of clarifier influent and RAS was determined by taking a series of trial measurements with different arbitrarily specified bin sizes. The upper limit was set as 50 μm because the samples had extremely small number of particles beyond that size. The other bin sizes were allocated randomly. For each bin, an average particle size was designated by taking an average of the upper and lower limit of the corresponding size range. These average sizes are displayed along with corresponding bin sizes in Table 3.2. The average bin sizes were later used in calculating the average particle sizes of the seasonal samples.

As previously mentioned, a dilution factor of 55 was used in analyzing the clarifier influent and RAS samples, but the results tabulated within this report represent the original count as the particle counter automatically adjusts the results with the programmed dilution factor and background subtraction. Thus the results are also adjusted with background particle counts obtained from the dilution water. The results obtained from the influent analysis are shown graphically in Figure 3.9.

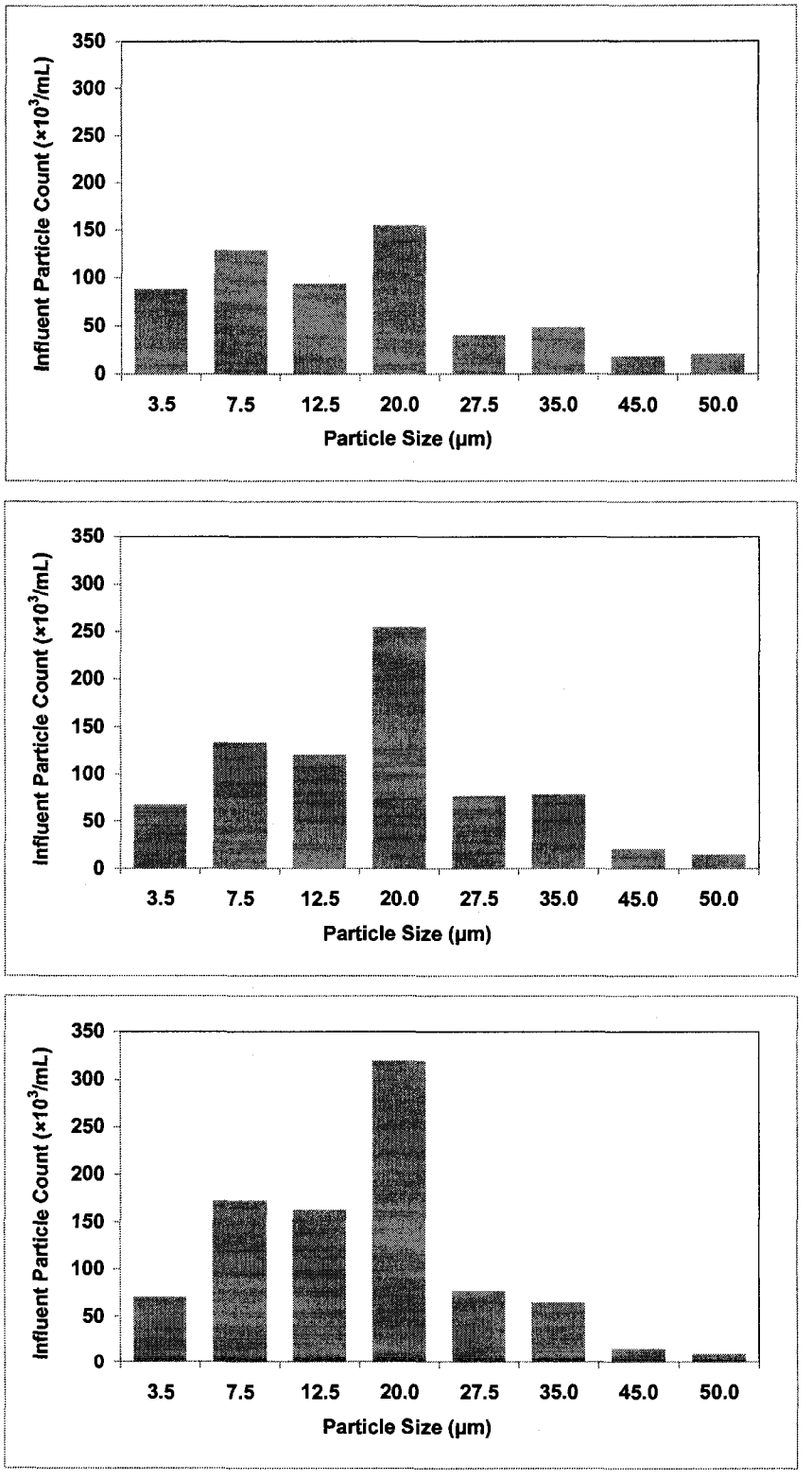

Figure 3.9: Particle Size Distribution for Clarifier Influent in a) October 2007 (top image), b) February 2008 (middle image) and c) April 2008 (bottom image)

Figure 3.9 shows the particle size distributions of the three seasonal samples of Clarifier Influent. Each plot was generated by taking an average over triplicate particle counting measurements. The raw data from the analyses is presented in Appendices A-8, 9 and 10. To make an effective comparison between the samples, the particle count scale (ordinate axis) on all of the plots was kept constant. The three seasonal samples had more or less similar particle size distributions providing a general idea about the influent to Clarifier #1. Most of the changes in between samples were observed within three bin sizes of 5-10, 10-15 and 15-25 μm. From the figure, it is evident that in October the samples had the lowest count within these bins while the count increased gradually in February followed by April. Samples within these size ranges had the highest count in April owing to the runoff event while the counts for the smaller bin sizes were lower in that month. Thus, it can be said that an increase in plant capacity caused by a runoff contributes mostly to the count of larger particles in terms of secondary clarifier influent.

Table 3.2: Particle Size Distribution for Clarifier Influent and RAS

Size range (μm)	Average Size (μm)	Differential Particle Count ($\times 10^3$/mL)			
		Oct-07	Feb-08	Apr-08	RAS
2-5	3.5	88.33	66.87	70.18	34.54
5-10	7.5	128.04	133.26	172.29	89.98
10-15	12.5	93.80	119.86	162.18	90.37
15-25	20.0	154.55	254.76	319.51	245.25
25-30	27.5	40.18	76.45	76.77	106.88
30-40	35.0	48.43	77.87	64.68	146.26
40-50	45.0	18.62	21.01	15.66	49.01
>50	50.0	21.08	14.77	10.00	32.73

Figure 3.10 shows the particle size distribution of the RAS sample collected in April, 2008. To compare the RAS distribution with the influent, the particle count scale was kept identical to the influent plots. The RAS distribution had higher counts than the influent in terms of larger particles while having lower counts for smaller particles. This is due to the formation of flocs during settling. The maximum count for the RAS sample was observed within the size range of 15-25 μm, just as the influent. Appendix A-13 contains the raw data.

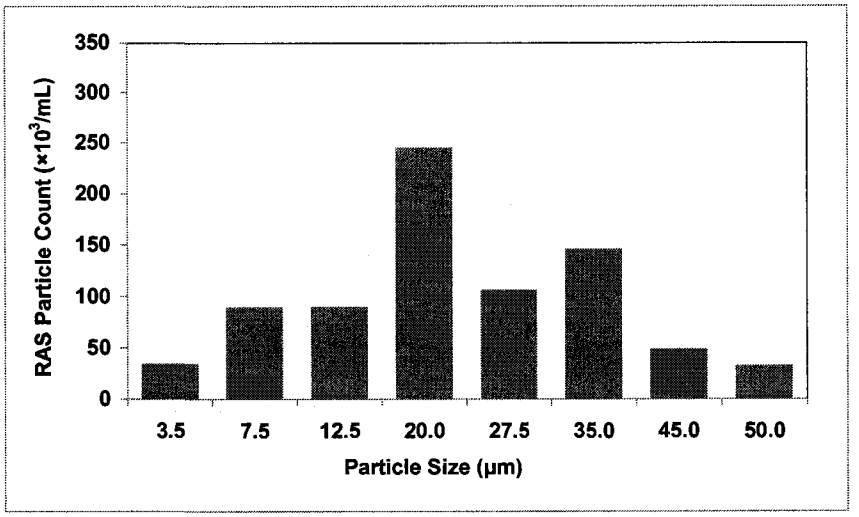

Figure 3.10: Particle Size Distribution for RAS

The seasonal particle size distributions for clarifier effluent are shown in Table 3.3. The size ranges specified for the analysis were determined by taking trial measurements with different arbitrarily specified bin sizes. The upper limit was set as 30 μm because the samples had negligible number of particles beyond that size. The other bin sizes were allocated randomly. For each bin, an average particle size was designated by taking an average of the upper and lower limit of the corresponding size range. The results obtained from the effluent analysis are shown graphically in Figure 3.11.

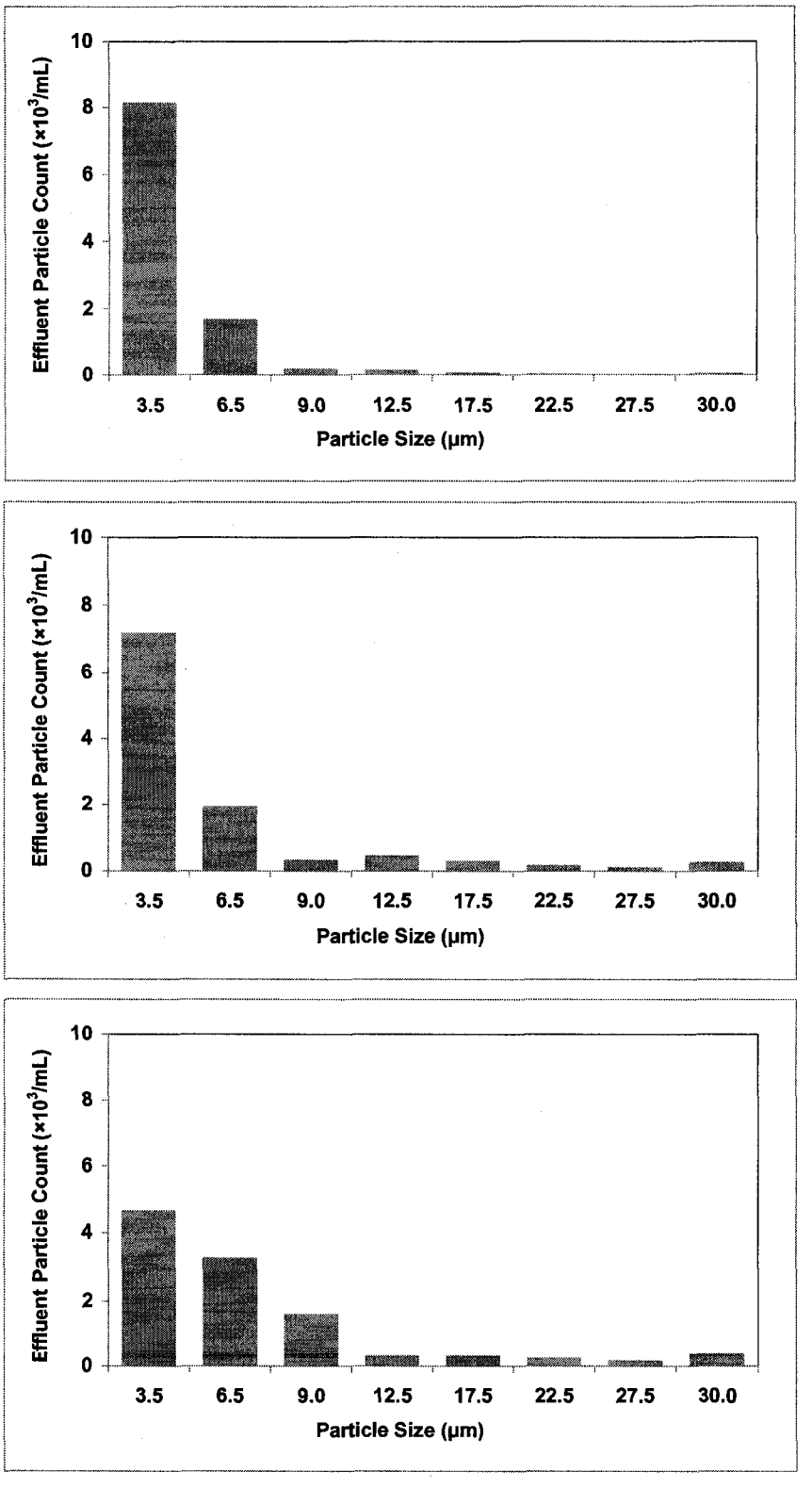

Figure 3.11: Particle Size Distribution for Clarifier Effluent in a) October 2007 (top image), b) February 2008 (middle image) and c) April 2008 (bottom image)

Figure 3.11 shows the particle size distributions of the three seasonal samples of clarifier effluent. Each plot was generated by taking an average over triplicate particle counting measurements. The raw data from the analyses is presented in Appendices A-11, 12 and 13. To make an effective comparison between the samples the particle count scale (ordinate axis) on all of the plots were kept identical. The three seasonal samples had more or less similar particle size distributions providing a general idea about the effluent from Clarifier #1. The lower size ranges had the prevailing counts for all of the samples while having very small counts of larger particles. In October, the smallest size range of 2-5 μm had the highest count while this count decreased gradually in February followed by April. The April samples had the smallest count within the 2-5 μm range, as compared to the other seasons, but there was a significant increase in count within the size ranges of 5-8 and 8-10 μm. This may be caused by the runoff event.

Table 3.3: Particle Size Distribution for Clarifier Effluent

Size range (μm)	Avg. Size (μm)	Differential Particle Count ($\times 10^3$/mL)		
		Oct-07	Feb-08	Apr-08
2-5	3.5	8.13	7.19	4.67
5-8	6.5	1.70	1.93	3.27
8-10	9.0	0.19	0.33	1.61
10-15	12.5	0.16	0.46	0.33
15-20	17.5	0.07	0.29	0.33
20-25	22.5	0.04	0.16	0.24
25-30	27.5	0.02	0.10	0.17
>30	30.0	0.05	0.25	0.39

As mentioned previously, the average bin sizes were used in calculating the average particle size for each seasonal sample. To calculate this, the average bin sizes were multiplied with the corresponding differential count and the sum of these values were then divided by the total count for each seasonal sample. The total particle count for a sample was determined by using the cumulative particle counts of the bin sizes. These numbers are presented with the raw data in the Appendices. The following table shows the average particle size for the seasonal samples along with the corresponding total particle count.

Table 3.4: Total Particle Count and Avg. Particle Size for Influent, Effluent and RAS

	Clarifier Influent		Clarifier Effluent		RAS	
Month	Total Particle Count ($\times 10^4$/mL)	Avg. Particle Size (μm)	Total Particle Count ($\times 10^3$/mL)	Avg. Particle Size (μm)	Total Particle Count ($\times 10^4$/mL)	Avg. Particle Size (μm)
Oct-07	59.30	17.24	10.36	4.56		
Feb-08	76.48	18.75	10.72	6.11		
Apr-08	89.13	17.43	11.02	7.62	79.50	23.56

The results documented in Table 3.4, are shown graphically in Figure 3.12. From the numbers, it is evident that the RAS sample collected in April had a lower total count than the corresponding influent sample. This is most unlikely, as the solids content of the RAS is much higher than the influent, as shown earlier with the TS and TSS analyses. This discrepancy might be due to the deterioration of the sample before analysis or it might have been caused by poor dilution rendering the sample concentration higher than the maximum allowable number concentration of the instrument.

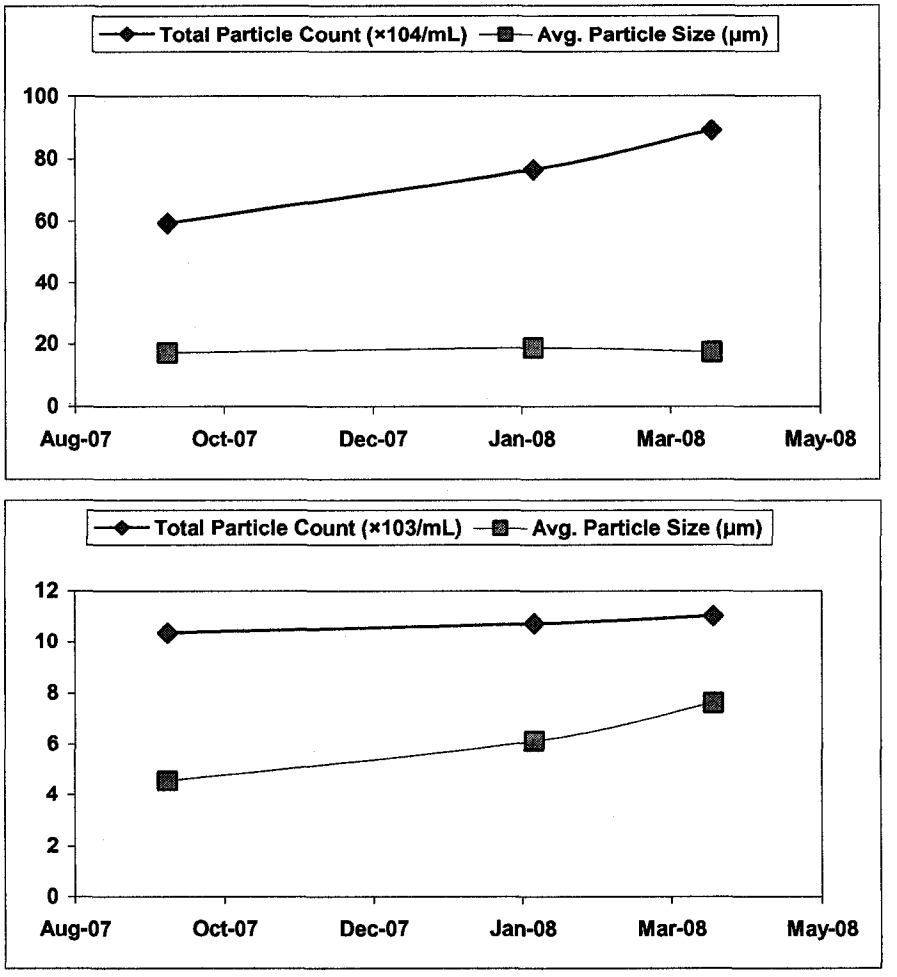

Figure 3.12: Total Count and Avg. Particle Size for Clarifier a) Influent (top image) and b) Effluent (bottom image)

Figure 3.12 shows the total particle count and avg. particle size for the clarifier influent and effluent seasonal samples. From the figure, it is evident that the total particle count increased from October to February followed by April for both the influent and effluent samples. The increase was sharper in terms of influent samples. In case of average particle size, the effluent sample in April had a higher average size, probably owing to the runoff, as compared to the other two months. The influent samples had similar average sizes throughout the three seasons. These results closely match the TSS analyses presented within this chapter and are comparable to Figures 3.6 and 3.8.

4.0. Study of Settling Characteristics

Sedimentation or gravity settling is the main objective of a final clarifier in an advanced wastewater treatment plant. The clarifier unit is designed to obtain concentrated sludge, activated with microbial population, by means of settling and to return this sludge to the preceding biological nutrient removal system. Due to the complex nature of the treatment techniques, the settling operation within the clarifier also becomes very complex, depending on a lot of factors. In order to effectively design a pilot-scale model of the selected unit, the suspension properties and corresponding settling characteristics of the original unit needs to be identified. This was done to make sure that the proper variables are taken into account at the time of design. This chapter deals with the study of the settling characteristics occurring within Clarifier #1 at Gold Bar WWTP and it discusses the corresponding results obtained.

4.1. Sample Collection

Three types of tests were performed to understand the settling behavior within the chosen unit. The first test was to determine the Sludge Volume Index (SVI) of the influent sludge. This analysis was done with the intention of observing seasonal effect on the SVI of the incoming sludge. Thus, collection of samples was carried out in three seasonal batches along with the samples collected for the TS, TSS and turbidity analyses, as discussed in the previous chapter. The next test was a Type II settling column test and it was done in the month of February, 2008, while the final tests were a series of batch settling tests performed in April, 2008.

As mentioned in the preceding chapter, all the samples were collected as grab samples from the sampling rack of Final Clarifier #1 at Gold Bar WWTP (Figure 3.1). The SVI analyses and the Type II settling column test were done on site (right next to the sampling rack) therefore the time between sampling and analysis was zero. The Type II settling column (Figure 4.1) was connected with the sampling line using rubber tubing and clamps. The sampling line was connected to the bottom of the column and the column was filled using the pressurized flow from the sample port. For each run, approximately 42.6 L of sample was used and after the test, the sludge was disposed through a nearby drain. In case of the batch settling tests, they were performed in temperature controlled rooms at the University. So, influent sludge samples were collected and transported from Gold Bar to the University. Four 20 L plastic containers were used for sample transportation, providing a total sample volume of around 80 L. In all cases, before collecting the samples, the sampling line was flushed for at least one minute to clear away any residuals and contaminants.

4.2. Analytical Procedures

4.2.1. Sludge Volume Index

The sludge volume index is a property that indicates the settle-ability of sludge in the final clarifier. It is defined as the volume in milliliters occupied by 1 g of a suspension after 30 minutes of settling. This parameter is typically used to monitor the settling characteristics of activated sludge and other biological suspensions. SVI has been proven to be useful in routine monitoring and control of biological processes by means of experience. The SVI is sometimes used for activated sludge plant control in determining

the RAS flow rate and frequency and volume of sludge wasting. To find out the SVI, the suspended solids concentration or TSS of a well-mixed sample of the suspension is determined along with the 30-min settled sludge volume. A dilute sludge sample cannot be analyzed using this method, because of the small volume of settled material.

The TSS of the clarifier influent samples, representing three different times of the year, were determined as discussed in the previous chapter. During the sampling operation, the 30-min settled sludge volume of each corresponding sample was also determined on site. A 1 L graduated glass cylinder was used for the purpose. The cylinder was graduated in mL with graduation interval of 50 to 1000 mL in 10mL subdivisions. The volumetric tolerance was ±5 mL and the approximate height of the cylinder from the base to the 1000 mL mark was measured with a measuring tape to be 46 cm. The approximate radius (r) of the cylinder was then calculated to be 2.631 cm using the volume and the height of the cylinder. All the volumetric readings (V) from the experiment were converted to sludge interface height as, $h=10\times V/\pi r^2$ in mm.

For each run, after flushing the sampling line for at least one minute, sample was collected into a 1 L Nalgene® bottle. The temperature of the sludge in the bottle was recorded using an alcohol thermometer. The bottle was then capped and shaken briskly before transferring the sludge carefully into the cylinder. It was made sure that the cylinder does not get overfilled past the 1000 mL mark. This was done in a quick manner to ensure that the sludge does nott settle before finishing the transfer. The timer or stopwatch was started at the moment when the transfer of the suspension was finished. The suspension was then allowed to settle for 45 minutes under quiescent condition.

Volume occupied by the settled suspension was recorded at measured time intervals of 5, 10, 15, 20, 30 and 45 minutes. When the experiment was finished, the final temperature of the sludge was recorded again to account for any temperature change during the experiment. No notable change in temperature was detected in any of the three cases.

The settled sludge volume of the suspension for each indicated time interval was recorded in mL/L, as a fraction of the original volume of the suspension. The sludge interface height for each corresponding settled sludge volume was calculated using the method discussed above. Finally, the SVI was calculated as per section 2710D of Standard Methods (American Public Health Association, 1999):

SVI (mL/g) = [30-min Settled Sludge Vol. (mL/L) / sample TSS (mg/L)] × 1000 (4.1)

Interferences may be caused by variations in suspension temperature, sampling and agitation methods, dimensions of settling column, and time between sampling and analysis. Quality assurance measures were taken during TSS analysis as discussed in the preceding chapter. In addition, on site testing was done to eliminate the time between sampling and analysis and to maintain the original sludge temperature. Also, the same glass cylinder and similar sampling and agitation methods were employed for all the analyses in order to ensure quality of the results. The results are presented and discussed in section 4.3.1 of this chapter and raw data from the experiment is tabulated in Appendix B-4.

4.2.2. Type II Settling Test

Among the four types of settling, discussed in chapter 2 of this report, the Type II or flocculent settling is investigated by this test. In case of flocculent settling, the particles tend to form flocs and settle by gravity thereafter. Larger flocculated particles settle more quickly and the depth of the tank allows room for particles to flocculate. Because of the floc formation, removal of particles by means of settling becomes a function of depth as well as the overflow rate (American Water Works Association, 1999). Velocity gradients within the system and particle concentration and size range also affect the extent of clarification. The results from a Type II settling test conducted on a flocculent suspension are used to design a full-scale basin intended for the settling of that particular suspension.

The test is conducted by filling a Type II settling column with a flocculent suspension which is thoroughly mixed prior to the start of the experiment. Ideally, the column depth should be at least as great as that of the basin being designed with sample ports installed at uniform depth intervals. Mixing is stopped and samples are withdrawn from the sample ports at predetermined time intervals. The samples are then analyzed for TSS and results are reported against the corresponding depth and time. The percent removal, as compared to the TSS of the original suspension, is computed for each sample and is plotted on a chart of depth vs. time. Lines of equal percent removal (iso-removal lines) are drawn on the chart by means of interpolation. This chart is then used for the full-scale design by using the targeted percent removal. For a full-scale design, the overflow rate, obtained from this test, is usually multiplied by a factor of 0.65, while the hydraulic retention time is multiplied by a factor of 1.5 to 2.0. This is done to account for non-idealities in a continuous flow system (American Water Works Association, 1999).

The purpose of conducting a Type II settling test for this research was to investigate the extent of flocculent settling within Clarifier #1 at Gold Bar WWTP. Although the sludge entering the clarifier had very high TSS, the possibility of flocculent settling was investigated, because biological suspensions are usually flocculent in nature. The settling column used in this experiment was made of transparent plastic and had five sample ports placed at equal depth intervals. A surface line was marked near the top of the column to indicate how much of the column needed to be filled. The distance from the column base to the top surface mark was 2.4 m. The first port was 0.4 m below the surface mark and the fifth port was 0.4 m above the column base with subsequent ports placed at equal intervals of 0.4 m. The approximate diameter of the column was 150 mm and the approximate volume of sample held by the column (up to the top surface mark) was 42.6 L. Figure 4.1 shows a schematic of the Type II settling column used in this experiment.

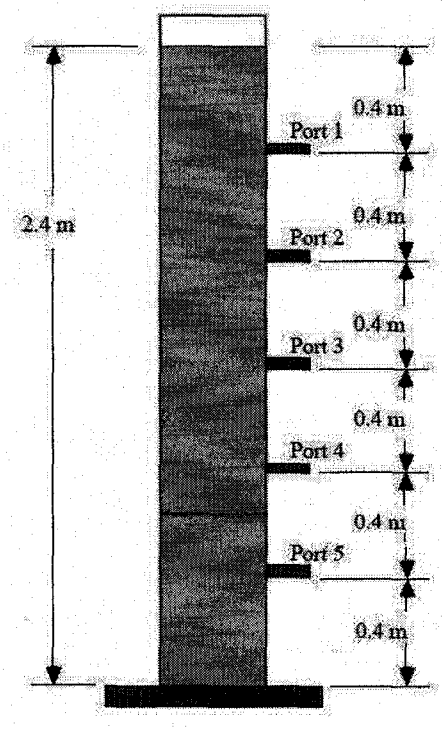

Figure 4.1: Schematic of the Type II Settling Column

As mentioned before, the experiment was conducted on site and the column was filled from bottom using rubber tubing connected to the Clarifier #1 sampling port. Before filling the column, initial sample was collected from the port in a 500 mL Nalgene® bottle. This sample served to indicate the sludge TSS at the beginning of the experiment. The pressurized flow from the sampling port was used to provide mixing throughout the column and to keep particles in suspension prior to the start of the experiment. Once the suspension reached the top surface mark, the sampling port was closed and the timer was started immediately, allowing the suspension to settle within the column. Samples were withdrawn from each sample port into 200 mL Nalgene® bottles at predetermined time intervals of 5, 10, 15, 20, 30 and 45 minutes. Due to the height of the column a step ladder was used to collect samples from the higher ports. Temperature of the sludge was recorded from time to time, using an alcohol thermometer, to account for the changes in temperature over the duration of the experiment. At the end of the experiment, a sample was collected from the drain line to determine TSS of the settled sludge. After the experiment was over, the remaining sludge was discarded through a nearby drain.

This method was employed for testing both the influent and effluent of Clarifier #1. The effluent testing was done in order to investigate the settling within the supernatant zone of the clarifier. Before conducting the test on the effluent, the whole column was rinsed once with effluent sample by filling it up and draining it. Also, during the experiment, the effluent samples were collected in 500 mL Nalgene® bottles in place of the 200 mL bottles. The collected sample bottles were tightly capped and placed into a cooler filled with ice packs, in order to maintain the quality of the samples. The samples

were then transported to the University for the analysis of suspended solids. The analytical procedure employed for determining the TSS of the samples is discussed in the preceding chapter. Quality control measures were employed during both the experiment and the analysis. The results of this experiment are presented and discussed in section 4.3.2 of this chapter and raw data from the experiment is tabulated in Appendix B-1.

4.2.3. Batch Settling Tests

Suspensions with high concentrations of suspended solids, settle in the zone settling regime followed by the compression regime. The zone settling regime, occurring under quiescent conditions, is characterized by the formation of a distinct interface between the supernatant liquor and the settled sludge zone. In case of batch settling test, several concentrations of the original sludge are prepared and are allowed to settle, under quiescent conditions, in individual columns. The height of the distinct settled sludge interface is reported against time for each batch. The interface height is plotted against time and the ZSV is calculated as the slope of the straight line through data points, ignoring initial shoulder and compression shoulder. The solids flux for each concentration is calculated by multiplying the sample concentration with the corresponding ZSV. This data is used in the design, operation, and evaluation of settling basins and gravity thickeners. Details about the different settling regime, the solids flux theory and the batch settling tests are discussed in Chapter 2 of this report. This section explains the methodology and analytical procedures employed in performing the batch settling column tests using the influent sludge of Clarifier #1 at Gold Bar WWTP.

As previously mentioned, three batch settling tests were performed in temperature controlled rooms in order to observe the seasonal effect on the ZSV of clarifier influent sludge. The first experiment was performed at around 4°C representing sludge settling in Winter, the second test was done at around 15°C representing sludge settling in Fall or Spring and the last experiment was carried out at around 27°C to investigate sludge settling in Summer. For each of these experiments, six different sludge concentrations were used with corresponding 4 L settling columns. The concentrations were prepared manually and hence were not identical among the individual experiments. The initial concentrations were determined later, by laboratory analysis.

For each experiment, one batch of original sludge was used as control. As mentioned earlier, a total of 80 L clarifier influent in four containers was transported from Gold Bar to the University. To prepare a dilution, first a sludge container was vigorously shaken to resuspend any settled matter and then predetermined volume of the well-mixed sludge sample was poured into a 2 L graduated cylinder. The known volume of sludge was then transferred into a graduated 4.5 L Nalgene® beaker. Estimated volume of tap water was added into the beaker, using a graduated cylinder, to make the final volume 4100 mL. Using a wooden spatula, the whole suspension was stirred vigorously within the beaker and the suspension was then transferred into the settling column until it reaches the 4 L mark. The remaining 100 mL of sample was transferred from the beaker into a sampling bottle for TS and TSS analysis that would indicate the initial solids concentration for the batch. In order to prepare other dilutions, the same method was employed except for varying the volumes of sludge and tap water added to the beaker.

To prepare a concentrated sludge sample, well-mixed sludge from a well shaken container was first poured into two graduated 4.5 L Nalgene® beakers. The beakers were then left untouched for 15 minutes and the sludge was allowed to settle under quiescent condition. After that time, predetermined volume of clear supernatant was transferred from the beakers into a 2 L graduated cylinder and then was disposed. This was done very carefully so as not to disturb the settled sludge layer. The settled sludge from one beaker was then transferred into the other to make the final volume 4100 mL. The suspension was stirred vigorously within the beaker using a wooden spatula and it was then transferred into a settling column by filling the column up to the 4 L mark. The remaining 100 mL of sample was transferred into a sampling bottle for initial TS and TSS analysis. To prepare other concentrations of thicker sludge, the same method was employed except for varying the volumes of supernatant disposed from the beakers.

The concentrations for each test were prepared in the corresponding temperature control room prior to the experiment and it was made sure that the sludge temperature matched with the room temperature before the settling was started. Settling trials were conducted using custom made columns with 4 L capacity equipped with 1 rpm stirrers. Each column was made of transparent plastic and had an inner diameter of approximately 101 mm. The columns were graduated on the outside in both length scale and volumetric fraction. In length scale, the columns were graduated in mm with graduation interval of 0 to 500 mm (from 4 L mark to column base) in 5 mm subdivisions. This graduation was in place to facilitate the measurement and recording of sludge interface height. For each column, a stirring mechanism, consisting of a rectangular closed loop thin rod extending the length of the column and positioned within two rod diameters of the cylinder wall,

was provided. The stirring rod was powered by a 1 rpm electrical stirrer and the mechanism was supported by a frame that was fitted to the wide base of the column by means of three vertical poles. Figure 4.2 shows a schematic of the apparatus used.

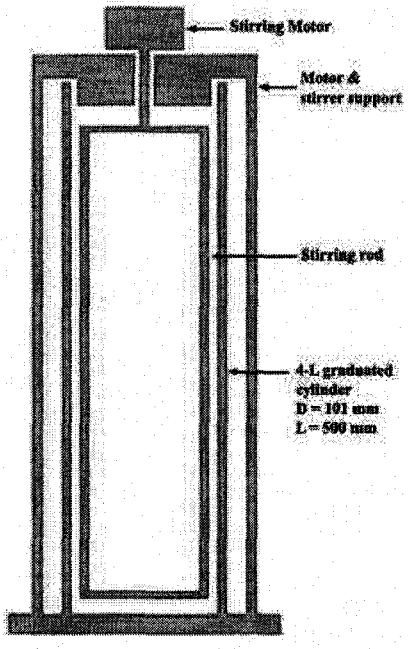

Figure 4.2: Schematic of the 4 L Batch Settling Column

After preparing the concentrations, contents were transferred into the appropriate settling column as quickly as possible to minimize pre-transfer settling. When the transfer was complete, the stirring mechanism was mounted quickly and the timer was started. Three of these columns were put into operation at a time and to facilitate recording, a fixed time interval was allowed between filling columns. The initial sludge interface height was recorded at time zero and subsequent readings were taken for two hours. For the first 30 minutes, readings were taken every 5 minutes and as the settling velocity decreased, the frequency was reduced to every 10 minutes. After the two hour settling period was over, supernatant sample was drawn off from each column using a plastic

syringe coupled with a thin rubber tube. These samples were collected before removing the column stirring mechanisms, to be analyzed for TSS and turbidity. For thicker sludge samples, very small volume of supernatant was available, so less volume was used to measure TSS with reduced accuracy. After collection was done, the remaining supernatant was removed and discarded from each column, being careful not to disturb the settled sludge. Finally, the entire volume of the settled sludge from each column was transferred into a large beaker and gentle stirring was provided with a wooden spatula to achieve a homogenous blend. The available settled sludge for each concentration was then collected and stored in a number of 500 L Nalgene® bottles to be analyzed for TS. All samples were stored in a refrigerator at 4°C until they were analyzed. Room temperature and temperature of the sludge were measured from time to time, using an alcohol thermometer, to account for the changes in temperature over the duration of the experiment. The analytical procedure employed for determining the TS and TSS of the samples is discussed in the preceding chapter.

The results of this experiment may be affected by the suspended solids concentration, suspension characteristics, dimensions of settling column used and analytical errors. Usually, it is recommended to use longer columns with wider diameter in order to investigate the settling rate. But the method employed in this experiment is acceptable because columns with exactly the same dimensions were used for all the batches, which facilitates the comparison of the results obtained. Quality control measures were employed during both the experiment and the analysis. The results of this experiment are presented and discussed in section 4.3.3 of this chapter and raw data from the experiment is tabulated in Appendices B-5, 6 and 7.

4.3. Results & Discussion

4.3.1. Sludge Volume Index

The seasonal SVI results for clarifier influent are shown in Table 4.1 along with the 30-min settled sludge volumes and the Mixed Liquor Suspended Solids (MLSS) concentration. The settled sludge volume was divided by the TSS data to obtain an SVI of 140 mL/g for the October sample, 144 mL/g for the February sample and 113 mL/g for the April sample. This means that 1 g of the October sample occupies a volume of 140 mL while the sludge from the same amount of February sample occupies a volume of 144 mL and that of April sample occupies a volume of 113 mL, after 30 minutes of settling.

Table 4.1: Sludge Volume Index (SVI) Data for Clarifier Influent

Date	Sludge Temp. (°C)	MLSS Conc. (mg/L)	Settled Sludge Volume @ 30 min (mL/L)	SVI (mL/g)
October 16, 2007	15	3116	435	140
February 28, 2008	7	3658	525	144
April 28, 2008	19	3890	440	113

The MLSS concentration increased from fall to winter followed by spring. But the 30-min settled sludge volume and the SVI was lowest for the spring sludge. This indicates that the suspended solids in the spring sample settled faster as compared to the other two samples and per unit mass of the settled sludge occupied lesser volume. The highest settled sludge volume and SVI value was produced by the influent sample collected in winter. This indicates that the suspended solids in the winter sludge sample settled slower than the other two. Although the settled sludge volume for the winter sample was the highest but owing to its larger MLSS, both the fall and winter samples

produced SVI results close to each other. The slower settling in winter and the faster settling in spring can be explained by the corresponding temperatures of the two samples. The spring sludge had the highest temperature among the three while the winter sludge had the lowest temperature. At lower temperatures, the viscosity of the water increases providing higher resistance towards settling of suspended solids. This phenomenon is again displayed in the sludge interface height vs. time plot shown in Figure 4.3.

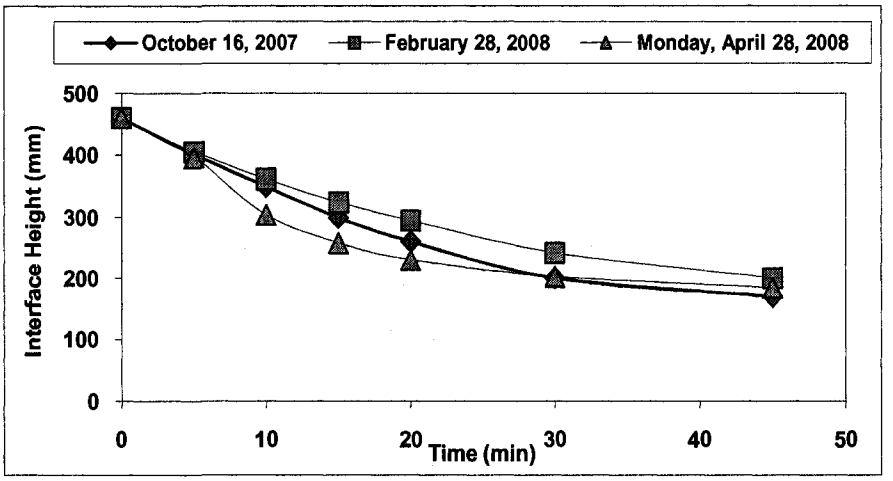

Figure 4.3: Sludge Interface Height vs. Time for SVI Measurements

As mentioned earlier, all the volumetric readings, taken during the course of the SVI analyses, were converted into interface height of the settled sludge, using the dimensions of the graduated cylinder. The interface height readings in mm were then plotted against time as shown in Figure 4.3. The three curves shown within this figure represent the settling behavior of the corresponding sludge samples under the same experimental conditions. As can be seen from the figure, all three of the sludge samples settled at a similar rate for the first five minutes of the experiment. Thereafter the settling of the spring sample took place at an accelerated rate, as compared to the other two samples, until it reached a flat region. This region is representative of settling governed by Type

IV or compression regime. The lowest settling rate was observed in case of the winter sample. The curves are consistent with the SVI results obtained from the experiment. In all cases, the curves start to flatten out after about 30 minutes of settling. For the April curve, a shoulder can be observed during the first five minutes of settling. This may be caused by flocculation or by unintended agitation induced within the sample, deterring the settling. The results obtained from the SVI analysis and the interface height vs. time plot given within this section are not totally representative of the true settling within the original tank. This is because the dimensions of the graduated cylinder used for this experiment are extremely small as compared to the dimensions of the clarifier. In order to truly represent the settling phenomenon within the clarifier, a deeper and wider settling column is necessary. But still the analysis is useful as a means to evaluate the seasonal effect on the settling. Thus, in order to facilitate an effective comparison, the same apparatus and experimental conditions were employed for all thee samples.

4.3.2. Type II Settling Test

Although the suspended solids concentration of the clarifier influent was very high (close to 4000 mg/L), a Type II settling test was conducted on the influent to observe the effect of flocculent settling. This was done in view of the highly flocculent nature of the biological suspension entering the clarifier. As expected, no results could be obtained from the test, indicating negligible flocculent settling occurring within the sludge zone of the clarifier. From the test data, a sludge interface vs. time plot was generated (not shown in this report) which resembled the plots shown in Figure 4.3. The settling rate, as observed from the figure, represents the governance of Type III (zone/hindered) and

Type IV (compression) settling regime. For such suspensions, after a period of settling, the curve reaches a flat region, with gradually decreasing settling rate, representing the transition from zone into compression regime. But for flocculent regime, the settling rate increases with the formation of floc and particle growth. From this test, it was confirmed that zone and compression settling regime governs within the lower part of settling zone and sludge zone of the clarifier. This indicates that the sludge zone within the clarifier acts as a gravity thickener.

Although the suspended solids concentration in the effluent was very low (close to 18 mg/L), a Type II settling test was conducted on clarifier effluent in view of the absence of large particles in the effluent and the highly flocculent nature of the clarifier suspension. During the experiment, time and depth representative samples were collected for TSS analysis from the settling column. Percent suspended solids removal was determined for each sample, for corresponding depth and time. The obtained results are presented graphically in Figure 4.4. Raw data and calculated percent removals are reported in Appendix B-1.

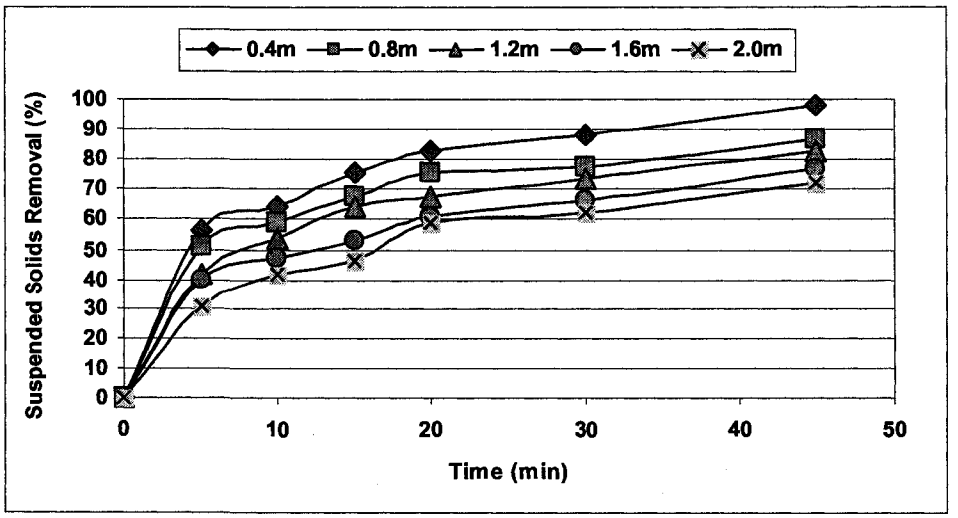

Figure 4.4: Rate of Suspended Solids Removal at Different Depth

Figure 4.4 shows the percent suspended solids removal from clarifier effluent at different settling time and depth. It is evident from the figure that all the curves followed similar traits but took place at different rates depending on the depth of sample collection. For a specific percentage removal, settling time increased with increasing depth. For a specific depth, the solids removal increased with time caused by gravity settling. The removal rate was faster at the very beginning of the experiment but slowed down gradually with time, possibly because of the absence of particles. In case of the test with clarifier influent it was observed that for a certain depth, the solids removal would be steady for some time and as soon as the settled sludge interface crossed that depth, there would be a spike in the removal followed again by a steady reading. This is explained by the theory of compression settling where all the solid particles in the suspension settle together at the same rate forming a distinct interface with the supernatant. This was not the case for the effluent, which proves the presence of flocculent settling.

As a next step of analysis, lines parallel to the abscissa were drawn, as shown in Figure 4.4, representing specific percent suspended solids removals. For each removal, the corresponding required settling time was determined from the plot and was noted accordingly. This data is reported in Appendix B-2. This data was then used to generate an iso-removal plot for clarifier effluent as shown in Figure 4.5. The iso-removal plot includes lines of equal suspended solids removal, providing information of required settling time at a certain depth.

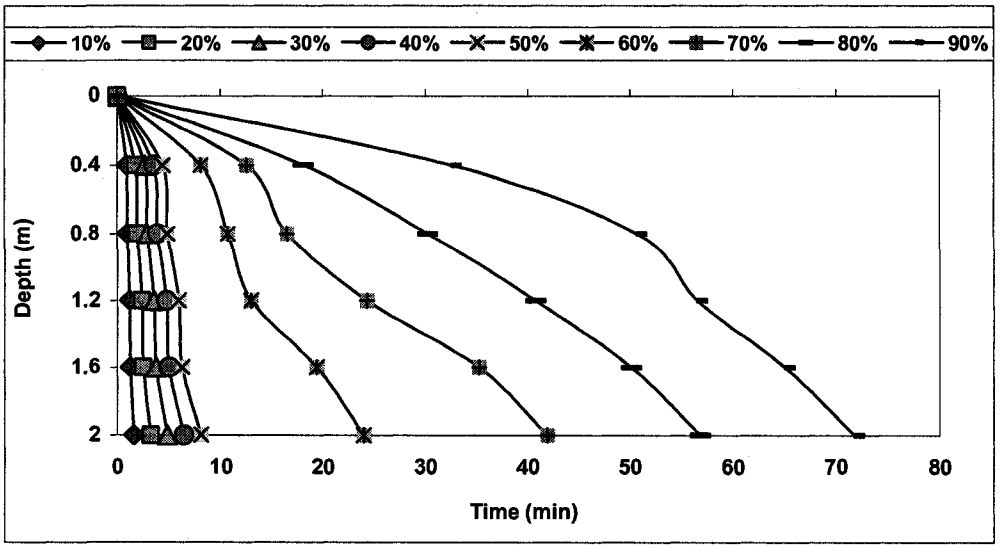

Figure 4.5: Iso-Removal Plot for Clarifier Effluent

Figure 4.5 clearly indicates flocculent settling of the effluent sample, as the iso-removal lines, within the figure, resemble the typical behavior of a flocculent sample. From the plot, it is evident that 50% suspended solids removal was achieved within the first ten minutes of the experiment. For solids removal beyond 50 %, the required settling time drastically increased. This is because the light unflocculated particles that stay in suspension require longer time to form flocs due to unavailability of solids. During the experiment, the solids removal at 0.8 and 1.2 m depth did not reach 90% and the removal did not reach 80% at 1.6 and 2 m depth. Data was extrapolated to obtain the higher removals at higher depth in order to construct the iso-removal plot. Although the plot represents solids removal at a maximum depth of 2 m and the original tank has an approximate depth of 4 m, the data is useful as the experiment was conducted to understand settling behavior in the supernatant zone of the clarifier. Also, in the original tank, the effluent is collected from the surface by means of weirs so the removal at smaller depth is of concern here.

For a specific suspended solids removal, each depth was divided by the corresponding settling time required. This produced the overflow rate corresponding to a specific solids removal at a specific depth. The calculated overflow rates for different iso-removal are tabulated in Appendix B-3 and the results are plotted in Figure 4.6.

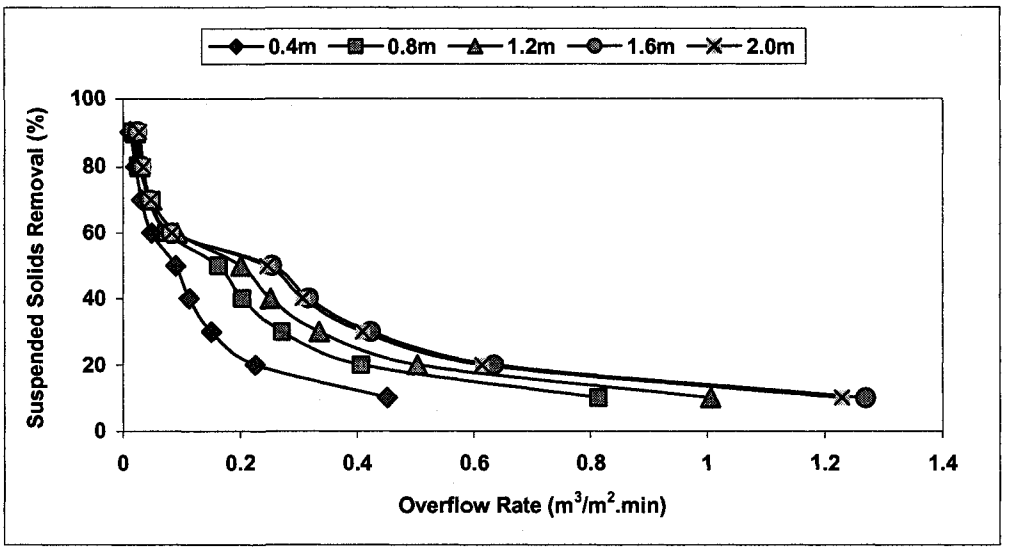

Figure 4.6: Solids Removal vs. Overflow Rate at Different Depth

From the figure, it is evident that the solids removal decreases with increasing overflow rate. For a particular percentage removal, larger depths can handle higher overflow rates and for a particular overflow rate, more removal is achieved at larger depths. This behavior is also distinctive of a flocculent suspension indicating the depth-dependent settling. Near the surface, small change in overflow rate affects the suspended solids removal noticeably while the effect is smaller with increasing depth. For all depths, a high percentage removal can only be achieved at very small overflow rates. At 0.4 m depth, 90% removal can be achieved if the overflow rate is 0.012 m^3/m^2.min or less while at 2m depth, the overflow rate should be 0.028 m^3/m^2.min or less to achieve the same removal. The overflow rate of a clarifier is obtained by dividing the volumetric flow rate

with the tank surface area. For Clarifier #1 at Gold Bar WWTP, the overflow rate is approximately 0.011 m^3/m^2.min based on an average flow of 30 ML/day and 0.018 m^3/m^2.min based on a high flow of 50 ML/day. This indicates that over 80% removal of the suspended solids can be achieved near the top water surface within the clarifier.

The Type II settling test results for the clarifier effluent, given within this section, represents the settling phenomena occurring within the upper part of the settling zone and the outlet zone of the clarifier. Thus by conducting this test, it was proven that flocculent settling is the governing settling regime within the supernatant region of the final clarifier. The results of this test can be used in estimating the solids removal by flocculation under different operating capacity of the clarifier.

4.3.3. Batch Settling Tests

From the Type II settling test, it was confirmed that the high suspended solids concentration in the clarifier influent was consistent with zone settling and compression settling. The batch settling tests were therefore conducted in order to find out the settling behavior of the clarifier influent sludge. As mentioned before, the tests were conducted in three different temperatures, each with six concentration batches, to observe the seasonal effects on settling. For each temperature, the prepared concentrations were designated as 1 to 6 in order of increasing suspended solids concentration, 1 being most dilute and 6 being most concentrated. After finishing the experiments, the recorded sludge interface depth was plotted against corresponding time for each individual experiment, as shown in Figure 4.7. An estimate of percent sludge volume reduction was also calculated for each

sample using the percent increase in sludge interface depth. Corresponding raw data and sludge volume reduction are tabulated in Appendices B-5, 6 and 7.

As can be seen from the figure, the influent sludge exhibited typical zone and compression settling behavior throughout the experiment at all the temperatures. At each temperature, for lower concentrations, the depth of the settled sludge interface increased rapidly providing a very high settling rate, right after the start of the experiment. The settling rate then decreased sharply, indicating the transition from zone to compression settling regime. With higher concentrations, the initial settling rate decreased and the change from zone to compression settling became less sharp. At the highest concentration, an initial shoulder is observed indicating a small period of re-flocculation.

The original sludge samples for the three experiments are represented by the sample numbers 5°C-5, 15°C-4 and 27°C-4. For the experiment at 5°C, in addition to the original sludge, four dilute and one concentrated samples were used. For each of the experiments conducted at 15°C and 27°C, three dilute and two concentrated samples were used in addition to the original sludge. For the 5°C experiment, the lower concentration samples exhibit the highest initial settling rate and the sharpest transition into compression. The original sludge sample shows somewhat similar settling behavior in all three of the experiments.

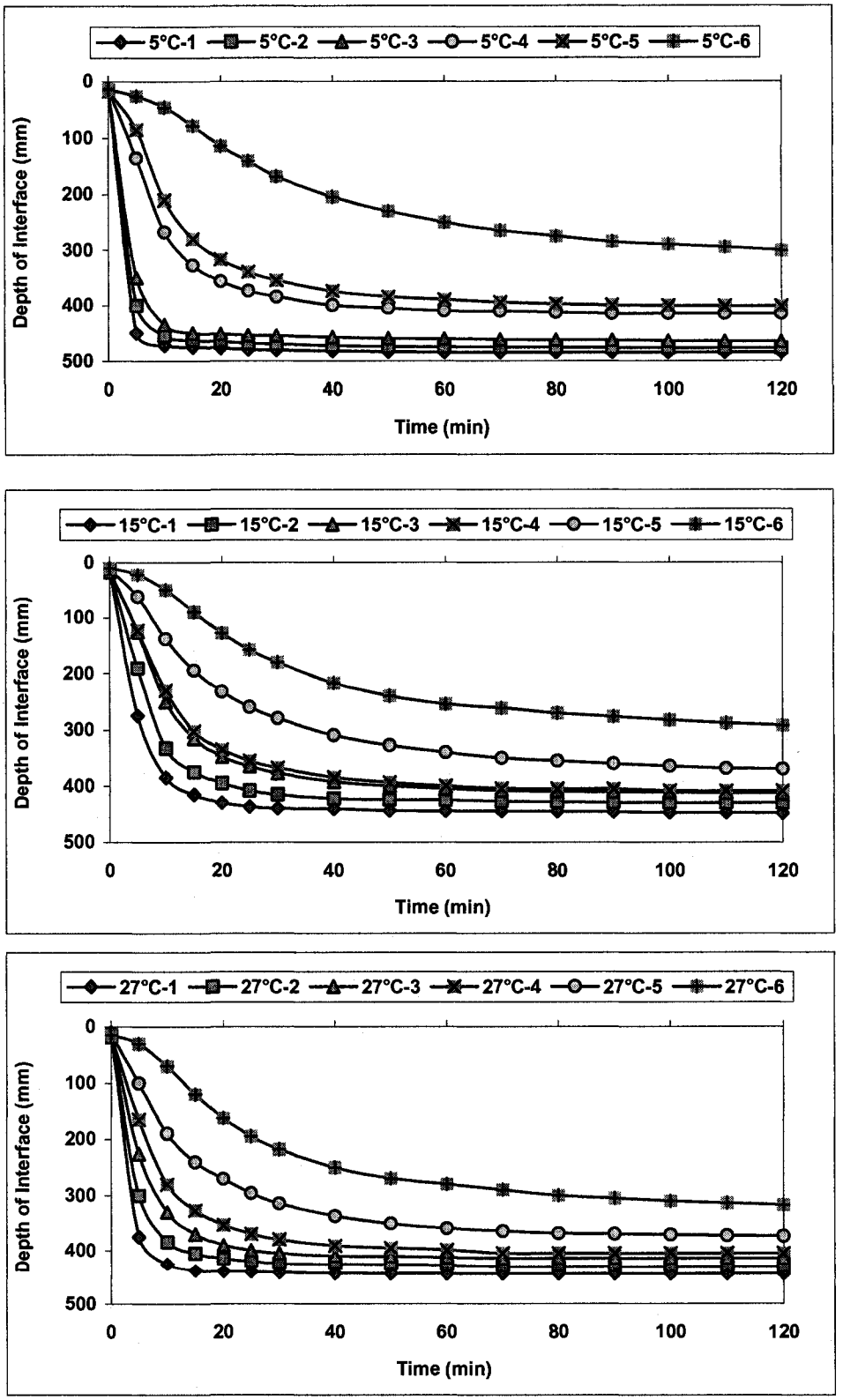

Figure 4.7: Interface vs. Time Plots for Clarifier Influent at a) 5°C (top image), b) 15°C (middle image) and c) 27°C (bottom image)

It must be mentioned here that during the course of the experiment a number of unexpected events occurred. In case of the 5°C experiment, everything went as planned and the data generated were reliable. But for the experiments conducted at higher temperatures, the sludge settling was poor because of the rising sludge phenomena. This problem, associated with the settling of biological suspensions, is discussed in Chapter 2 of this report. If a biological suspension in a biological nutrient removal system contains high levels of nitrate, then under favorable condition the bacteria present within the suspension starts the denitrification process releasing nitrogen gas into the atmosphere. The gas bubbles entrained within the sludge reduces its specific gravity and deters the settling. After sufficient exposure to the denitrifying process, some portions of the settled sludge may become too buoyant and start to break away from the settled mass, rising to the surface, which is referred to as rising sludge.

The rising sludge was encountered only at the higher temperature experiments while the 5°C experiment went smoothly. This indicates that warmer temperatures are favorable for the denitrifying bacteria. However, the extent of sludge rising was highest in case of the 15°C experiment, which indicates that too high temperature may slow down the denitrification. Also, visible effects of the sludge rising started after sufficient amount of time (close to 40 minutes) had been spent and settling had taken place up to a considerable extent. Before this time, there was no visible sign of the associated problem. For this reason, the sludge rising was not encountered during the SVI experiments. The sludge rising affected the settling rate of the samples, producing lower settling velocities and difficult to record data. Thus the data generated from the 15°C and 27°C experiments may not be as consistent as the 5°C experiment.

From the interface vs. time plots, the ZSV was determined for each sample at each temperature, using the slope of the initial linear settling period. The settling velocity was then multiplied by the corresponding suspended solids concentration of the sample to produce the solids flux. The solids flux represents the mass of solids passing through a unit area per unit time. The calculated zone settling velocity data in addition to the solids flux is tabulated in Appendix B-8. The settling velocity, solids flux and sludge volume reductions were plotted against the initial sludge concentration as shown in Figures 4.8, 4.9 and 4.10 respectively.

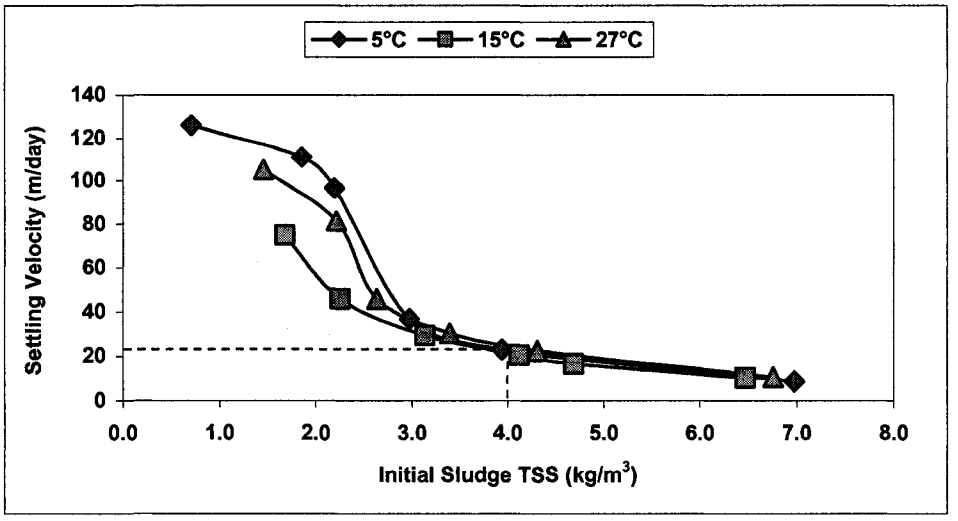

Figure 4.8: Zone Settling Velocity of Influent Sludge Samples

Figure 4.8 depicts the change in ZSV of sludge samples with different initial concentrations, at different temperatures. From the figure, it is evident that the ZSV of sludge samples at different temperatures produced very similar values, at concentrations higher than the original sludge. But at lower concentrations, the settling velocities were noticeably different from each other. In Figure 4.8, at lower concentrations, the 5°C sample had the highest settling velocity as compared to the other two samples. This is

unlikely because at lower temperatures, lower settling velocities are expected owing to the higher viscosity of water providing higher resistance towards settling of solids. This can be explained by the sludge rising, described previously, which occurred during the 15°C and 27°C experiments. This also explains the lowest settling velocity exhibited by the 15°C sample. However, all the samples exhibited somewhat comparable traits with a sharp decrease of settling rate, associated with the transition from zone to compression settling. This was followed by a steady region with low settling velocity at higher concentrations, associated with the governance of compression settling regime. According to the analyses results given in the preceding chapter, the original clarifier influent has a suspended solids concentration of approximately 3.9 kg/m^3 during wet-weather conditions. Thus, from the plot, a corresponding value of ZSV is determined to be approximately 24 m/day. As previously mentioned the solids flux for each sample at each temperature was then calculated, and was plotted as a function of initial sludge TSS, as shown in Figure 4.9.

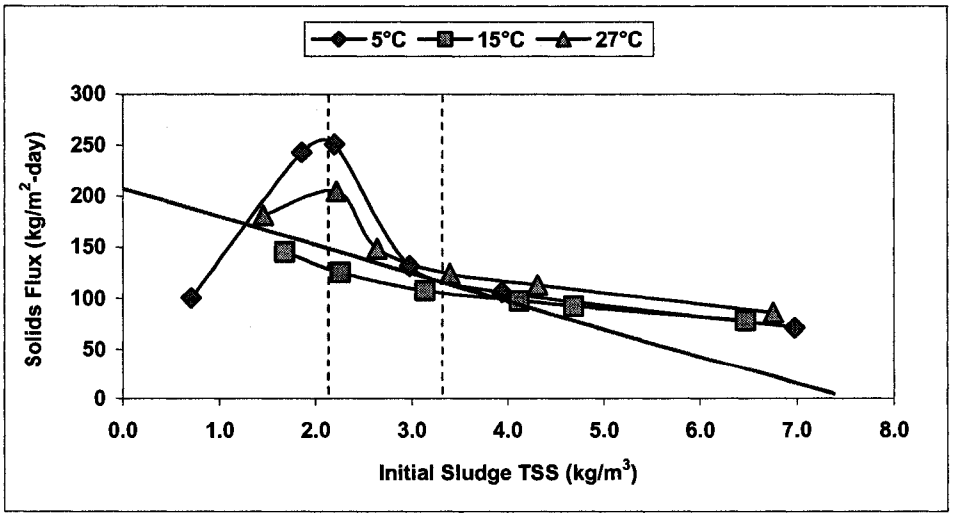

Figure 4.9: Solids Flux Curve for Influent Sludge Samples

From the solids flux curve, it is evident that the maximum flux at 5°C was much higher than the other two temperatures, while the maximum flux at 15°C has the lowest value. This can be explained by the sludge rising described earlier. At higher concentrations, the flux values are somewhat close to each other as were the settling velocities. The point at which zone settling gives way to compression regime, is called the inflection point and it is associated with the final change in slope, within the solids flux curve.

From the shapes of the three curves, it can be said that the samples at all three temperatures reached the peak of maximum flux and went into compression settling at around the same initial sludge concentration. However, due to the irregularity of the data produced at 15°C and 27°C, only the solids flux curve generated at 5°C will be used for further calculations. The peak of the curve, *i.e.* the maximum flux, was achieved at slightly more than 2.0 kg/m^3 of initial sludge concentration while the inflection point was associated with a sludge concentration of about 3.3 kg/m^3. This indicates that when the sludge concentration rises above 2.0 kg/m^3, a distinct layer forms between the settled sludge and the supernatant and the ZSV starts to decrease producing lower solids flux. When the sludge concentration rises beyond 3.3 kg/m^3 the whole suspension settles homogeneously by means of gravity. As determined in the previous chapter, the influent to the original tank has a suspended solids concentration of approximately 3.9 kg/m^3 during wet-weather conditions. This means that compression settling is the governing settling regime within the sludge zone of the clarifier and the clarifier actually performs as a gravity thickener.

The solids flux curve represents the flux associated with the solids movement based on the ZSV. It does not take account of the bulk flow velocity that takes place in the compression zone of the clarifier. The bulk flow velocity is determined by dividing the volumetric flow rate of clarifier underflow (combined flow rate of RAS and WAS) by the cross sectional area of the tank. The solids flux curve has been effectively used in designing final clarifiers and thickeners for activated sludge systems. The plot is also used in determining the Limiting Solids Flux (F_L) for a certain operation, using the flow rate (Q_u) and suspended solids concentration (C_u) of clarifier underflow. To determine F_L from the solids flux curve, a tangent is drawn starting from the underflow concentration value on the abscissa, touching the underside of the curve and not intersecting the curve twice. The point where the tangent line touches the flux curve is the inflection point and the intercept of this tangent line indicates the F_L value for the clarifier operation. The limiting solids flux can be compared with the operational solids loading of the clarifier unit indicating if there is a problem of solids overloading.

As determined in the previous chapter, for the original tank, during wet-weather conditions, the influent suspended solids concentration (C_o) is approximately 3.9 kg/m^3 and an underflow or RAS concentration (C_u) of approximately 7.3 kg/m^3. With the underflow concentration value, a tangent line was drawn on the flux curve (indicated by the tangent line in Figure 4.9), which gave an F_L value of approximately 210 kg/m^2.day. By dividing this value with a scale factor of 1.5, the practical value was calculated as 140 kg/m^2.day.

Again, if the negligible amount of suspended solids leaving the clarifier with the effluent is ignored, a mass balance around the clarifier produces,

$$Q_o \times C_o = Q_u \times C_u \qquad (4.2)$$

Assuming a peak flow rate (Q_O) of 50,000 m^3/day (50 ML/day) gives:

$$Q_u = (Q_o \times C_o)/C_u = 26{,}712\ m^3/day \approx 27\ ML/day \qquad (4.3)$$

Thus, for an influent flow rate of 50 ML/day, the operational underflow rate is approximately 27 ML/day. About 90% of this underflow is recycled as RAS giving a recycle ratio of about 49%. Further, with a surface area of (76.2m×25.8m) 1968.4 m^2, the operational solids loading at wet-weather conditions of the clarifier is approximately 99 kg/m^2.day. This value is less than the F_L value of approximately 140 kg/m^2.day, which indicates that the original clarifier unit at Gold Bar is not overloaded with suspended solids. Also, the operational bulk flow velocity within the compression zone of the clarifier, obtained by dividing the underflow (Q_u) with the clarifier surface area, is approximately 14 m/day as compared to the approximate ZSV of 24 m/day.

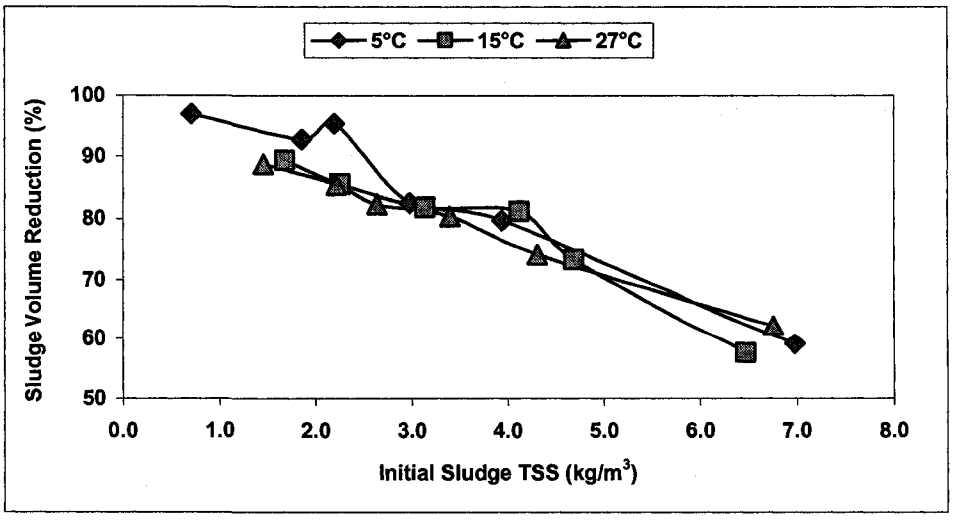

Figure 4.10: Volume Reduction of Influent Sludge Samples

Figure 4.10 depicts the change in volume reduction of sludge samples with different initial concentrations, at different temperatures. From the plot, it is evident that the volume reduction decreases with increasing sludge concentrations. This is natural, because when highly concentrated sludge settle, consolidation occurs as the settled solids are compressed under the weight of overlying solids. The void spaces in between the particles are gradually diminished and water is squeezed out of the matrix. Thus, with increasing sludge concentration, the inter-particle space diminishes with lower reduction in settled sludge volume. Figures 4.11 and 4.12 provide the depiction of settled sludge and supernatant properties as a function of initial sludge concentration. Corresponding raw data are tabulated in Appendices B-9, 10, 11 and 12.

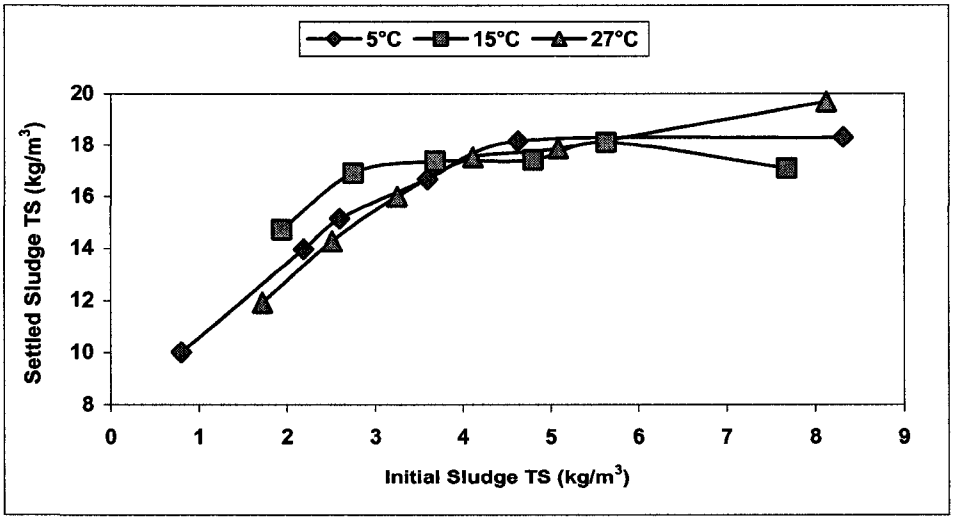

Figure 4.11: Settled Sludge TS vs. Initial Sludge TS

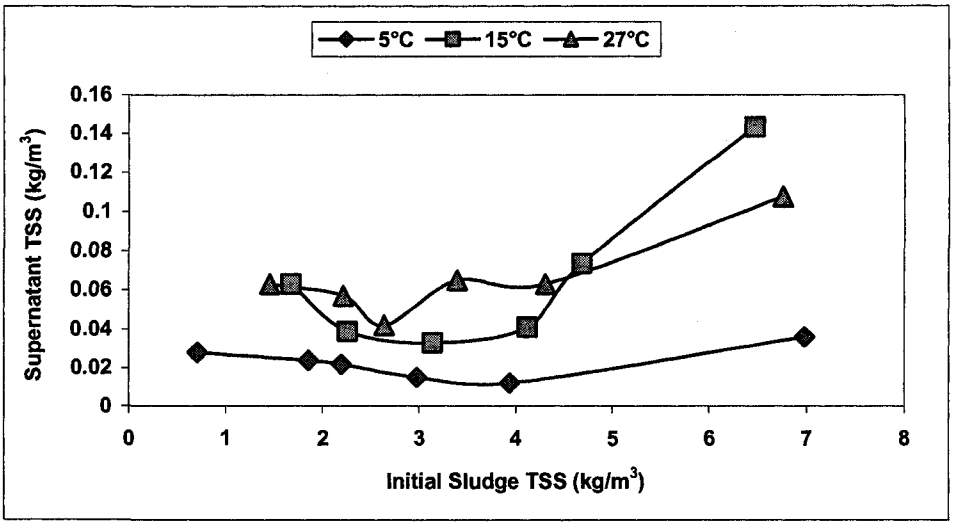

Figure 4.12: Supernatant TSS vs. Initial Sludge TSS

From Figure 4.11, it is evident that the solids concentration of the settled sludge increased with increasing initial sludge concentration. The curves reached a plateau at higher sludge concentrations, which is consistent with the previously determined inflection or compression point. The settled sludge concentration for the 15°C experiment shows a decrease near the highest TS value. This can be explained by the rising sludge phenomena described previously. TSS analysis was not done on the settled sludge samples in view of the very high solids content that might clog the filters. Figure 4.12 depicts the trend of the supernatant TSS as a function of the initial sludge TSS. Supernatant at 15°C and 27°C produced very high TSS values at higher concentrations owing to the sludge rising. For those cases, it was very difficult to collect supernatant samples because of the scum floating on the top. The supernatant turbidity vs. initial sludge TSS plot is not shown here because it was almost exactly similar to this plot.

The results obtained from both the sludge property evaluation and the settling tests are tabulated in Table 4.2 in approximate numbers. From the results, it is evident that Clarifier #1 does not have a problem of solids overloading. The operational data acquired during the experiments indicate a steady and efficient operation in terms of solids removal. But the problems encountered during the batch settling test indicate presence of high levels of nitrate in the MLSS, coming from the fourth pass of the preceding bioreactor. The nitrate level in the MLSS is supposed to be reduced by the internal recycle within the bioreactor. Thus, reduced performance of the clarifier may indicate a poor operation of the bioreactor.

Table 4.2: Summary of Approximate Results from Batch Settling Test

Peak Flow Rate (ML/day)	Total Underflow (ML/day)	Influent MLSS Conc. (kg/m^3)	Underflow Conc. (kg/m^3)
50	27	3.9	7.3
Zone Settling Velocity (m/day)	**Bulk Flow Velocity (m/day)**	**Limiting Solids Flux ($kg/m^2.day$)**	**Operational Solids Flux ($kg/m^2.day$)**
24	14	140	99

4.3.4. Settling Velocity Models

Many empirical relationships between the settling velocity and sludge concentration have been proposed to facilitate the direct analysis of settling tank behavior. Some of the most accepted models are discussed in Chapter 2 of this report. These models were tested using the settling velocity data obtained from the batch settling test. This was done in order to find an appropriate mathematical model for the system which would effectively assist in any future study.

Among the settling velocity models, formulas given by Vesilind (1968) and Dick and Young (1972) provided the most accurate response. According to the Vesilind formula:

$$\ln V_s = - nX_o + \ln V_o \qquad (4.4)$$

While, the Dick and Young formula yields the relationship:

$$\ln V_s = - n(\ln X_o) + \ln V_o \qquad (4.5)$$

where, V_s is the ZSV obtained from batch settling tests and X_o is the MLSS or clarifier influent concentration. Thus, to determine the model parameters (n and V_o) for the Vesilind and Dick and Young model, $\ln V_s$ was plotted against X_o and $\ln X_o$ respectively. Both datasets generated approximate straight lines with high R^2 values for all three temperatures. These plots are presented in Appendices B-13 and B-14. Model generated settling velocities and the corresponding raw data are tabulated in Appendix B-15.

Table 4.3: Parameters for Settling Velocity Models

Sample	Vesilind Model			Dick & Young Model		
	Model Parameters		Model Fit	Model Parameters		Model Fit
	n (m^3/kg)	V_o (m/day)	R^2	n	V_o (m/day)	R^2
5°C	0.47	199.94	0.931	1.24	143.45	0.809
15°C	0.40	118.51	0.958	1.45	155.09	0.999
27°C	0.44	170.37	0.940	1.57	218.98	0.974

The model parameters were different for the three different experiments as shown in Table 4.3. Also, both models generated the highest R^2 value with the 15°C data. This is unusual because during the experiments conducted at 15°C and 27°C, the normal settling operation was interrupted by sludge rising. Hence, to compare the response of the two models, only the data from the 5°C experiment was used.

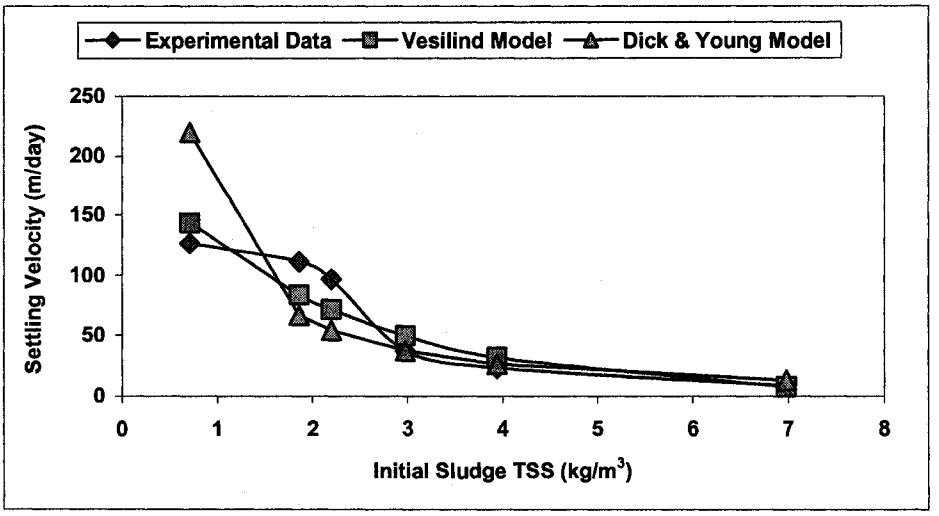

Figure 4.13: Batch Settling Data (5°C) and Response of Settling Velocity Models

As shown in Figure 4.13, both models provided good predictions, in terms of settling velocity, at high MLSS concentration. From the study, it is evident that the Vesilind model produced a more accurate response for the 5°C data as compared to the Dick and Young model.

5.0. Design of Pilot-Scale Clarifier Unit

One of the key objectives of this thesis was to design and manufacture a pilot scale unit of the selected clarifier at Gold Bar WWTP. In order to do this, the original tank design was thoroughly investigated along with a study of the sludge properties and the associated settling characteristics. This chapter deals with the pilot-scale design while the rest of the studies are described in preceding chapters within this report. The chapter consists of a detailed description of the existing design, scale down method, design calculation and finally, verification of the pilot-scale model including tracer study.

5.1. Original Tank Design

In order to scale down the selected clarifier unit, the original design was scrupulously investigated to identify each and every one of the tank's characteristic dimensions. Design data along with technical drawings of the unit were supplied by Gold Bar, for this purpose. List of engineering drawings included the original 1957 design of the unit followed by all the major modifications to date.

As mentioned in Chapter 1, Gold Bar WWTP has 11 operational rectangular horizontal flow final clarifiers. The tanks are almost identical to each other in terms of basic design but some of them have in-tank baffles in place. For the purpose of this research, Clarifier #1 was selected for scale down. As in the case of rectangular horizontal flow clarifiers, the tank is essentially an extremely long and shallow basin. The length is approximately three times the width and nineteen times the depth of the tank. The MLSS coming from the fourth pass of the preceding bioreactor flows into a common channel which then feeds into the clarifier in a distributed manner. The clarifier has five

parallel bays separated from each other near the influent end by concrete structure. The structures do not separate the settling zone of the clarifier completely and the tank acts as a continuous basin downstream. Each parallel bay near the influent end of the clarifier has two rectangular feed ports controlled by slide gates, placed at the top of the inlet wall. Thus, the whole unit has ten rectangular distributed inlets along the width of the tank. Each rectangular inlet to the clarifier is about 0.419 m (1.37 ft) wide and 1.168 m (3.83 ft) deep and the inlets within each bay are placed at an equal distance from each other. The momentum of the influent flow into the tank is dissipated by placing an inlet baffle near the influent end of the unit. The inlet baffle is located at a distance of about 0.508 m (1.67 ft) from the inlet wall and it stretches across the full width of the tank with a depth of about 1.905 m (6.25 ft).

The tank is equipped with a sludge hopper, running along the width of the tank, where the settled sludge is collected and then transferred to either recycle or waste. According to the original plan, the selected clarifier unit was designed as a variation of the Gould Type I clarifier, where the hopper was located near the effluent end of the clarifier. The unit was subsequently modified to Gould Type II clarifier by retaining the hopper and by adding a launder section to the end of the unit. The length of the selected clarifier unit is about 76.192 m (250 ft) with a launder section, starting from the end of the hopper. The sludge hopper is located at a distance of about 46.634 m (153 ft) from the influent end and 25.900 m (85 ft) from the effluent end. The sludge hopper is about 3.658 m (12 ft) wide and 1.524 m (5 ft) deep with a length equal to the width of the clarifier. The hopper is built with inclined side walls near the top, on both sides, so that the settled sludge can easily slide into it. The side walls of the hopper are vertical near the bottom in

order to store the sludge. The sloped portion of the hopper on each side has a depth and width of 0.914 m (3 ft). Each parallel bay near the influent end of the clarifier is about 5.167 m (17 ft) wide, yielding a total width of 25.835 m (85 ft) for the whole clarifier unit. The side water depth of the clarifier is about 3.963 m (13 ft) at the influent and effluent ends, sloping to a depth of about 4.115 m (13.5 ft) at the sludge hopper.

The inclined floor of the clarifier promotes any settled sludge to move into the hopper under the influence of gravity. The sludge hopper has a cross collector that moves the settled sludge to a discharge point at one end of the hopper. Sludge removal within the clarifier is achieved by employing a chain and flight system. The flights in the influent section scrape the settled sludge toward the sludge hopper, in the same direction as the flow. In the effluent section, a separate chain and flight system is used, where the flights scrape the sludge to the sludge hopper in a direction opposite to the flow. The flights in the sludge removal system move at a speed of approximately 4 ft/min. Scum removal is accomplished by a surface skimming action, controlled by an automatically operated ducking skimmer in each of the five compartments of the clarifier.

The effluent section or outlet zone of the clarifier consists of two sets of five launders or troughs. The troughs are arranged perpendicular to the flow and discharging into a single central channel. The central channel is located along the direction of the flow right in the middle of the effluent section and the two sets of troughs are placed on either side of the channel. Each trough has a depth of about 0.510m (1.67 ft) and a width of about 0.710 m (2.33 ft) and the troughs are placed at an equal distance of 2.640 m (8.66 ft) from each other. The first trough is at a distance of 0.451 m (1.48 ft) from the beginning of the

central outlet channel and the last trough is 2.896 m (9.50 ft) away from the outlet wall. The troughs are slightly sloped towards the central channel for the efficient discharge of effluent. Each trough is topped on both interior faces by v-notched weir plates. The central channel discharges the effluent into the next transfer conduit through a single rectangular outlet and it has a sloped bottom towards this final outlet. The central channel is approximately 17.455 m (57.27 ft) long and 1.200 m (3.94 ft) wide with a depth of about 0.762 m (2.50 ft) near the first trough and 2.300 (7.55 ft) at the end. The final outlet from the clarifier is about 1.200 m (3.94 ft) wide and 1.790 m (5.87 ft) deep.

Before conducting the pilot-scale design, some operational parameters and performance indicators of the full-scale clarifier were calculated using the design dimensions of the unit. These numbers were evaluated by comparing with values of common design criteria obtained from literature, as shown in Table 5.1. From the data shown in the table, it is evident that the secondary clarifier operates within the standard and typical range of key design criteria.

Table 5.1: Secondary Clarifier Design Criteria for Activated Sludge Plants

Design Criteria	Surface Loading ($m^3/m^2.day$)	Solids Loading ($kg/m^2.day$)	Water Depth (m)	Weir Overflow ($m^3/m.day$)	Recycle Ratio (%)	SVI (mL/g)
Canadian Standard[1]	40.61 max	245 max	3.7 min	251 max	25 to 75	
Typical Values[2]	16 to 41	96 to 144	3 to 5.5	125 to 190	43 to 60	100 to 150
Gold Bar WWTP	13 to 25	50 to 99	3.96	102 to 203	~ 49	113 to 144

[1]Chinniah (2006); [2]WEF-ASCE (1992)

5.2. Pilot-Scale Design

5.2.1. Scaling Theory for Hydraulic Modeling

The pilot-scale unit was designed based on the fundamental theories of hydraulic modeling and similitude criteria were established to verify the design. Hydraulic modeling, which is a form of physical modeling, is used widely to investigate design and operational issues of larger hydraulic structures. These physical models are often used with appropriate computational models to adequately describe complicated flow situations. Hydraulic models may be intended to simulate a specific physical process (process models) or they may be intended to evaluate the effects of proposed design modifications (design models). Although hydraulic models are built to replicate the design and processes of a selected unit, it is not possible to achieve exact replication. Such shortcomings of a physical model are known as scale effects (Ettema *et al.*, 2000).

In order to design and build an appropriate physical model, due considerations of similitude must be made. The principles of similitude were developed to relate the experimental data generated from a hydraulic model to the full-scale unit. For an ideal design, geometric, kinematic and dynamic similarity should be maintained between the two systems. To obtain geometric similitude, the distance between any two points on the model must bear a constant ratio to the distance between the corresponding two points in the full-scale system. To ensure kinematic similarity, the velocity at a point in the model must bear a constant ratio to the velocity at the corresponding point in the full-scale system. To satisfy the dynamic similitude criteria, forces at geometrically equivalent points must be related by a constant ratio within the two systems. If geometric similitude

is satisfied, kinematic similitude is achieved automatically, but practical conditions make it difficult to satisfy all three of the criteria (Schmidtke and Smith, 1983).

In the following discussion, different criteria are presented to verify similitude between a model and a full-scale unit. In this context, the subscripts r, m and f denote ratio, model and full-scale values, respectively. For geometric similitude, the primary parameter is known as the length (L) ratio, expressed as:

$$L_r = L_f / L_m \tag{5.1}$$

The area (A) and volume (V) ratios are thus given as:

$$A_r = L_r^2;\ V_r = L_r^3 \tag{5.2}$$

To describe kinematic similitude, the time (t) ratio is described as:

$$t_r = t_f / t_m \tag{5.3}$$

Based on the time ratio, the velocity (u) and acceleration (a) ratios can be given as:

$$u_r = L_r / t_r;\ a_r = L_r / t_r^2 \tag{5.4}$$

Also, the flow rate (Q) ratio is given as:

$$Q_r = u_r \times A_r = L_r^3 / t_r \tag{5.5}$$

The first step in determining the conditions for satisfying dynamic similitude is the identification of the critical dimensionless parameters for a specific system. This is usually done by either direct establishment upon inspection of relevant forces or by using dimensional analysis (Ettema *et al.*, 2000). An example of the first method is given below.

If the system experiences momentum transport, the inertial force (F_i) becomes critical, which according to Newton's second law is a function of mass (M) and acceleration (a). Mass can again be expressed as a function of density (ρ) and volume (V) while

acceleration is a function of velocity (u) and time (t). Thus, the inertial force (F_i) is given as:

$$F_i = (M)(a) = (\rho V)(u/t) = (\rho L^3)(u/t) = \rho L^2 u(L/t) = \rho L^2 u^2 \qquad (5.6)$$

Similarly, the gravity force (F_g) acting on a system may be given as a function of the mass (M) and gravitational acceleration (g):

$$F_g = (M)(g) = (\rho V)(g) = \rho L^3 g \qquad (5.7)$$

A ratio of these two forces represents the dimensionless parameter well known as the Froude number (Fr):

$$F_i / F_g = \rho L^2 u^2 / \rho L^3 g = u^2 / Lg \equiv Fr^2 \qquad (5.8)$$

For a system in which the above two forces are critical, dynamic similitude criteria is established when the Froude numbers for the model and the full-scale system are set as equal, *i.e.* $Fr_r = 1$:

$$u_f^2 / L_f g_f = u_m^2 / L_m g_m \qquad (5.9)$$

$$u_r^2 = (L_r / t_r)^2 = L_r g_r \qquad (5.10)$$

If the full-scale system and the model are under the same gravitational field ($g_r = 1$), then the Froude number criterion for dynamic similitude is given as:

$$u_r = t_r = \sqrt{L_r} \text{ and } Q_r = L_r^{2.5} \qquad (5.11)$$

The dynamic similitude criterion presented above is specifically applicable for modeling using the Froude number (Fr). If, for a system, a different dimensionless parameter is considered *e.g.* Reynolds number (Re) or Weber number (We), the criteria for dynamic similitude turn out to be completely different, giving rise to conflicting scale ratios. Only two among these three parameters can be simultaneously used to establish dynamic similitude. But it is possible only by manipulating fluid properties, which is

extremely difficult. Strict similitude is impossible to achieve using all these parameters. Therefore, in order to build an accurate physical model of a system, the most important forces acting on the system must be identified and an appropriate force ratio or dimensionless parameter must be chosen to establish the dynamic similitude criteria.

In case of a single-phase flow, considerations must be made for forces and fluid properties such as fluid inertia, gravity, fluid viscosity and surface tension. The Froude number (Fr) is the dominant similitude parameter for gravity driven free surface flows:

$$Fr = u / \sqrt{(gd)} \qquad (5.12)$$

where, u = fluid velocity and d = depth of flow. The Froude number criterion for dynamic similitude is presented in the preceding paragraph. The Reynolds number (Re), which represents the ratio of inertial to viscous forces, becomes important in terms of viscous flow conditions:

$$Re = ud\rho / \mu \qquad (5.13)$$

where, ρ = fluid density and μ = dynamic viscosity of fluid. To model systems where the flow is prone to air-entraining vortices, the surface tension of the fluid is the significant force. In such cases, the Weber number (We), which represents the ratio of inertial to surface tension forces, is the dominant similitude parameter:

$$We = \rho du^2 / \sigma \qquad (5.14)$$

where, σ = surface tension strength of fluid. In most cases, surface tension exerts negligible influence in large free surface flows, as compared to the other forces described here.

For hydraulic modeling, it is impossible to simultaneously satisfy the equality of both Reynolds and Froude number without manipulating fluid properties. Usually, when the Froude number criterion is satisfied ($Fr_r = 1$), Reynolds number in the model is much smaller than in the full-scale system. However, the Reynolds number should remain within the same range of flow behavior, *i.e.* if the full-scale system has fully turbulent flow then the flow in the model should also be turbulent. If the fluid density and viscosity remain same ($\rho_r = \mu_r = 1$), then the ratio of Reynolds number can be expressed as a function of the length ratio, under the Froude number criterion ($u_r = \sqrt{L_r}$):

$$Re_r = u_r d_r \rho_r / \mu_r \qquad (5.15)$$

$$Re_r = L_r^{1.5} \qquad (5.16)$$

This reduced value of Reynolds number at model scale may shift the flow from fully turbulent, which prevails at full-scale, into a transition or a laminar flow. The shift in flow region signifies a change in local flow pattern near boundaries and increased viscous flow resistance in the model. To solve this problem, a smaller scale ratio may be used for the design and if that is not possible then vertical distortion may be employed. Vertical distortion implies the use of a smaller vertical length scale than a horizontal length scale. This increases the value of Re in terms of flow depth. Vertical distortion is commonly used for reproducing stream wise flow patterns and when flow resistance is of primary concern. Use of vertical distortion reduces accuracy of geometric and dynamic similitude, exaggerates secondary currents and increases bottom slopes. It is inappropriate for models that are intended to replicate complete flow patterns of the full-scale system.

For a fluid flow carrying suspended matter, the buoyancy effects become particularly significant in addition to the inertia, gravity and viscous forces. These effects are caused

by differences in densities that result in the buoyancy forces strongly affecting the flow dynamics, producing buoyancy modified flows. The density difference may be caused by a temperature gradient or by the difference in suspended solids concentration while buoyancy modified flows may include density stratification within the system. The dynamic similitude of such flows usually requires the densimetric Froude number (Fr_D) to be equal in the model and the full-scale system (Ettema *et al.*, 2000).

$$Fr_D = u / \sqrt{[(\Delta\rho/\rho)gd]} = Fr\sqrt{(\rho/\Delta\rho)} \qquad (5.17)$$

$$\Delta\rho = c[(\rho_p - \rho) / \rho] \qquad (5.18)$$

where, $\Delta\rho$ = differential density, c = suspended solids concentration and ρ_p = density of dried solids. Thus, for dynamic similitude, the satisfaction of the densimetric Froude number criterion ($Fr_{Dr} = 1$) requires the satisfaction of Froude number criterion ($Fr_r = 1$) and similarity of suspension properties in terms of density ($[\rho/\Delta\rho]_r = 1$). Hence, to achieve satisfactory dynamic similitude for such systems, suspensions from the full-scale system can be used effectively for the hydraulic model.

5.2.2. Assumptions and Considerations

The primary purpose of the hydraulic model building was to closely reproduce the flow phenomena of the original tank. In addition, the pilot-scale unit will serve to observe and validate the effect of certain design changes on the tank hydrodynamics. In view of this purpose, the biological activity taking place within the original tank was overlooked during scaling. The major dimensions of the pilot-scale model were designed under the geometric and kinematic similitude criteria, while the flow rate was selected to satisfy the dynamic similitude criteria.

The first step of the model design was to select an appropriate scale factor. Two things were considered in the selection of this factor. The full-scale clarifier had to be scaled down to fit in the laboratory while the depth of the model had to be maintained at a reasonable range to represent flow behavior. Consequently, a length ratio, $L_r = 25$ was chosen for the scaling. The next step was to recognize the most important forces acting on the system and to select an appropriate dimensionless parameter. Good understanding of the full-scale flow system and relevant forces allowed direct establishment of suitable dimensionless parameter without the use of dimensional analysis. Because the free surface flow in the original system involves momentum transport and is governed by gravity, the Froude number criterion was established for dynamic similitude, as shown in the preceding section. As a result of this selection, the resistance to flow caused by fluid viscosity and the effects of fluid surface tension was considered negligible. In order to simplify the design process, identical fluid properties were assumed for the model and the full-scale system. Thus, single phase flow of water at 20°C was assumed to establish the similitude criteria.

In determining the inlet and outlet area of the pilot-scale model, several considerations were made. First of all, the inlet and outlet openings were designed to be circular, as opposed to the rectangular openings in the full-scale system, to accommodate for conventional plumbing arrangements. Attempts were made to keep the ratio of the inlet-outlet areas consistent with the geometric similitude criteria, but some restrictions were experienced. For the inlet, 10 equidistant openings were placed on the inlet wall, each with a diameter of 1¼". However, to facilitate plumbing, two identical openings were placed at the end of the central outlet channel in stead of a single, much larger

opening. The width of the central outlet channel allowed a maximum diameter of 2" for each opening. Due to manufacturing limitations, the troughs or launders in the pilot-scale model were not equipped with V-notch weir system. In stead, vertical channels were manually cut along the length of each trough to facilitate effluent transport from the tank into the launders.

Clear acrylic was used as material of construction for the pilot-scale model. Acrylic (Polymethyl-Methacrylate or PMMA), otherwise known as Plexiglas®, is an optically transparent thermoplastic that offers high light transmittance and has a large strength to weight ratio. Owing to the high level of optical clarity, acrylic was chosen for constructing the model in order to permit future study using laser measurement techniques like Planar Laser Induced Fluorescence (PLIF) and Particle Image Velocimetry (PIV). Also, acrylic was chosen because prolonged exposure of acrylic to moisture or even total immersion in water, does not significantly affect its mechanical or optical properties. Usually, commercial acrylics are UV (ultraviolet) stabilized for good weatherability and resistance to prolonged sunlight exposure. In addition to aqueous solutions, acrylics are unaffected by the majority of laboratory chemicals, detergents, cleaners, dilute inorganic acids, alkalis and aliphatic hydrocarbons. However, acrylics are not recommended for use with chlorinated or aromatic hydrocarbons, esters or ketones (Boedeker Plastics Inc., 2008).

Acrylic with a thickness of ¾" was used for building the main walls of the pilot-scale unit, while a thickness of ¼" was used for internal structures like the launders. For smooth operation and in order to keep the tank from spilling, a 50 mm clearance above

the desired fluid depth was provided within the design. Also, the uneven shape of the tank floor was used as a false bottom, supported on a flat sheet of ¾" acrylic. This increased the load bearing capacity of the tank base and facilitated the placement of the tank on flat surfaces.

5.2.3. Design Calculation

As a first step of the design calculation, all linear dimensions of the full-scale tank were scaled down using the scale factor of 25. The dimensions of the original tank and the pilot-scale model are tabulated in Appendix C-1. Using these dimensions the surface area, tank volume, average depth, flow area and inlet-outlet area for both the pilot-scale model and full-scale system were calculated as shown below. For each tank, the total volume was calculated by considering different geometric shapes at the tank base and the hopper, while the average tank depth was calculated from the tank volume. The approximate flow area was calculated using the average depth of each tank.

For the full-scale system,

Tank surface area, $A_{S\text{-}f} = 76.192\ m \times 25.835\ m = 1968.420\ m^2$

Volume of sloped bottom = $[0.5 \times (46.634 + 25.900)\ m \times (4.115 - 3.963)\ m] \times 25.835\ m$
$= 142.418\ m^3$

Volume of hopper = $[0.914\ m \times 0.914\ m + (3.658 - 0.914 \times 2)\ m \times 1.524\ m] \times 25.835\ m$
$= 93.634\ m^3$

Total tank volume, $V_{T\text{-}f} = 142.418\ m^3 + 93.634\ m^3 + (76.192\ m \times 25.835\ m \times 3.963\ m)$
$= 8036.902\ m^3$

Average tank depth, $d_f = 8036.902\ m^3 / 1968.420\ m^2 = 4.083\ m$

Approximate flow area, $A_f = 25.835\ m \times 4.083\ m = 105.484\ m^2$

Inlet area, $A_{in\text{-}f} = 10 \times 1.168\ m \times 0.419\ m = 4.894\ m^2$

Outlet area, $A_{out\text{-}f} = 1.200\ m \times 1.790\ m = 2.148\ m^2$

For the pilot-scale model,

Tank surface area, $A_{S\text{-}m} = 3.048\ m \times 1.036\ m = 3.158\ m^2$

Volume of sloped bottom = $[0.5 \times (1.865 + 1.036)\ m \times (0.165 - 0.158)\ m] \times 1.036\ m$
$= 0.011\ m^3$

Volume of hopper = $[0.037\ m \times 0.037\ m + (0.147 - 0.037 \times 2)\ m \times 0.061\ m] \times 1.036\ m$
$= 0.006\ m^3$

Total tank volume, $V_{T\text{-}m} = 0.011\ m^3 + 0.006\ m^3 + (3.048\ m \times 1.036\ m \times 0.158\ m)$
$= 0.516\ m^3$

Average tank depth, $d_m = 0.516\ m^3 / 3.158\ m^2 = 0.163\ m$

Approximate flow area, $A_m = 1.036\ m \times 0.163\ m = 0.169\ m^2$

Inlet area, $A_{in\text{-}m} = 10 \times \pi \times (1.25 \times 2.54 / 100)^2 / 4 = 7.92 \times 10^{-3}\ m^2$

Outlet area, $A_{out\text{-}m} = 2 \times \pi \times (2 \times 2.54 / 100)^2 / 4 = 4.05 \times 10^{-3}\ m^2$

In the following two pages, Figures 5.1, 5.2 and 5.3 show the design drawings of the scaled model. In the drawings, all the dimensions are in mm. For convenience of presentation, the trough system is not shown in these drawings. Apart from the original design, the model was equipped with some provisions of design modification in terms of baffle channels. These baffle channels will allow the placement of full-width, in-tank baffles at different positions along the length of the settling zone. The baffle channels were also designed to allow the baffles to be placed at alternating depths within the tank. The baffles were not used in this research but they will aid in the future study to find out optimum number and placement of in-tank baffles, in order to improve clarifier hydrodynamic performance.

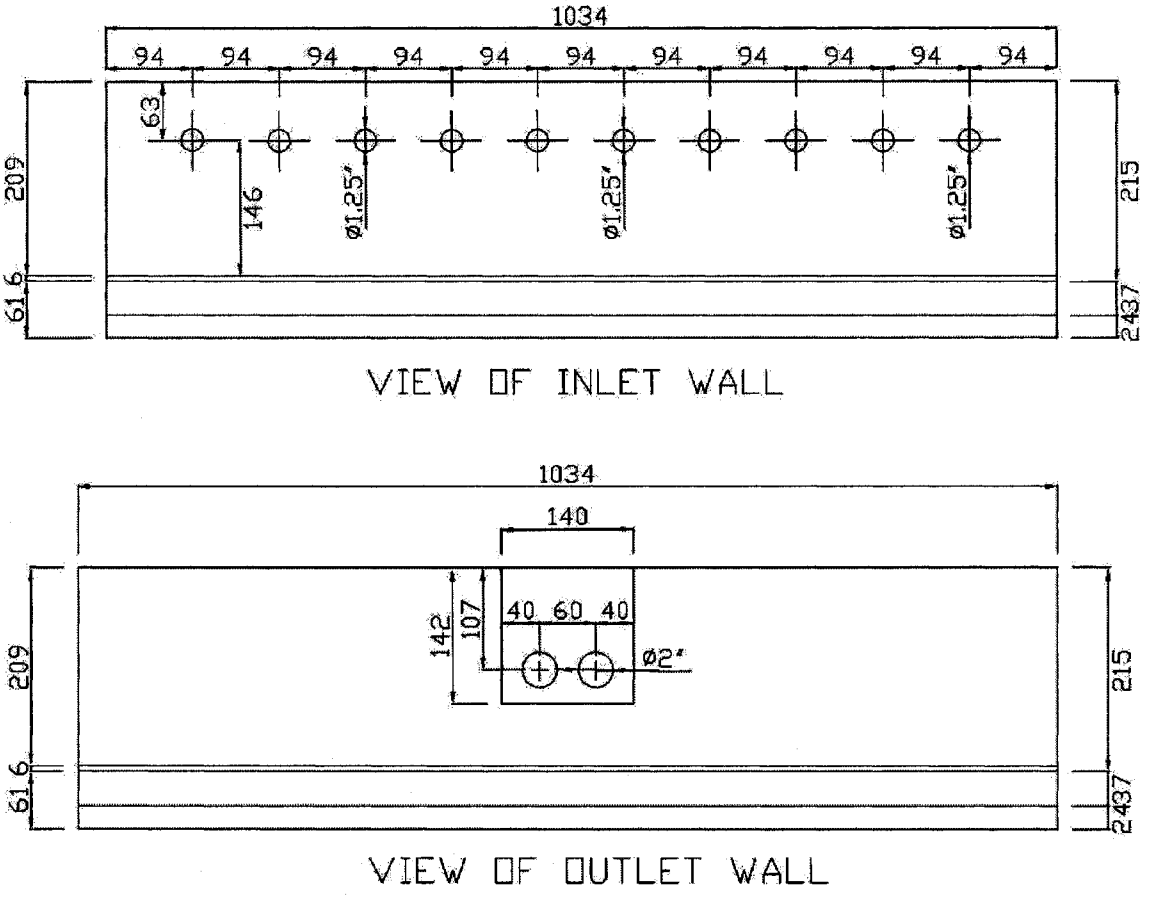

Figure 5.1: Inlet and Outlet Wall View of Pilot-Scale Secondary Clarifier

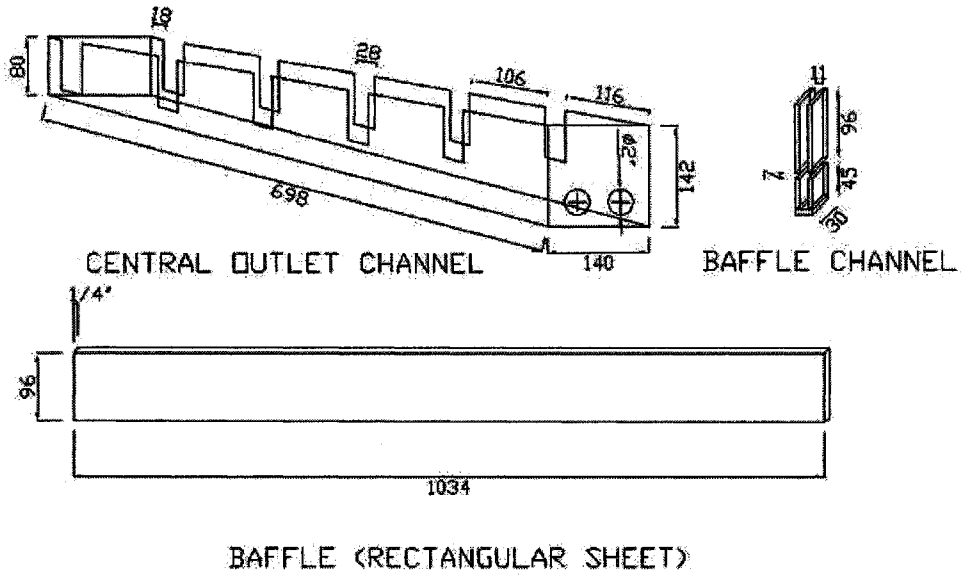

Figure 5.2: Details of Central Outlet Channel, Baffle Channel and In-Tank Baffles

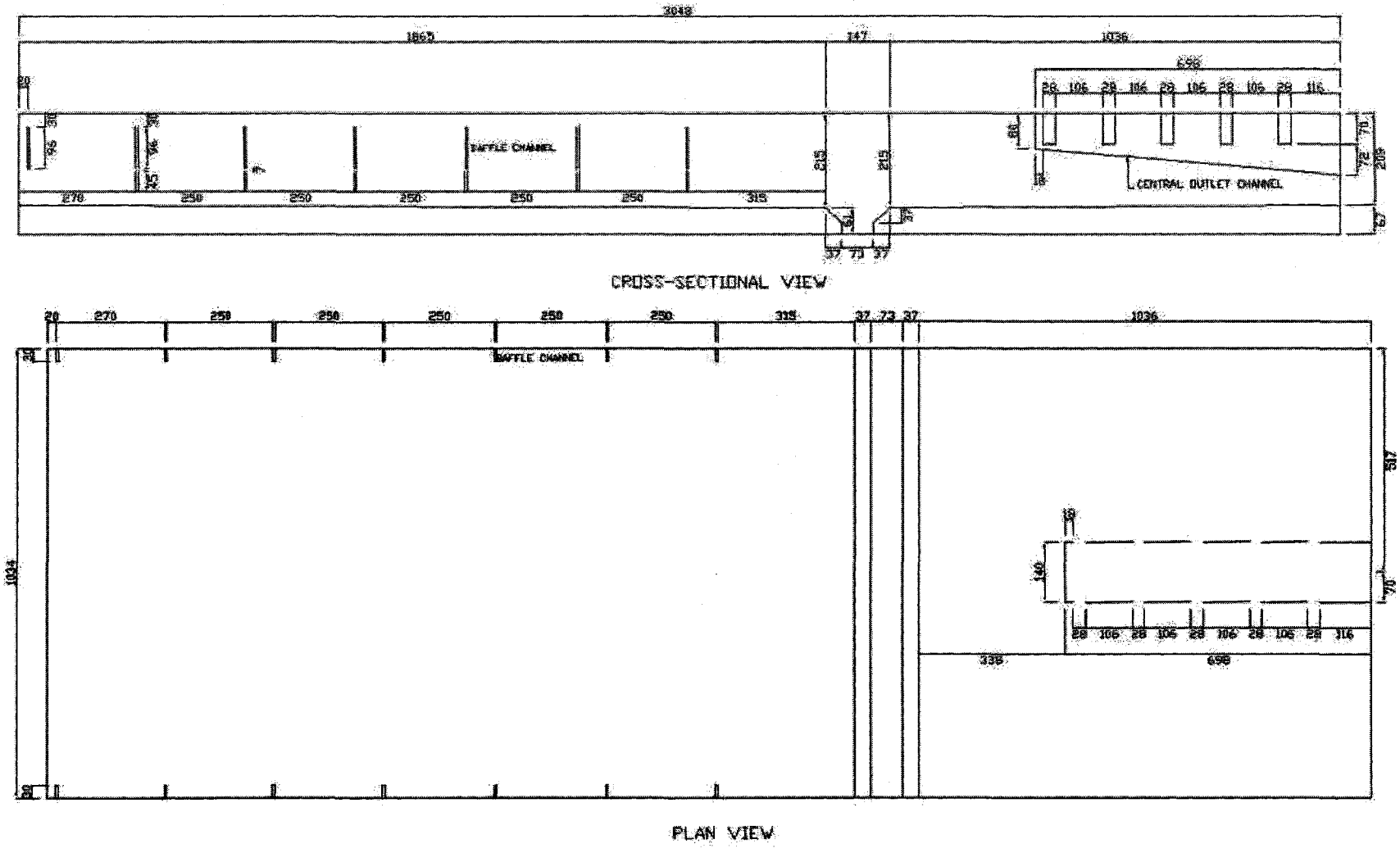

Figure 5.3: Cross-Sectional and Plan View of Pilot-Scale Secondary Clarifier

The original tank was designed to handle a minimum flow rate of 25 ML/day (0.289 m^3/s) with a high flow of 50 ML/day (0.579 m^3/s). In accordance, the weir system in the launder section of the pilot-scale model was designed to handle a range of flow from 1.5 gpm (9.45×10^{-5} m^3/s) to 3 gpm (1.89×10^{-4} m^3/s). Thus,

Q_f = 0.289 to 0.347 m^3/s and $Q_m = 9.45\times10^{-5}$ to 1.89×10^{-4} m^3/s.

Considering the minimum flow, the average flow velocity, hydraulic retention time, Reynolds number and Froude number for both systems were calculated as shown below. To calculate the Reynolds number inside tank, a single phase flow of water at 20°C (ρ = 998.2 kg/m^3, μ = 0.001 kg/m.s) was considered for both systems.

For the full-scale system,

Volumetric flow rate, $Q_f = 0.289\ m^3/s$

Average flow velocity, $u_f = Q_f / A_f = (0.289\ m^3/s) / (105.484\ m^2) = 2.74\times10^{-3}$ m/s

Hydraulic retention time, $\tau_f = V_{T\text{-}f} / Q_f = (8036.902\ m^3) / (0.289\ m^3/s) = 463$ min

Reynolds number, $Re_f = u_f d_f \rho_f / \mu_f$

$= (2.74\times10^{-3}\ m/s) \times (4.083\ m) \times (998.2\ kg/m^3) / (0.001\ kg/m.s)$

$= 11{,}145$

Froude number inside tank, $Fr_f = u_f / \sqrt{(g d_f)}$

$= (2.74\times10^{-3}\ m/s) / \sqrt{[(9.81\ m/s^2) \times (4.083\ m)]}$

$= 4.33\times10^{-4}$

Flow velocity at inlet, $u_{in\text{-}f} = Q_f / A_{in\text{-}f} = (0.289\ m^3/s) / (4.894\ m^2) = 0.059$ m/s

Froude number at inlet, $Fr_{in\text{-}f} = u_{in\text{-}f} / \sqrt{(g d_{in/out})}$

$= (0.059\ m/s) / \sqrt{[(9.81\ m/s^2) \times (3.963\ m)]}$

$= 9.46\times10^{-3}$

Flow velocity at outlet, $u_{out\text{-}f} = Q_f / A_{out\text{-}f} = (0.289\ m^3/s) / (2.148\ m^2) = 0.135$ m/s

Froude number at outlet, $Fr_{out\text{-}f} = u_{out\text{-}f} / \sqrt{(g d_{in/out})}$

$= (0.135\ m/s) / \sqrt{[(9.81\ m/s^2) \times (3.963\ m)]}$

$= 0.022$

For the pilot-scale model,

Volumetric flow rate, $Q_m = 9.45\times10^{-5}$ m^3/s

Average flow velocity, $u_m = Q_m / A_m = (9.45\times10^{-5}\ m^3/s) / (0.169\ m^2) = 5.59\times10^{-4}$ m/s

Hydraulic retention time, $\tau_m = V_{T\text{-}m} / Q_m = (0.516\ m^3) / (9.45\times10^{-5}\ m^3/s) = 91$ min

Reynolds number, $Re_m = u_m d_m \rho_m / \mu_m$

$= (5.59\times10^{-4}\ m/s) \times (0.163\ m) \times (998.2\ kg/m^3) / (0.001\ kg/m.s)$

$= 91$

Froude number inside tank, $Fr_m = u_m / \sqrt{(g d_m)}$

$= (5.59\times10^{-4}\ m/s) / \sqrt{[(9.81\ m/s^2) \times (0.163\ m)]}$

$= 4.42\times10^{-4}$

Flow velocity at inlet, $u_{in\text{-}m} = Q_m / A_{in\text{-}m} = (9.45\times10^{-5}\ m^3/s) / (7.92\times10^{-3}\ m^2) = 0.012$ m/s

Froude number at inlet, $Fr_{in\text{-}m} = u_{in\text{-}m} / \sqrt{(g d_{in/out})}$

$= (0.012\ m/s) / \sqrt{[(9.81\ m/s^2) \times (0.158\ m)]}$

$= 9.64\times10^{-3}$

Flow velocity at outlet, $u_{out\text{-}m} = Q_m / A_{out\text{-}m} = (9.45\times10^{-5}\ m^3/s) / (4.05\times10^{-3}\ m^2)$

$= 0.023$ m/s

Froude number at outlet, $Fr_{out\text{-}m} = u_{out\text{-}m} / \sqrt{(g d_{in/out})}$

$= (0.023\ m/s) / \sqrt{[(9.81\ m/s^2) \times (0.158\ m)]}$

$= 0.018$

Before construction, the selected material thickness was verified on the basis of flexural yield strength of acrylic. The flexural strength, also known as fracture strength or modulus of rupture, is measured in terms of stress and is given as: $\sigma = FL/bd^2$; where, F = load or force at fracture point, L = length of support, b = width of support and d = thickness of material. The average flexural yield strength of optical grade acrylic is σ_m = 96.2 MPa (Automation Creations Inc., 2008). The average height of the tank including the 50 mm clearance (h = 0.213 m) and a single phase flow of water at 20°C (ρ = 998.2 kg/m^3) was considered in calculating the flexural stress on the tank walls.

Force on the tank floor = $(h \times \rho \times g) \times A_{S\text{-}m}$

$= (0.213\ m \times 998.2\ kg/m^3 \times 9.81\ m/s^2) \times 3.158\ m^2 = 6587\ N$

Flexural stress on tank floor, $\sigma = (6587\ N \times 3.048\ m) / (1.034\ m \times 0.0191^2\ m^2)$

$= 53.22\ MPa < \sigma_m$ (satisfactory)

Force on the inlet/outlet walls = $W_m \rho g \int_0^{0.213} h dh$

$= 1.034\ m \times 998.2\ kg/m^3 \times 9.81\ m/s^2 \times (0.213)^2/2\ m^2$

$= 230\ N$

Flexural stress on inlet/outlet walls, $\sigma = (230\ N \times 1.034\ m) / (0.213\ m \times 0.0191^2\ m^2)$

$= 3.06\ MPa < \sigma_m$ (satisfactory)

Force on the side walls = $L_m \rho g \int_0^{0.213} h dh$

$= 3.048\ m \times 998.2\ kg/m^3 \times 9.81\ m/s^2 \times (0.213)^2/2\ m^2$

$= 677\ N$

Flexural stress on side walls, $\sigma = (677\ N \times 3.048\ m) / (0.213\ m \times 0.0191^2\ m^2)$

$= 26.56\ MPa < \sigma_m$ (satisfactory)

From the above calculation, it is evident that the stresses on the base and walls of the tank are well below the threshold limit. This confirms that the tank will not experience any fracture or breakage once filled with fluid. The difference between actual stress value and the critical limit ensures smooth operation, if any other fluid is used in stead of water. In addition, the scaled tank was equipped with braces, placed on top and along the width of the tank, to prevent the side walls from bending.

5.2.4. Model Validation

The built pilot-scale model was validated by conducting a similitude analysis to ensure the satisfaction of geometric, kinematic and dynamic similitude criteria. The results of the analysis are shown below. In this context, the term ratio represents the ratio of a value in the full-scale unit to the corresponding value in the pilot-scale model. As before, the subscripts r, m and f denote ratio, model and full-scale values, respectively.

In order to satisfy geometric similitude, different length ratios (tank length, width and depth), area ratios (tank surface area, flow area and inlet-outlet area) and tank volume ratio were evaluated in terms of the scale factor, $L_r = 25$.

Length ratio,

$$L_r = L_f / L_m = 76.192 \text{ m} / 3.048 \text{ m} \approx 25$$

Width ratio,

$$W_r = W_f / W_m = 25.835 \text{ m} / 1.034 \text{ m} \approx 25$$

$$W_r = L_r$$

Average depth ratio,

$$d_r = d_f / d_m = 4.083 \text{ m} / 0.163 \text{ m} \approx 25 = L_r$$

$$d_r = L_r$$

Tank surface area ratio,

$$A_{S\text{-}r} = A_{S\text{-}f} / A_{S\text{-}m} = 1968.420 \text{ m}^2 / 3.158 \text{ m}^2 = 623$$

$$\sqrt{A_{S\text{-}r}} \approx L_r$$

Approximate flow area ratio,

$$A_r = A_f / A_m = 105.484 \text{ m}^2 / 0.169 \text{ m}^2 = 624$$

$$\sqrt{A_r} \approx L_r$$

Inlet area ratio,

$$A_{in\text{-}r} = A_{in\text{-}f} / A_{in\text{-}m} = 4.894 \text{ m}^2 / 7.92 \times 10^{-3} \text{ m}^2 = 618$$

$$\sqrt{A_{in\text{-}r}} \approx L_r$$

Outlet area ratio,

$$A_{out\text{-}r} = A_{out\text{-}f} / A_{out\text{-}m} = 2.148\ m^2 / 4.05\times10^{-3}\ m^2 = 530$$

$$\sqrt{A_{out\text{-}r}} < L_r$$

Total tank volume ratio,

$$V_{T\text{-}r} = V_{T\text{-}f} / V_{T\text{-}m} = 8036.902\ m^3 / 0.516\ m^3 = 15575$$

$$\sqrt[3]{V_{T-r}} \approx L_r$$

To ensure the satisfaction of kinematic similitude, ratios of different time, flow rate and velocity were evaluated in terms of the Froude number criterion ($t_r^2 = \sqrt[2.5]{Q_r} = u_r^2 = L_r$), which was determined in section 5.2.1 of this chapter.

Hydraulic Retention Time (HRT) ratio,

$$\tau_r = \tau_f / \tau_m = 463\ min / 91\ min \approx 5$$

$$\tau_r^2 = L_r$$

Volumetric flow rate ratio,

$$Q_r = Q_f / Q_m = (0.289\ m^3/s) / (9.45\times10^{-5}\ m^3/s) = 3058$$

$$\sqrt[2.5]{Q_r} \approx L_r$$

Average flow velocity ratio,

$$u_r = u_f / u_m = (2.74\times10^{-3}\ m/s) / (5.59\times10^{-4}\ m/s) \approx 5$$

$$u_r^2 = L_r$$

Inlet flow velocity ratio,

$$u_{in\text{-}r} = uin_f / u_{in\text{-}m} = (0.059\ m/s) / (0.012\ m/s) \approx 5$$

$$u_{in\text{-}r}^2 = L_r$$

Outlet flow velocity ratio,

$$u_{out\text{-}r} = u_{out\text{-}f} / u_{out\text{-}m} = (0.135\ m/s) / (0.023\ m/s) = 6$$

$$u_{out\text{-}r}^2 > L_r$$

Finally, to validate the model through satisfaction of dynamic similitude, ratios of Froude number and Reynolds number were evaluated.

Froude number ratio inside tank,

$$Fr_r = Fr_f / Fr_m = 4.33\times10^{-4} / 4.42\times10^{-4} \approx 1$$

Froude number ratio at inlet,

$$Fr_{in\text{-}r} = Fr_{in\text{-}f} / Fr_{in\text{-}m} = 9.46\times10^{-3} / 9.64\times10^{-3} \approx 1$$

Froude number ratio at outlet,

$$Fr_{out\text{-}r} = Fr_{out\text{-}f} / Fr_{out\text{-}m} = 0.022 / 0.018 = 1.22$$

Reynolds number ratio inside tank,

$$Re_r = Re_f / Re_m = 11{,}145 / 91 = 123 \approx L_r^{1.5}$$

As can be seen from the analysis shown above, apart from a few exceptions, the built pilot-scale model rigorously satisfies the criteria for geometric, kinematic and dynamic similitude. A small discrepancy in terms of similitude can be observed in the design of the outlet opening of the scaled model. The discrepancy arose from replacing rectangular opening of the original tank with circular openings. This issue has been discussed in section 5.2.2 with other assumptions and considerations for design. This disagreement in terms of similitude can be ignored without any effect on the performance of the tank because the actual outlet openings are completely separated from the normal flow of the tank by the effluent collection system or troughs. Hence the disparity in area, flow velocity or Froude number at the outlet opening of the tank will not affect the purpose of the pilot-scale model.

Another noteworthy inconsistency is attributed to the Reynolds number inside the tank. As can be seen from the design calculation, shown in the previous section, the Reynolds number in the original tank is quite high and evidently in the turbulent flow region. Although the full-scale system is operated under almost quiescent conditions with little to no disturbance and very small flow velocity, the flow becomes turbulent owing to the magnitude of the tank dimensions. Consequently, the flow in the scaled model generates a very small Reynolds number which obviously represents Laminar flow conditions.

As previously discussed, the Reynolds number for a hydraulic model should remain in the same flow region as the original unit, although this is not always possible for designs based on the Froude number criterion. The only solution to this problem is a vertically distorted model, which in this case would completely spoil the purpose of the scaling. A vertically distorted model would not be able to represent the complete flow pattern of the original system with corresponding hydrodynamic trends. Thus, the Reynolds number criterion for dynamic similitude was relaxed during design with the assumption that the resistance to flow caused by fluid viscosity is negligible. The dynamic similitude was therefore satisfied in terms of inertial and gravity forces, which are the most significant forces acting on the system.

Thus, all the required similitude criteria are satisfied rendering the built pilot-scale model a valid one.

5.3. Operation of Pilot-Scale Model

After building the pilot-scale model, normal operation of the scaled unit was investigated by conducting a tracer study. Before doing the tracer study, the large tank was placed in an appropriate laboratory space with necessary plumbing arrangements. The tank was connected to a reservoir via a 1.5 HP reciprocating pump for continuous feed. Copper manifolds and rubber hoses were used to connect the pump outlet to the ten inlets of the tank. An in-line ball valve coupled with a rotameter was placed before the manifolds for flow monitoring and control. Hoses with appropriate diameter were connected to the outlet and one end of the hopper for discharge and draining of the tank. A unique metal structure was built using Unistrut® products to lay the tank. Proper fittings and struts were selected on the basis of load bearing capacity and load distribution of the fully filled tank. Images showing different features of the connected and operational scaled tank are presented in Appendix D.

5.3.1. Tracer Study

A tracer study is conducted on a reactor or process unit by injecting a tracer at the inlet of the tank and measuring the concentration of tracer coming out from the outlet, at fixed time intervals. The generated tracer concentration data, when normalized and plotted against corresponding times, gives the Residence Time Distribution (RTD) curve. The RTD curve helps to develop an understanding of the mixing characteristics within a vessel. Two idealized models exist in terms of mixing in a reactor. They are the Continuous-flow Stirred Tank Reactor (CSTR) and the Plug Flow Reactor (PFR). The CSTR behaves as a homogeneously mixed tank with infinite dispersion and back-mixing

while the PFR model assumes zero back-mixing and zero axial dispersion within the tank (Levenspiel, 1996). When a tracer is injected into a CSTR, instantaneous mixing occurs and the concentration inside the tank is assumed to be equal to the concentration exiting the tank. In a PFR, the tracer moves through the tank as plugs of fluid and exits the tank, after a time delay, with exactly the same trends as it was injected. For an ideal PFR, the time delay represents the Hydraulic Retention Time (HRT) of the vessel. Under practical conditions, the mixing characteristics in a reactor usually falls somewhere between the two ideal categories. A tracer study helps determine the level of axial dispersion, short circuiting and closeness to ideal behavior in terms of mixing for a reactor or vessel.

While conducting a tracer study, the tracer should be non-reactive in nature and should be introduced into the fluid stream at the inlet of the vessel without upsetting its hydrodynamic condition. The two most common methods for introducing tracer are pulse or slug input and step input. In case of a pulse input, a small amount of tracer with predetermined concentration is injected into the inlet stream of the reactor instantaneously, much like a pulse or a slug. While for a step input, known concentration of tracer is injected into the vessel in a steady and continuous manner to approach a step function. The tracer response from a step input often tends to flatten out some of the details in flow condition while a pulse response can reveal them quite distinctively.

A pulse input was chosen for the study and 45 mL of an aqueous Potassium Chloride (KCl) solution with a concentration of 1.61 M was used as the tracer. The tracer was introduced into the flow stream at the outlet of the reservoir, preceding the pump, using a disposable syringe. Steady state operation was ensured before the tracer injection and the

flow rate was maintained at 1.65 gpm (6.25 L/min) throughout the experiment. The flow rate falls within the operational range of the unit and represents a full-scale flow rate of about 28 ML/day. This corresponds to a theoretical HRT of about 83 min for the pilot-scale model. A summary of the experimental conditions for the tracer study are stated in Table 5.2. Raw data from the study is tabulated in Appendix C-3.

Table 5.2: Summary of Experimental Parameters for Tracer Study

Tank Flow Rate, v (L/min)	Tank Volume, V (L)	Avg. Flow Velocity, u (m/s)	Theoretical HRT, τ (min)	Used Tracer Conc. (mg/L)	Used Tracer Volume (mL)	Mass of Tracer, M (mg)	M/v (mg.min/L)
6.25	516.128	0.000616	83	119892	45	5395.13	863.88

The tracer response was continuously monitored and recorded in terms of conductivity, measured as μS/cm, using a conductance-resistance meter (YSI Model 34) and a dip conductivity cell (YSI 3417). The conductivity measurements were taken by immersing the cell in the central outlet channel and readings were taken until the response data reached a steady region, close to the value at time zero. Both the conductivity meter and the conductivity cell were calibrated at 20°C before the tracer experiment and a calibration curve was generated as shown in Figure 5.4. The calibration data are listed in Appendix C-2. For all instances, a control measurement was taken using DI water before taking any other measurements. Also, system temperature was monitored and recorded throughout the experiment. Necessary adjustments for the control and temperature were applied to the conductivity data collected during the experiment. Subsequently, the conductivity values were converted into concentration values using the

calibration curve. Time scale for the recordings was adjusted by subtracting the lag time required for the tracer to reach tank inlet from the injection point.

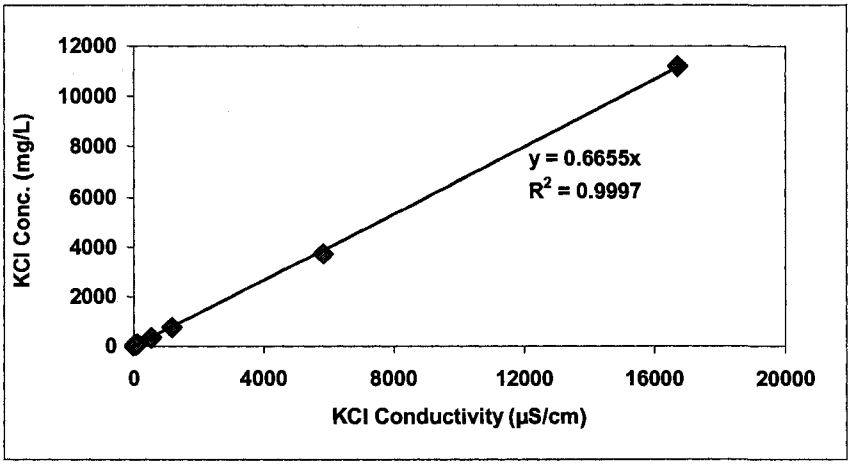

Figure 5.4: KCl Calibration Curve at 20°C

5.3.2. Results and Discussion

The first step in presenting the results of a tracer study is the construction of the tracer response curve in terms of tracer concentration vs. time as shown in Figure 5.5. This experimental curve is then converted into the RTD curve or E_t curve by changing the concentration (C) scale so that the area under the curve is unity. This is achieved simply through dividing the concentration readings by the numerical value of M/v. The E_t curve can be further modified into an E curve, in which both the area and mean are unity. This is done by converting the E_t scale into dimensionless E_θ scale and converting the time (t) scale into dimensionless θ scale. In order to do this, the E_t values are multiplied with and the t values are divided by the mean residence time ($\bar{t}$) (Levenspiel, 1996).. All of the curves, *i.e.* the response curve, the E_t curve and the E curve, have the same shape.

$$E_t = \frac{v}{M}C,\ E_\theta = \bar{t}E_t \text{ and } \theta = \frac{t}{\bar{t}} \qquad (5.19)$$

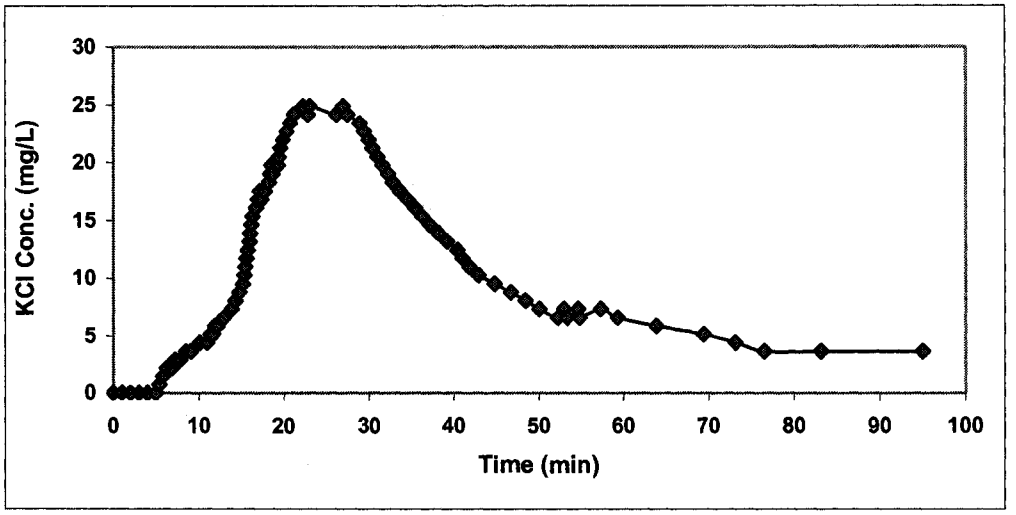

Figure 5.5: Tracer Response Curve

From the response curve shown above, it is evident that the mean residence time is reached well ahead of the theoretical HRT. This type of early curve is a sure sign of stagnant backwaters and short circuiting. Because of the presence of stagnant volume, most of the tracer enters the active vessel volume and leaves earlier than the theoretical HRT generating a short circuit. Some of the tracer, that enters the relatively stagnant region, leaves the vessel very slowly producing a long tail as evident in the figure. Thus, ignoring the long tail gives an approximation of the active vessel volume and the difference between this and the total tank volume gives the relatively stagnant vessel volume. According to mass balance, the total area under the response curve should be equal to the value of M/v as given in Table 5.2. Thus, the results of the tracer study were checked for consistency by evaluating the area under the curve.

Two more characteristic measures for describing tracer curves are the mean residence time ($\bar{t}$) and the variance (σ^2). The mean residence time represents the value of observed HRT for the vessel, while the variance gives an idea about how spread out the curve is.

Based on the data collection method, these values were calculated from the tracer response by using the following formulas (Levenspiel, 1996) and the results are given in Table 5.3.

$$\text{Area under the curve} = \int_0^\infty C dt = \sum_{i=1}^{n} C_i \Delta t_i \tag{5.20}$$

$$\bar{t} = \frac{\int_0^\infty tCdt}{\int_0^\infty Cdt} = \frac{\sum_{i=1}^{n-1}(t_{i+1}+t_i)(C_{i+1}+C_i)(t_{i+1}-t_i)}{2\sum_{i=1}^{n-1}(C_{i+1}+C_i)(t_{i+1}-t_i)} \tag{5.21}$$

$$\sigma^2 = \frac{\int_0^\infty t^2 Cdt}{\int_0^\infty Cdt} - \bar{t}^2 = \frac{\sum_{i=1}^{n-1}(t_{i+1}+t_i)^2(C_{i+1}+C_i)(t_{i+1}-t_i)}{4\sum_{i=1}^{n-1}(C_{i+1}+C_i)(t_{i+1}-t_i)} - \bar{t}^2 \tag{5.22}$$

Table 5.3: Summary of Experimental Results from Tracer Response Curve

Model	Theoretical HRT, τ (min)	Observed HRT, $\bar{t}$ (min)	$\bar{t}/\tau$	Area Under Curve (mg.min/L)	Observed Variance, σ^2	Active Vessel Volume (m^3)	Stagnant Vessel Volume (m^3)
Pilot-Scale	83	39	0.472	842.83	432	168.622	347.506
Full-Scale†	254	122	0.480	--	--	--	--

†The full-scale data was collected from a clarifier study conducted at Gold Bar WWTP by CPE Services Inc. in 2002.

The data from Table 5.3 clearly indicates that the pilot-scale model behaved in a closely similar fashion as the full-scale system. The ratio of the observed hydraulic retention time to the theoretical value is close to each other for the two systems. The area under the curve was slightly less than the value of M/v, as given in Table 5.2, which indicates that not all of the tracers have left the system. However, the values are pretty close indicating a consistent and valid study. From the tracer response curve an

approximation of the active and relatively stagnant vessel volume was determined, as shown in the table, by ignoring the long tail of the curve. Upon ignoring the long tail, a mean residence time of 27 min was obtained, from which the active vessel volume was calculated. According to the study, only about 33% of the total volume of the vessel was active while the rest (about 67%) was relatively stagnant.

Different methods are available for analyzing the results of a tracer study in order to explain the flow behavior of the vessel. Among them the most common methods are the Axial Dispersion and Tanks-in-Series models (Levenspiel, 1996) and the Point Analysis method (Thirumurthi, 1969). The axial dispersion model is based on the ideal plug flow behavior of a vessel with a superimposed component for axial dispersion or diffusion. The magnitude of the axial dispersion is quantified by the dimensionless Dispersion Number (N_D), given by:

$$N_D = \frac{D}{uL} = \frac{1}{Pe} \qquad (5.23)$$

where, D is the longitudinal dispersion coefficient, u is the average flow velocity, L is the characteristic length of the vessel and Pe represents the Peclet number.

For an ideal PFR, zero axial dispersion is present, hence $N_D = 0$, $Pe = \infty$, while for an ideal CSTR, infinite axial dispersion renders $N_D = \infty$, $Pe = 0$. The dispersion number is determined by studying the tracer response or RTD curve and taking measurements of observed HRT or mean residence time ($\bar{t}$) and variance (σ^2). The method for determining the dispersion number varies depending on the extent of deviation from ideal plug flow behavior. For large deviations from ideal behavior, which is the case for this study, the dispersion model is highly influenced by the boundary conditions of the reactor. The

boundary conditions for a tracer study imply the point of tracer injection and the point of measurement. The system under investigation represents a closed system because the tracer was introduced into the fluid stream well before entering the tank, while the measurements were taken in the central outlet channel, which is completely separated from the normal flow of the tank. For such a system, the dispersion number maintains the following relationship (Levenspiel, 1996):

$$\sigma_\theta^2 = \frac{\sigma^2}{\bar{t}^2} = 2(N_D) - 2(N_D)^2\left(1 - e^{-1/N_D}\right) \qquad (5.24)$$

From the above relationship, the dispersion number for the system was calculated using the Solver function of Microsoft Excel. Consequently, the dispersion coefficient was determined from the dispersion number using the length and average flow velocity of the tank. The obtained value of the dispersion number was evaluated by comparing the shape of the E curve with published information (Levenspiel, 1996) corresponding to a dispersion number of 0.2. The results of this analysis are presented in Table 5.4.

Table 5.4: Results of Axial Dispersion Model Analysis

$\bar{t}$ (min)	σ^2	σ_θ^2	Dispersion Number, D/uL	Peclet number, Pe	Dispersion Coefficient, D (m^2/s)
39	432	0.282	0.17	5.88	0.00032

In the tanks-in-series model, the flow behavior in a reactor is characterized by a series of N equal volume hypothetical CSTRs. The number of tanks (N), given by an integer, represents the extent of axial dispersion within the reactor. At N = 1, infinite dispersion exists indicating an ideal CSTR, while N = ∞ indicates ideal plug flow behavior. One

method of determining the appropriate value of N is to construct E curves for various N and compare them with experimentally obtained E curves. For the tanks-in-series model, the E curves are generated using the following relationship (Levenspiel, 1996):

$$E_\theta = \frac{N(N\theta)^{N-1}}{(N-1)!} e^{-N\theta} \qquad (5.25)$$

Several E curves were generated and compared to the experimentally obtained E curve, using different values of N. For this experiment, the closest approximation by the tanks-in-series model was generated at N = 7, as shown in Figure 5.6. As seen from the figure, the variances or spreads of the two curves are close to each other but the curve generated by the model exhibits slightly delayed response than the actual one. This indicates that the generated model response does not fully account for the short-circuiting taking place within the tank. In this situation, the axial dispersion model was found to provide a better and closely matching response than the tanks-in-series model.

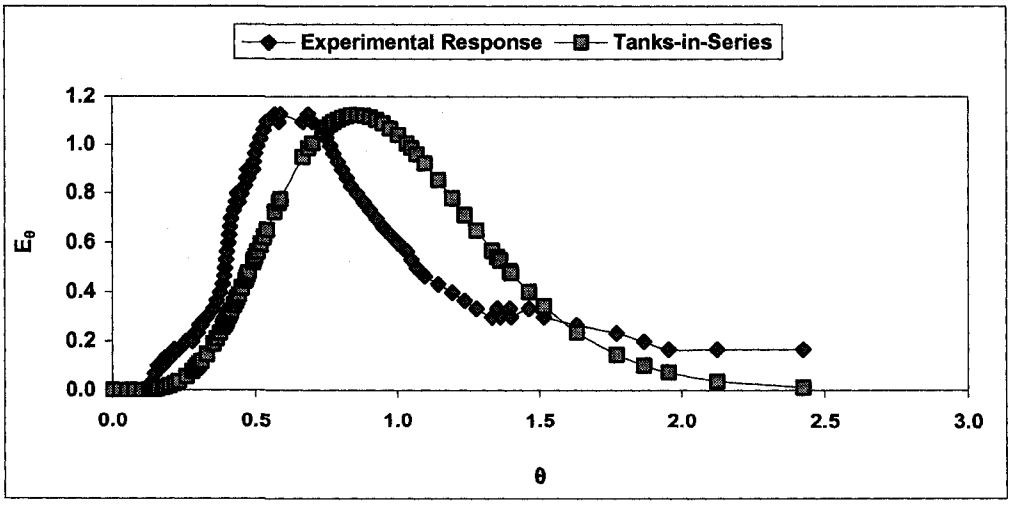

Figure 5.6: Experimental Data and Tanks-in-Series Model Response

The method of point analysis depends on examination of the experimental response curve at various points of time. These points include t_{10}, t_{90}, t_p and t_g. Values of t_{10} and t_{90} represent, respectively, the times for 10% and 90% of the tracer to exit reactor. The value of t_p provides the time to reach maximum tracer concentration and t_g gives the time to reach center of gravity of the curve or the mean residence time ($\bar{t}$). An estimate of mixing or axial dispersion can be represented by the Morrill Index of mixing, given as t_{90}/t_{10}. Also, the index of short-circuiting is provided by the value of $1-t_p/t_g$. Calculated results from the point analysis are provided in Table 5.5. The results indicate high level of short-circuiting which is consistent with the experimental response.

Table 5.5: Results of Point Analysis

t_{10} (min)	t_{90} (min)	t_p (min)	t_g or $\bar{t}$ (min)	Morill Index of Mixing (t_{90}/t_{10})	Index of Short-Circuiting [$1-(t_p/t_g)$]
17.56	72.16	23.07	39	4.11	0.41

5.3.3. Visual Observation

In addition to the tracer study, the operation of the scaled tank was closely observed, by visual means, using a fluorescent dye. This was done in order to have an idea of the different hydrodynamic occurrences within the tank. Operation of the tank was visually examined at different flow rates and the observations indicated the presence of density waterfall at all flow rates. Although an inlet baffle was present, but the baffle did not break off the density waterfall completely. Figure 5.7 shows an image of the actual density waterfall in the scaled tank.

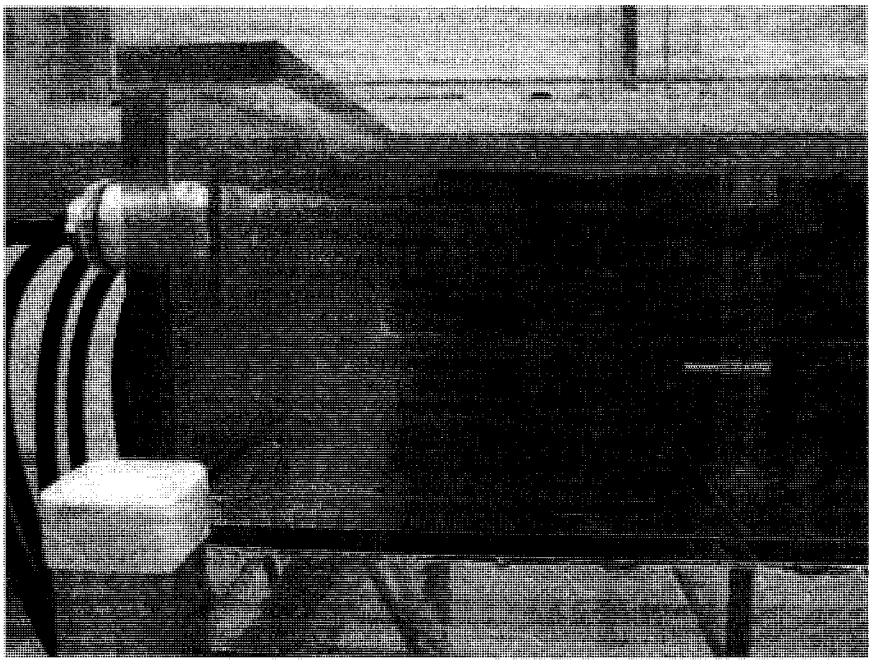

Figure 5.7: Density Waterfall in Pilot-Scale Model

For each observation, the density waterfall at the inlet zone of the tank quickly developed into a density current. The density current is dependent on the difference in densities between the influent stream and the fluid within the tank. In this case, the density difference was mainly caused by the temperature difference between the water in the tank and that in the reservoir. It was noted that a very small difference in temperature caused the formation of density currents. Also, the development and behavior of density currents varied greatly with only minor change in conditions in terms of temperature. Figure 5.8 shows the images of two different formations of density currents under almost similar conditions. Both the images were taken right after the inlet zone, when the density waterfall developed into the currents. The image on the left shows a density current which is traveling along the surface of the tank while the image on the right indicates a bottom density current. The bottom density current is actually representative of the full-scale clarifier operation.

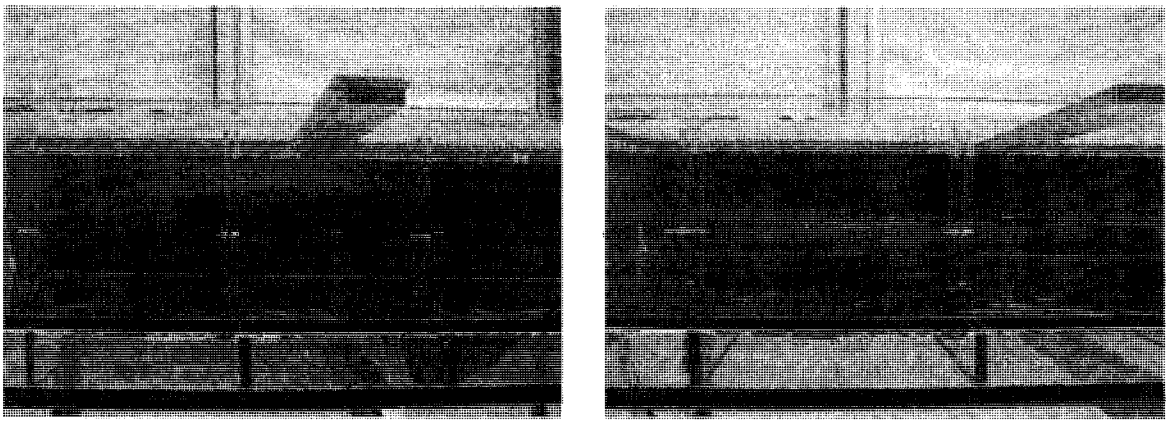

Figure 5.8: Formation of Density Currents in Pilot-Scale Model

Because of the different formation of density currents under slightly changed conditions, the scaled tank operation was unstable, thus it was extremely hard to generate consistent data from conventional tracer study. Conventional tracer study is based on the measurement of tracer concentration at a single point, which is insufficient for this system. If a cross-sectional plane is selected along the direction of the flow near the outlet zone and the concentration passing through the plane is measured over time then the collected data would generate a more stable and consistent response. This can be achieved by employing the laser measurement technique known as Planar Laser Induced Fluorescence (PLIF). Visual observation confirmed roughly uniform flow distribution along the width of the tank, which means that the measurement plane can be located anywhere along the tank width.

As a part of visual observation, the flow condition of the tank was examined by placing an in-tank full width baffle halfway in the settling zone. The baffle was placed at a depth so as to allow the flow to pass through the bottom of the tank. The baffle interrupted and cut off the bottom density current and as a result the current was dissipated further down the flow path, as shown in Figure 5.9. In the figure, the right

hand image indicates the interruption of the density current by the baffle, while the left image shows the resulting dissipation of the current.

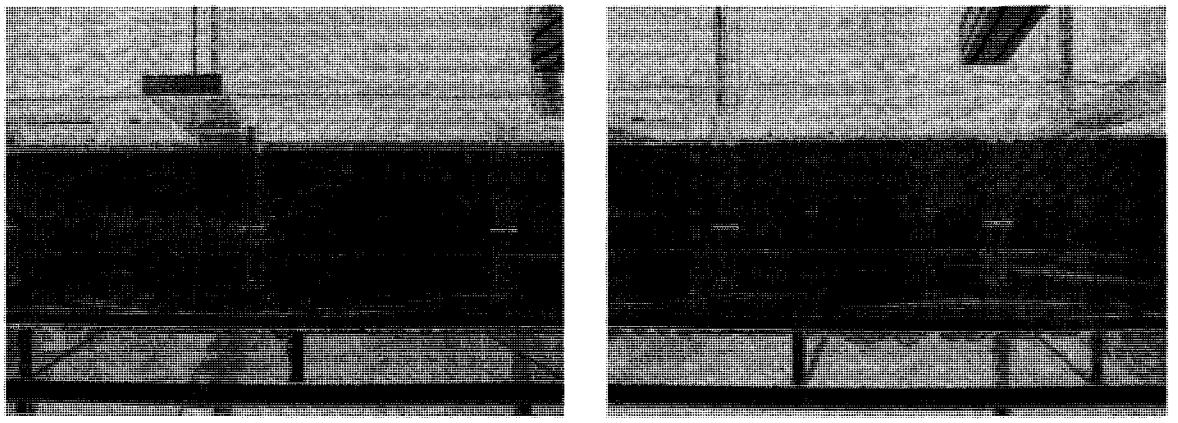

Figure 5.9: Effect of Baffle on Bottom Density Current

The presence of density current induces short-circuiting and generates a relatively stagnant region within the secondary clarifier system. By placing in-tank baffles, the extent of this stagnant region can be reduced considerably, thereby increasing the effective HRT of the system. The pilot-scale model was designed and equipped with provisions of future study that will help in determining the optimum number and placement of baffles in order to improve the overall hydrodynamics of the system.

6.0. Conclusions and Recommendations

The concluding chapter of this study reflects on different highlighted aspects that were revealed and discussed in the previous chapters. Based on the findings from the literature review, research was conducted to understand the activated sludge properties, sludge settling characteristics and the existing hydrodynamics of the unit. The results of these studies are presented in the preceding three chapters. Major findings from the research are briefly presented herewith.

6.1. Conclusions

The properties of incoming MLSS, return sludge and effluent from the selected final clarifier were evaluated in three different times of the year to observe the seasonal variation.

- For influent sludge, the fraction of suspended solids was higher in winter than the other two seasons due to the low amount of dissolved solids in winter.
- The suspended and total solids concentration in return sludge samples increased consistently from fall to spring through winter.
- In case of clarifier effluent, the spring samples, corresponding to the spring runoff, had higher suspended solids concentration than the other seasons. The spring samples had slightly higher suspended solids than the best practicable standard.
- The seasonal differences were quite small in terms of percentage suspended solids removal. Highest removal among the three was during the winter operation while spring operation exhibited the lowest removal owing to the runoff event.

- In terms of particle size distribution, the three seasonal influent samples exhibited more or less similar trend in the characteristic size range of 2-50 μm.
- Based on the results, it can be said that an increase in plant capacity caused by a runoff contributes mostly to the count of influent particles in the 15-25 μm size range.
- For effluent particle size distribution, samples had negligible number of particles beyond the size of 30 μm. The lower size range of 2-5 μm had the prevailing counts for all of the samples while having very small counts of larger particles.

Settling column experiments were carried out to investigate sludge settling behavior. Also, SVI of the clarifier influent was determined in three seasons to have an idea of the seasonal sludge settle-ability.

- The settled sludge volume and the SVI were lowest for the spring sludge indicating that the sludge settled faster and per unit mass of the settled sludge occupied lesser volume, as compared to the other two samples.
- The highest settled sludge volume and SVI were produced by the winter influent sample, indicating slower settling than the other two seasons.
- By conducting a Type II settling test, it was proven that flocculent settling is the governing settling regime within the supernatant region of the final clarifier.
- Under normal operating conditions and overflow rate, more than 80% removal of suspended solids can be achieved near the top water surface within the clarifier.
- Results from batch settling tests confirmed that compression settling is the governing settling regime within the sludge zone of the clarifier.
- The zone settling velocity of the influent sludge was approximately 24 m/day for an influent suspended solids concentration of about 3.9 kg/m^3 during wet-weather conditions.

- For a high influent flow rate of 50 ML/day, the operational underflow rate is approximately 27 ML/day with a sludge recycle ratio of about 49%.
- The operational solids loading at wet-weather conditions of the clarifier is approximately 99 kg/m^2.day, less than the limiting solids flux of about 140 kg/m^2.day, which indicates that the secondary clarifier does not have a problem of solids overloading.
- Rising sludge problems encountered during the batch settling test indicate presence of high levels of nitrate in the MLSS, coming from the fourth pass of the preceding bioreactor.
- A study of model fit, conducted with the batch settling data, indicated that the Vesilind model produced a better fit as compared to the other settling velocity models.

The current design and flow distribution of the selected secondary clarifier was studied and based on the acquired data a pilot-scale reproduction of the clarifier was designed and manufactured. The design of the pilot-scale unit was validated and the unit was prepared for further study and enhancement in design.

- Study of the design and operation of the existing clarifier indicated that the unit operates within the standard and typical range of key design criteria like overflow rate, solids loading rate, weir overflow rate, sludge recycle etc.
- From the results of the tracer study, it was found that the pilot-scale model behaved in a closely similar fashion as the full-scale system, in terms of the ratio of observed hydraulic retention time to its theoretical value.
- Results from the tracer study indicated presence of stagnant backwaters and short circuiting. According to the study, only about 33% of the total volume of the vessel was active while the rest (about 67%) was relatively stagnant.

- Analysis of the tracer response results produced an axial dispersion number of 0.17 and an index of short-circuiting of 0.41.
- Visual examination of the operational scaled tank at different flow rates indicated the presence of density waterfall followed by density currents at all flow rates.

6.2. Recommendations

Based on the results of this research, some operational problems associated with the selected clarifier at Gold Bar WWTP were identified. One of the major problems was the rising sludge caused by the presence of nitrates in the MLSS. In order to abate this problem, the biological denitrification process in the preceding bioreactors should be evaluated. The amount of internal recycle within the bioreactor may be increased to encourage denitrifiaction in the bioreactor. Also, the retention time of the settled sludge in the secondary clarifier can be reduced to prevent this problem. This can be done by increasing the sludge recycle ratio.

Tracer study conducted on the scaled tank indicated high levels of short-circuiting and relatively stagnant regions within the clarifier. This problem may be solved by placing in-tank baffles that will reduce the extent of stagnant region, thereby increasing the effective hydraulic retention time of the system. Another major problem in terms of tank hydrodynamics was identified through visual examination of the scaled tank operation. This problem is the formation of density waterfall and density currents within the tank. This again can be reduced by the strategic placement of in-tank baffles. To facilitate further study in determining the optimum number and placement of baffles, the pilot-scale model was designed and equipped with appropriate provisions.

While conducting further experimental study with the scaled tank, PLIF technique is recommended for use. This is because the laser technique can take measurements over a cross-sectional plane and hence can capture the density currents traveling at different depths. The visual observation of the scaled tank indicated that most of the hydrodynamic anomaly within the system is caused by differential density, which is best described by the dimensionless densimetric Froude number. Hence, to completely reproduce the flow phenomena, the densimetric Froude numbers in the scaled model and the full-scale system should be equal. To satisfy the similitude of densimetric Froude number, MLSS from the secondary clarifier at Gold Bar can be used in the scaled tank.

References

Adams, E. W. and Rodi, W. (1990); Modeling flow and mixing in sedimentation tanks; *Journal of Hydraulic Engineering*; **116**(7); 895-913.

Akca, L., Kinaci, C. and Karpuzcu, M. (1993); Model for optimum design of activated sludge plants; *Water Research*; **27**(9); 1461-1468.

American Public Health Association (1999); *Standard Methods for the Examination of Water and Wastewater*; 20th Ed.; American Public Health Association; Washington.

American Water Works Association (1999); *Water Quality and Treatment : A Handbook of Community Water Supplies*; 5th Ed.; McGraw-Hill; New York.

Anderson, N. E. (1945); Design of final settling tanks for activated sludge; *Sewage Works Journal*; **17**(1); 50-63.

Andreadakis, A. D. (1993); Physical and chemical properties of activated sludge floc; *Water Research*; **27**(12); 1707-1714.

Automation Creations Inc. (2008); http://www.matweb.com/search/DataSheet.aspx?MatGUID=ff7e01a9f8dd4d9aac49418fe4f4b337; Retrieved: January 3, 2008.

Barahona, L. and Eckenfelder, W. W., Jr. (1984); Relationships between organic loading and zone settling velocity in the activated sludge process; *Water Research*; **18**(1); 91-94.

Barber, J. B. and Veenstra, J. N. (1986); Evaluation of biological sludge properties influencing volume reduction; *Journal Water Pollution Control Federation*; **58**; 149-156.

Barbusinski, K. (2000); Influence of floc size on activated sludge volume index; *Environmental Protection Engineering*; **26**(1); 45-53.

Barbusinski, K. and Koscielniak, H. (1995); Influence of substrate loading intensity on floc size in activated sludge process; *Water Research*; **29**(7); 1703.

Battistoni, P., Fava, G. and Ruello, M. L. (1993); Heavy metal shock load in activated sludge uptake and toxic effects; *Water Research*; **27**(5); 821-827.

Blackall, L. L., Tandoi, V. and Jenkins, D. (1991); Continuous culture studies with *Nocardia amarae* from activated sludge and their implications for foaming control; *Research Journal of the Water Pollution Control Federation*; **63**(1); 44-49.

Boedeker Plastics Inc. (2008); http://www.boedeker.com/acryl_p.htm; Retrieved: January 3, 2008.

Bond, A. W. (1961); Behaviour of suspensions; *Institution of Water Engineers -- Journal*; **15**(7); 494-516.

Bradley, T. and Kharkar, S. (1996); Foam factors: bursting some bubbles in management mythology; *Water Environment and Technology*; **8**(3); 49.

Bretscher, U., Krebs, P. and Hager, W. H. (1992); Improvement of flow in final settling tanks; *Journal of Environmental Engineering*; **118**(3); 307-321.

Bye, C. M. and Dold, P. L. (1998); Sludge volume index settleability measures: Effect of solids characteristics and test parameters; *Water Environment Research*; **70**(1); 87-93.

Camp, T. R. (1946); Sedimentation and the design of settling tanks; *Transactions of the American Society of Civil Engineers*; **111**; 895-936.

Camp, T. R. (1953); Studies of sedimentation basin design *Sewage and Industrial Wastes*; **25**(1); 1-12.

Casey, T. G., Ekama, G. A., Wentzel, M. C. and Marais, G. R. (1995); Filamentous organism bulking in nutrient removal activated sludge systems paper 1: a historical overview of causes and control; *Water S.A.*; **21**(3); 231-238.

Casey, T. G., Wentzel, M. C., Ekama, G. A., Loewenthal, R. E. and Marais, G. (1994); Hypothesis for the causes and control of anoxic-aerobic (AA) filament bulking in nutrient removal activated sludge systems; *Water Science and Technology*; **29**(7); 203-212.

Chen, G. W., Chang, I. L., Hung, W. T. and Lee, D. J. (1996); Regimes for zone settling of waste activated sludges; *Water Research*; **30**(8); 1844-1850.

Chinniah, K. (2006); *Standards and Guidelines for Municipal Waterworks, Wastewater, and Storm Drainage Systems*; Alberta Environment.

Cho, S. H., Colin, F., Sardin, M. and Prost, C. (1993); Settling velocity model of activated sludge; *Water Research*; **27**(7); 1237-1242.

Chua, H., Yu, P. H. F., Sin, S. N. and Cheung, M. W. L. (1999); Sub-lethal effects of heavy metals on activated sludge microorganisms; *Chemosphere*; **39**(15); 2681-2692.

Chudoba, J., Cech, J. S., Farkac, J. and Grau, P. (1985); Control of activated sludge filamentous bulking: experimental verification of a kinetic selection theory; *Water Research*; **19**(2); 191-196.

Clarke, A. R. and Forster, C. F. (1983); Significance of ATP in the settlement of activated sludge; *Journal of Chemical Technology and Biotechnology*; **33**(2); 127-135.

Clayfield, G. W. (1974); Respiration and denitrification studies on laboratory and works activated sludges; *Water Pollution Control (Maidstone, England)*; **73**(1); 51-76.

Coe, H. S. and Clevenger, G. H. (1916); Laboratory method for determining the capacities of slime-settling tanks; *Transactions of the American Institute of Mining Engineers*; **55**; 356 - 384.

Daigger, G. T. (1995); Development of refined clarifier operating diagrams using an updated settling characteristics database; *Water Environment Research*; **67**(1); 95-100.

Daigger, G. T. and Roper, R. E. (1985); The relationship between SVI and activated sludge settling characteristics; *Journal Water Pollution Control Federation*; **57**(8); 859-866.

Deininger, A., Gunthert, F. W. and Wilderer, P. A. (1996); The influence of currents on circular secondary clarifier performance and design; *Water Science and Technology*; **34**(3-4); 405-412.

Dick, R. I. (1971); Role of activated sludge final settling tanks; *Journal of the Sanitary Engineering Division-Asce*; **97**(NSA5); 759-&.

Dick, R. I. (1972); Gravity thickening of sewage sludges; *Effluent & Water Treatment Journal*; **12**(11); 597-605.

Dick, R. I. (1976); Folklore in the design of final settling tanks; *Journal Water Pollution Control Federation*; **48**(4); 633-644.

Dick, R. I. and Ewing, B. B. (1967); Evaluation of activated sludge thickening theories; *Journal of the Sanitary Engineering Division Proceedings of the American Society of Civil Engineers*; **93**(SA4); 9-29.

Dick, R. I. and Vesilind, P. A. (1969); The sludge volume index - what is it?; *Journal Water Pollution Control Federation*; **41**(7); 1285-&.

Dick, R. I. and Young, K. W. (1972); *Analysis of thickening performance of final settling tanks*; Proceedings of 27th Purdue Industrial Waste Conference; Lafayette, Indiana, USA; Purdue University; 33-54.

Dixon, D. C. (1978); Momentum balance aspects of free-settling theory III, transient compression resistance; *Separation Science and Technology*; **13**(9); 753-766.

Dixon, D. C. (1982); Compression effects in batch settling tests; *American Society of Civil Engineers, Journal of the Environmental Engineering Division*; **108**(EE6); 1171-1191.

Dupont, R. and Dahl, C. (1995); One-dimensional model for a secondary settling tank including density current and short-circuiting; *Water Science and Technology*; **31**(2); 215-224.

Dupont, R. and Henze, M. (1992); Modelling of the secondary clarifier combined with the Activated Sludge Model No. 1; *Water Science and Technology*; **25**(6); 285-300.

Eikelboom, D. H. (1977); Identification of filamentous organisms in bulking activated sludge; *Progress in Water Technology*; **8**(6); 153-161.

Ekama, G. A., Barnard, J. L., Günthert, F. W., Krebs, P., McCorquodale, J. A., Parker, D. S. and Wahlberg, E. J. (1997); *Secondary settling tanks: theory, modelling, design and operation*; IAWQ Scientific and Technical Report no. 6; IAWQ; London, England.

Ekama, G. A. and Marais, G. v. R. (1986); Sludge Settlability and Secondary Settling Tank Design Procedures; *Water Pollution Control (Maidstone, England)*; **85**(1); 101-113.

Ettema, R., Arndt, R., Roberts, P. and Wahl, T. (2000); *Hydraulic modeling : concepts and practice*; American Society of Civil Engineers; Reston, VA.

Finch, J. and Ives, H. (1950); Settleability indexes for activated sludge; *Sewage and Industrial Wastes*; **22**(6); 833-839.

Finstein, M. S. and Heukelekian, H. (1967); Gross dimensions of activated sludge flocs with reference to bulking; *Water Pollution Control Federation -- Journal*; **39**(1); 33-40.

Fitch, B. (1962); Sedimentation process fundamentals; *Society of Mining Engineers -- Transactions*; **223**(2); 129-136.

Fitch, B. (1966); A mechanism of sedimentation; *Industrial & Engineering Chemistry Fundamentals*; **5**(1); 129-&.

Fitch, B. (1975); Current theory and thickener design; *Filtration and Separation*; **12**(5-6); 480-488, 636-638.

Fitch, B. (1979); Sedimentation of flocculent suspensions: State of the art; *AIChE Journal*; **25**(6); 913-930.

Fitch, B. (1983); Kynch theory and compression zones; *AIChE Journal*; **29**(6); 940-947.

Fitch, B. and Kos, P. (1976); Towards a more meaningful index of sludge quality; *Journal Water Pollution Control Federation*; **48**(8); 1979-1987.

Fitch, E. B. (1957); The significance of detention in sedimentation; *Sewage and Industrial Wastes*; **29**(10); 1123-1133.

Font, R. (1988); Compression zone effect in batch sedimentation; *AIChE Journal*; **34**(2); 229-238.

Foot, R. J. (1992); Effects of process control parameters on the composition and stability of activated sludge; *Journal of the Institution of Water and Environment Management*; **6**(2); 215-228.

Foot, R. J., Robinson, M. S. and Forster, C. F. (1994); Systematic activated sludge bulking and foam control; *Water Science and Technology*; **29**(7); 213-220.

Ford, D. L. and Eckenfelder, J. W. W. (1967); Effect of process variables on sludge floc formation and settling characteristics; *Water Pollution Control Federation -- Journal*; **39**(11); 1850-1859.

Forster, C. F. (1968); Surface of activated sludge particles in relation to their settling characteristics; *Water Research*; **2**(11); 767-776.

Forster, C. F. (1971); Activated sludge surfaces in relation to the sludge volume index; *Water Research*; **5**(10); 861-870.

Forster, C. F. (1982); A further examination of mass flux theory as applied to activated sludge settlement; *Biotechnology Letters*; **4**(6); 381-386.

Forster, C. F. (1985a); Factors involved in the settlement of activated sludge I: nutrients and surface polymers; *Water Research*; **19**(10); 1259-1264.

Forster, C. F. (1985b); Factors involved in the settlement of activated sludge II: the binding of polyvalent metals; *Water Research*; **19**(10); 1265-1271.

Forster, C. F. and Dallas-Newton, J. (1980); Activated sludge settlement - some suppositions and suggestions; *Water Pollution Control (Maidstone, England)*; **79**(3); 338-351.

Ganczarczyk, J. J. (1970); Variation of the activated sludge volume index; *Water Research*; **4**(1); 69-77.

Ganczarczyk, J. J., Zahid, W. M. and Li, D. H. (1992); Physical stabilization and embedding of microbial aggregates for light microscopy studies; *Water Research*; **26**(12); 1695-1699.

George, D. B. and Keinath, T. M. (1978); Dynamics of continuous thickening; *Journal Water Pollution Control Federation*; **50**(11); 2560-2572.

Giokas, D. L., Daigger, G. T., Von Sperling, M., Kim, Y. and Paraskevas, P. A. (2003); Comparison and evaluation of empirical zone settling velocity parameters based on sludge volume index using a unified settling characteristics database; *Water Research*; **37**(16); 3821-3836.

Gohle, F., Finnson, A. and Hultman, B. (1996); Dynamic simulation of sludge blanket movements in a full-scale rectangular sedimentation basin; *Water Science and Technology*; **33**(1); 89-99.

Govoreanu, R., Saveyn, H., Van der Meeren, P. and Vanrolleghem, P. A. (2004); Simultaneous determination of activated sludge floc size distribution by different techniques; *Water Science and Technology*; **50**(12); 39-46.

Hartel, L. and Popel, H. J. (1992); A dynamic secondary clarifier model including processes of sludge thickening; *Water Science and Technology*; **25**(6); 267-284.

Hassett, N. J. (1964); Mechanism of thickening and thickener design; *Institution of Mining and Metallurgy -- Transactions*; **74**(Part 10); 627-656.

Hazen, A. (1904); On sedimentation; *Proceedings of the American Society of Civil Engineers*; **53**; 45-88.

Henze, M., Dupont, R., Grau, P. and De La Sota, A. (1993); Rising sludge in secondary settlers due to denitrification; *Water Research*; **27**(2); 231-236.

Hermanowicz, S. W. (1998); Secondary clarification of activated sludge: Development of operating diagrams; *Water Environment Research*; **70**(1); 10-13.

Heukelekian, H. and Weisberg, E. (1956); Bound water and activated sludge bulking; *Sewage and Industrial Wastes*; **28**(4); 558-574.

Hilligardt, D. and Hoffmann, E. (1997); Particle size analysis and sedimentation properties of activated sludge flocs; *Water Science and Technology*; **36**(4); 167-175.

Ho, C. F. and Jenkins, D. (1991); The effect of surfactants on *Nocardia* foaming in activated sludge; *Water Science and Technology*; **23**(4-6); 879-887.

Hossain, F. (2004); Activated sludge bulking: A review of causes and control strategies; *Journal of the Institution of Engineers (India): Environmental Engineering Division*; **85**(1); 1-6.

Hultman, B., Lowen, M., Karlsson, U., Li, P. H. and Molina, L. (1991); Prediction of activated sludge sedimentation based on sludge indices; *Water Science and Technology*; **24**(7); 33-42.

Imam, E., McCorquodale, J. A. and Bewtra, J. K. (1983); Numerical modeling of sedimentation tanks; *Journal of Hydraulic Engineering*; **109**(12); 1740-1754.

Javaheri, A. R. and Dick, R. I. (1969); Aggregate size variations during thickening of activated sludge; *Journal Water Pollution Control Federation*; **41**(5, Part 2, Research Suppl); 197-214.

Jenkins, D. and Richard, M. G. (1985); *Causes and control of activated sludge bulking*; Environmental Conference, Proceedings of the Technical Association of the Pulp and Paper Industry; Mobile, AL, USA; TAPPI Press; 197-201.

Jenkins, D., Richard, M. G. and Neethling, J. B. (1983); Causes and control of activated sludge bulking; *Water Pollution Control (Maidstone, England)*; **83**(4); 455-472.

Jorand, F., Boue-Bigne, F., Block, J. C. and Urbain, V. (1998); Hydrophobic/hydrophilic properties of activated sludge exopolymeric substances; *Water Science and Technology*; **37**(4-5); 307-315.

Kalinske, A. A. (1948); Settling characteristics of suspensions in water treatment processes; *American Water Works Association -- Journal*; **40**(2); 113-120.

Keinath, T. M. (1990); Diagram for designing and operating secondary clarifiers according to the thickening criterion; *Research Journal of the Water Pollution Control Federation*; **62**(3); 254-258.

Kim, M. H., Al-Ghusain, I. A., Hao, O. J. and Lim, B. S. (1994); Modeling of nitrate disappearance and sludge rising in a settling column system; *Water Research*; **28**(9); 1861-1872.

Kim, Y., Pipes, W. O. and Chung, P.-G. (1998); Control of activated sludge bulking by operating clarifiers in a series; *Water Science and Technology*; **38**(8-9 pt 7); 1-8.

Kjellerup, B. V., Keiding, K. and Nielsen, P. H. (2001); Monitoring and troubleshooting of non-filamentous settling and dewatering problems in an industrial activated sludge treatment plant; *Water Science and Technology*; **44**(2-3); 155-162.

Knocke, W. R. (1986); Effects of floc volume variations on activated sludge thickening characteristics; *Journal Water Pollution Control Federation*; **58**(7); 784-791.

Knudson, M. K., Williamson, K. J. and Nelson, P. O. (1982); Influence of dissolved oxygen on substrate utilization kinetics of activated sludge; *Journal Water Pollution Control Federation*; **54**(1); 52-60.

Kos, P. (1977); Gravity thickening of water-treatment-plant sludges *Journal of the American Water Works Association*; **69**(5); 272-282.

Krebs, P. (1991); The hydraulics of final settling tanks; *Water Science and Technology*; **23**(4-6); 1037-1046.

Krebs, P., Armbruster, M. and Rodi, W. (1998); Laboratory experiments of buoyancy-influenced flow in clarifiers; *Journal of Hydraulic Research/De Recherches Hydrauliques*; **36**(5); 831-851.

Krebs, P., Vischer, D. and Gujer, W. (1992); Improvement of secondary clarifiers efficiency by porous walls; *Water Science and Technology*; **26**(5-6); 1147-1156.

Krebs, P., Vischer, D. and Gujer, W. (1995); Inlet-structure design for final clarifiers; *Journal of Environmental Engineering*; **121**(8); 558-564.

Kynch, G. J. (1952); A theory of sedimentation; *Transactions of the Faraday Society*; **48**(2); 166-176.

Laquidara, V. D. and Keinath, T. M. (1983); Mechanism of clarification failure; *Journal Water Pollution Control Federation*; **55**(1); 54-57.

Larsen, P. (1977); *On the hydraulics of rectangular settling basins : Experimental and Theoretical studies*; Dept. of Water Resources Engineering; Lund Institute of Technology; Lund, Sweden.

Lau, A. O., Strom, P. F. and Jenkins, D. (1984); The competitive growth of floc-forming and filamentous bacteria: a model for activated sludge bulking; *Journal Water Pollution Control Federation*; **56**(1); 52-61.

Lechevalier, M. P. and Lechevalier, H. A. (1974); Nocardia amarae sp. nov., an actinomycete common in foaming activated sludge; *International Journal of Systematic Bacteriology*; **24**(2); 278-288.

Levenspiel, O. (1996); *The Chemical Reactor Omnibook*; 5th version.; OSU Book Stores, Inc.; Corvallis, OR.

Li, D. H. and Ganczarczyk, J. J. (1987); Stroboscopic determination of settling velocity, size and porosity of activated sludge flocs; *Water Research*; **21**(3); 257-262.

Li, D. H. and Ganczarczyk, J. J. (1988); Flow through activated sludge flocs; *Water Research*; **22**(6); 789-792.

Li, D. H. and Ganczarczyk, J. J. (1990); Structure of activated sludge flocs; *Biotechnology and Bioengineering*; **35**(1); 57-65.

Li, D. H. and Ganczarczyk, J. J. (1991); Size distribution of activated sludge flocs; *Research Journal of the Water Pollution Control Federation*; **63**(5); 806-814.

Li, D. H. and Ganczarczyk, J. J. (1992); Advective transport in activated sludge flocs; *Water Environment Research*; **64**(3); 236-240.

Lumley, D. J., Balmer, P. and Adamsson, J. (1988); Investigations of secondary settling at a large treatment plant; *Water Science and Technology*; **20**(4-5); 133-142.

Magara, Y., Nambu, S. and Utosawa, K. (1976); Biochemical and physical properties of an activated sludge on settling characteristics; *Water Research*; **10**(1); 71-77.

McCorquodale, J. A., Moursi, A. M. and El-Sebakhy, I. S. (1988); Experimental study of flow in settling tanks; *Journal of Environmental Engineering*; **114**(5); 1160-1174.

McCorquodale, J. A., Yuen, E. M., Vitasovic, Z. and Samstag, R. W. (1991); Numerical simulation of unsteady conditions in clarifiers; *Water Pollution Research Journal of Canada*; **26**(2); 201-222.

McCorquodale, J. A. and Zhou, S. (1993); Effects of hydraulic and solids loading on clarifier performance; *Journal of Hydraulic Research*; **31**(4); 461-477.

Metcalf and Eddy Inc. (2002); *Wastewater Engineering: Treatment, Disposal, and Reuse*; 4th Ed.; McGraw-Hill; New York.

Michaels, A. S. and Bolger, J. C. (1962); Settling rates and sediment volumes of flocculated kaolin suspensions; *Industrial and Engineering Chemistry -- Fundamentals*; **1**(1); 24-33.

Mines, R. O., Vilagos, J. L., Echelberger, W. F. and Murphy, R. J. (2001); Conventional and AWT mixed-liquor settling characteristics; *Journal of Environmental Engineering-Asce*; **127**(3); 249-258.

Mueller, J. A., Morand, J. and Boyle, W. C. (1967); Floc sizing techniques; *Applied Microbiology*; **15**(1); 125-134.

Neufeld, R. D. (1976); Heavy metals-induced deflocculation of activated sludge; *Journal Water Pollution Control Federation*; **48**(8); 1940-1947.

Nguyen, T. P., Hankins, N. P. and Hilal, N. (2007); A comparative study of the flocculation behaviour and final properties of synthetic and activated sludge in wastewater treatment; *Desalination*; **204**(1-3 SPEC ISS); 277-295.

Novak, L., Larrea, L., Wanner, J. and Garcia-Heras, J. L. (1993); Non-filamentous activated sludge bulking in a laboratory scale system; *Water Research*; **27**(8); 1339-1346.

Ostendorf, D. W. (1986); Hydraulics of rectangular clarifiers; *Journal of Environmental Engineering*; **112**(5); 939-952.

Oviedo, M. D. C., Marquez, D. S. and Alonso, J. M. Q. (2002); Toxic effects of metals on microbial activity in the activated sludge process; *Chemical and Biochemical Engineering Quarterly*; **16**(3); 139-144.

Ozbelge, T. A., Ozbelge, H. O. and Altinten, P. (2007); Effect of acclimatization of microorganisms to heavy metals on the performance of activated sludge process; *Journal of Hazardous Materials*; **142**(1-2); 332-339.

Ozinsky, A. E. and Ekama, G. A. (1995); Secondary settling tank modelling and design Part 2: linking sludge settleability measures; *Water S.A.*; **21**(4); 333-349.

Palm, J. C., Jenkins, D. and Parker, D. S. (1980); Relationship between organic loading, dissolved oxygen concentration and sludge settleability in the completely-mixed activated sludge process; *Journal Water Pollution Control Federation*; **52**(10); 2484-2506.

Pavoni, J. L., Tenney, M. W. and Echelberger Jr, W. F. (1972); Bacterial exocellular polymers and biological flocculation; **44**(3 pt 1); 414-31.

Pflanz, P. (1969); *Performance of (activated sludge) secondary sedimentation basins*; Advances in Water Pollution Research: Proceedings of the 4th International Conference; Prague; Pergamon Press, London; 569-581.

Pipes, W. O. (1969); Types of activated sludge which separate poorly; *Journal Water Pollution Control Federation*; **41**(5, Part 1); 714-724.

Pipes, W. O. (1978); Actinomycete scum production in activated sludge processes; *Journal Water Pollution Control Federation*; **50**(4); 628-634.

Pipes, W. O. (1979); Bulking, deflocculation and pin-point floc; *Journal Water Pollution Control Federation*; **51**(1); 71-77.

Pitman, A. R. (1985); Settling of nutrient removal activated sludges; *Water Science and Technology*; **17**(4-5 pt 2); 493-504.

Pitt, P. and Jenkins, D. (1990); Causes and control of Nocardia in activated sludge; *Research Journal of the Water Pollution Control Federation*; **62**(2); 143-150.

Price, G. A. and Clements, M. S. (1974); Some lessons from model and full-scale tests in rectangular sedimentation tanks; *Water Pollution Control (Maidstone, England)*; **73**(1); 102-113.

Pujol, R. and Boutin, P. (1989); Control of activated sludge bulking. From the lab to the plant; *Water Science and Technology*; **21**(6-7 pt 2); 717-726.

Renko, E. K. (1996); Model for batch settling curve; *Water S.A.*; **22**(4); 339.

Renko, E. K. (1998); Modelling hindered batch settling Part I: a model for linking zone settling velocity and stirred sludge volume index; *Water S.A.*; **24**(4); 325-330.

Rensink, J. H. (1974); New approach to preventing bulking sludge; *Journal Water Pollution Control Federation*; **46**(8); 1888-1894.

Richards, T., Nungesser, P. and Jones, C. (1990); Solution of Nocardia foaming problems; *Research Journal of the Water Pollution Control Federation*; **62**(7); 915-919.

Richardson, J. F. and Zaki, W. N. (1954); Sedimentation and fluidisation -- 1; *Institution of Chemical Engineers -- Transactions*; **32**(1); 35-52.

Saayman, G. B., Schutte, C. F. and van Leeuwen, J. (1998); Chemical control of filamentous sludge bulking in a full-scale biological nutrient removal activated sludge plant; *Ozone: Science and Engineering*; **20**(1); 1-15.

Sadar, M. J. and Molina, M. (2003); *The determination of settled sludge volume and sludge volume index using process methodologies*; Technical Papers of ISA: Safety Instrumented Systems for the Process Industry; Lake Buena Vista, FL, USA; ISA - Instrumentation, Systems, and Automation Society; **448**; 99-110.

Samstag, R. W., McCorquodale, J. A. and Zhou, S. P. (1992); Prospects for transport modeling of process tanks; *Water Science and Technology*; **26**(5-6); 1401-1410.

Sawyer, C. N. and Bradney, L. (1945); Rising of activated sludge in final settling tanks; *Sewage Works Journal*; **17**(6); 1191-1209.

Schmidtke, N. W. and Smith, D. W. (1983); *Scale-up of water and wastewater treatment processes*; Butterworth Publishers; Boston.

Seka, A. M., Van de Wiele, T. and Verstraete, W. (2001); Feasibility of a multi-component additive for efficient control of activated sludge filamentous bulking; *Water Research*; **35**(12); 2995-3003.

Sekine, T., Tsugura, H., Urushibara, S., Furuya, N., Fujimoto, E. and Matsui, S. (1989); Evaluation of settleability of activated sludge using a sludge settling analyzer; *Water Research*; **23**(3); 361-367.

Sezgin, M., Jenkins, D. and Palm, J. C. (1979); Floc size, filament length and settling properties of prototype activated sludge plants; *Progress in Water Technology*; **12**(3); 171-182.

Sezgin, M., Jenkins, D. and Parker, D. S. (1978); A unified theory of filamentous activated sludge bulking; *Journal Water Pollution Control Federation*; **50**(2); 362-381.

Shannon, P. T. and Tory, E. M. (1965); Settling of slurries - new light on an old operation; *Industrial and Engineering Chemistry*; **57**(2); 18-&.

Silveston, P. L., Cordobamolina, J. F. and Hudgins, R. R. (1981); The use of flow contractions to improve clarifier performance; *Water Science and Technology*; **13**(1); 385-394.

Sin, S. N., Chua, H., Lo, W. and Yu, P. H. F. (2000); Effects of trace levels of copper, chromium, and zinc ions on the performance of activated sludge; *Applied Biochemistry and Biotechnology*; **84-6**; 487-500.

Smollen, M. and Ekama, G. A. (1984); Comparison of empirical settling velocity equations in flux theory for secondary settling tanks; *Water S.A.*; **10**(4); 175-184.

Snidaro, D., Zartarian, F., Jorand, F., Bottero, J. Y., Block, J. C. and Manem, J. (1997); Characterization of activated sludge flocs structure; *Water Science and Technology*; **36**(4); 313-320.

Sorour, M. T. and Sayed-Ahmed, A. M. (2005); Combined effects of cadmium and zinc on both sequencing batch reactor and continuous activated sludge; *Environmental Technology*; **26**(9); 963-974.

Takacs, I., Patry, G. G. and Nolasco, D. (1991); A dynamic model of the clarification thickening process; *Water Research*; **25**(10); 1263-1271.

Talmage, W. P. and Fitch, E. B. (1955); Determining thickener unit areas; *Industrial and Engineering Chemistry*; **47**(1); 38-41.

Tambo, N. and Watanabe, Y. (1979); Physical characteristics of flocs I: The floc density function and aluminium floc; *Water Research*; **13**(5); 409-19.

Thirumurthi, D. (1969); A break-through in the tracer studies of sedimentation tanks; *Journal Water Pollution Control Federation*; **41**; 405-418.

Tiller, F. M. (1981); Revision of Kynch sedimentation theory; *AIChE Journal*; **27**(4); 823-829.

Tyagi, R. D., Couillard, D. and Tran, F. T. (1991); Analysis of final settling tank in relation to control of metal inhibition in the activated sludge process; *Canadian Journal of Chemical Engineering*; **69**(2); 534-543.

Urbain, V., Block, J. C. and Manem, J. (1993); Bioflocculation in activated sludge: An analytic approach; *Water Research*; **27**(5); 829-838.

Vaccari, D. A. and Uchrin, C. G. (1989); Modeling and simulation of compressive gravity thickening of activated sludge; *Journal of Environmental Science and Health, Part A: Environmental Science and Engineering*; **24**(6); 645-674.

Vesilind, P. A. (1968); Theoretical considerations: Design of prototype thickeners from batch settling tests; *Water and Sewage Works*; **115**(7); 302– 307.

Vesilind, P. A. and Jones, G. N. (1990); A reexamination of the batch-thickening curve; *Research Journal of the Water Pollution Control Federation*; **62**(7); 887-893.

Wagner, F. (1983); Studies on the causes and prevention of bulking sludge in Germany; *Water Science and Technology*; **16**(10-11); 1-14.

Wahlberg, E. J. and Keinath, T. M. (1988); Development of settling flux curves using SVI; *Journal Water Pollution Control Federation*; **60**(12); 2095-2100.

Wahlberg, E. J. and Keinath, T. M. (1995); Development of settling flux curves using SVI. An addendum; *Water Environment Research*; **67**(5); 872-874.

Waters, A. G. and Galvin, K. P. (1991); Theory and application of thickener design; *Filtration and Separation*; **28**(2); 110-116.

WEF-ASCE (1992); *Design of Municipal Wastewater Treatment Plants*; Water Environment Federation, American Society of Civil Engineers; Alexandria, Va., New York, N.Y.

White, M. J. D. (1975); *Settling of activated sludge*; Technical Report TR11; Water Research Centre; London, England.

Wilen, B.-M. and Balmer, P. (1999); Effect of dissolved oxygen concentration on the structure, size and size distribution of activated sludge flocs; *Water Research*; **33**(2); 391-400.

Wu, Y. C., Smith, E. D. and Novak, R. (1982); Filterability of activated sludge in response to growth conditions; *Journal Water Pollution Control Federation*; **54**(5); 444-456.

Xu, S. and Hultman, B. (1996); Experiences in wastewater characterization and model calibration for the activated sludge process; *Water Science and Technology*; **33**(12); 89-98.

Yoshioka, N., Hotta, Y., Tanaka, S., Naito, S. and Tsugami, S. (1957); Continuous thickening of homogeneous flocculated slurries; *Chemical Engineering, Tokyo*; **21**; 66-74.

Zahid, W. M. and Ganczarczyk, J. J. (1990); Suspended solids in biological filter effluents; *Water Research*; **24**(2); 215-220.

Zhang, D., Li, Z., Lu, P., Zhang, T. and Xu, D. (2006); A method for characterizing the complete settling process of activated sludge; *Water Research*; **40**(14); 2637-2644.

Zhou, S. and McCorquodale, J. A. (1992); Modeling of rectangular settling tanks; *Journal of Hydraulic Engineering*; **118**(10); 1391-1405.

Appendix A: Data for Chapter 3

Appendix A-1: TSS Data from October 16, 2007

	Control		Influent		Effluent		RAS	
Crucible No.	T4	T17	T99	T14	T42	T98	T29	T42
Sample (ml)	50.0	50.0	20.0	20.0	100.0	100.0	20.0	20.0
Initial wt (g)	16.9772	15.2206	15.6656	14.6438	15.8992	15.6368	16.1270	15.8998
Final wt (g)	16.9773	15.2207	15.7278	14.7063	15.9011	15.6385	16.2452	16.0169
Diff (g)	0.0001	0.0001	0.0622	0.0625	0.0019	0.0017	0.1182	0.1171
TSS (mg/L)	2.00	2.00	3110.00	3125.00	19.00	17.00	5910.00	5855.00
Std. dev.	0.00		10.61		1.41		38.89	
Avg. TSS	2.00		3117.50		18.00		5882.50	
Adjusted TSS			3115.50		16.00		5880.50	

Appendix A-2: TSS Data from February 28, 2008

	Control		Influent		Effluent		RAS	
Crucible No.	T25	T24	U24	T93	T50	U3	T40	T66
Sample (ml)	50.0	50.0	5.0	10.0	50.0	50.0	5.0	5.0
Initial wt (g)	16.2753	14.8269	16.0622	14.7148	16.7617	15.4588	15.6517	16.2292
Final wt (g)	16.2754	14.8270	16.0803	14.7518	16.7627	15.4598	15.6862	16.2633
Diff (g)	0.0001	0.0001	0.0181	0.0370	0.0010	0.0010	0.0345	0.0341
TSS (mg/L)	2.00	2.00	3620.00	3700.00	20.00	20.00	6900.00	6820.00
Std. dev.	0.00		56.57		0.00		56.57	
Avg. TSS	2.00		3660.00		20.00		6860.00	
Adjusted TSS			3658.00		18.00		6858.00	

Appendix A-3: TSS Data from April 28, 2008

	Control		Influent		Effluent		RAS	
Crucible No.	T20	U5	U24	U6	U24	T63	T22	T25
Sample (ml)	50.0	50.0	5.0	5.0	500.0	500.0	5.5	5.5
Initial wt (g)	15.2080	15.3162	16.0635	15.8796	16.0626	16.3885	15.3832	16.2769
Final wt (g)	15.2080	15.3162	16.0831	15.8989	16.0735	16.3992	15.4229	16.3178
Diff (g)	0.0000	0.0000	0.0196	0.0193	0.0109	0.0107	0.0397	0.0409
TSS (mg/L)	0.00	0.00	3920.00	3860.00	21.80	21.40	7218.18	7436.36
Std. dev.	0.00		42.43		0.28		154.28	
Avg. TSS	0.00		3890.00		21.60		7327.27	
Adjusted TSS			3890.00		21.60		7327.27	

Appendix A-4: TS Data from October 16, 2007				
	Influent 1	Influent 2	RAS	RAS
Crucible No.	40	22	9	77
Sample (ml)	25.0	25.0	25.0	25.0
Initial wt (g)	31.2894	30.5795	32.1028	30.9578
Final wt (g)	31.3892	30.6785	32.2794	31.1329
Diff (g)	0.0998	0.0990	0.1766	0.1751
TS (mg/L)	3992.00	3960.00	7064.00	7004.00
Std. dev.	22.63		42.43	
Avg. TS (mg/L)	3976.00		7034.00	

Appendix A-5: TS Data from February 28, 2008				
	Influent 1	Influent 2	RAS	RAS
Crucible No.	12	9	70	48
Sample (ml)	25.0	25.0	25.0	25.0
Initial wt (g)	30.2369	30.7386	30.8264	31.2119
Final wt (g)	30.3386	30.8421	31.0215	31.4116
Diff (g)	0.1017	0.1035	0.1951	0.1997
TS (mg/L)	4068.00	4140.00	7804.00	7988.00
Std. dev.	50.91		130.11	
Avg. TS (mg/L)	4104.00		7896.00	

Appendix A-6: TS Data from February 28, 2008				
	Influent 1	Influent 2	RAS	RAS
Crucible No.	18	82	11	17
Sample (ml)	25.0	25.0	25.0	25.0
Initial wt (g)	29.8230	33.6674	31.5717	32.8198
Final wt (g)	29.9386	33.7873	31.7876	33.0331
Diff (g)	0.1156	0.1199	0.2159	0.2133
TS (mg/L)	4624.00	4796.00	8636.00	8532.00
Std. dev.	121.62		73.54	
Avg. TS (mg/L)	4710.00		8584.00	

Appendix A-7: Turbidity Data for Clarifier Effluent			
	Oct, 07	Feb, 08	Apr, 08
Effluent Turbidity (NTU)	3.8	4.1	5.1
	4.5	3.6	5.9
	4.3	3.2	7.6
Std. dev.	0.36	0.45	1.28
Avg. Turb. (NTU)	4.2	3.6	6.2

App. A-8: Inf. Size Distribution for Oct, 07

	Size Range (μm)	Particle Count /mL	($\times 10^3$ /mL)	Cum. Count /mL
Replicate #1	2-5	93093	93.09	93093
	5-10	131109	131.11	224202
	10-15	97727	97.73	321929
	15-25	162060	162.06	483989
	25-30	42498	42.50	526487
	30-40	50960	50.96	577447
	40-50	19894	19.89	597341
	>50	22082	22.08	619423
Replicate #2	2-5	86359	86.36	86359
	5-10	126849	126.85	213208
	10-15	91633	91.63	304841
	15-25	151526	151.53	456367
	25-30	39334	39.33	495701
	30-40	47848	47.85	543549
	40-50	18026	18.03	561575
	>50	20648	20.65	582223
Replicate #3	2-5	85533	85.53	85533
	5-10	126175	126.18	211708
	10-15	92041	92.04	303749
	15-25	150074	150.07	453823
	25-30	38698	38.70	492521
	30-40	46492	46.49	539013
	40-50	17934	17.93	556947
	>50	20514	20.51	577461
Average of 3	2-5	88328	88.33	88328
	5-10	128044	128.04	216373
	10-15	93800	93.80	310173
	15-25	154553	154.55	464726
	25-30	40177	40.18	504903
	30-40	48433	48.43	553336
	40-50	18618	18.62	571954
	>50	21081	21.08	593036

App. A-9: Inf. Size Distribution for Feb, 08

	Size Range (μm)	Particle Count /mL	($\times 10^3$ /mL)	Cum. Count /mL
Replicate #1	2-5	63839	63.84	63839
	5-10	132899	132.90	196738
	10-15	119315	119.32	316053
	15-25	254155	254.16	570208
	25-30	76546	76.55	646754
	30-40	77846	77.85	724600
	40-50	21176	21.18	745776
	>50	14702	14.70	760478
Replicate #2	2-5	72645	72.65	72645
	5-10	134773	134.77	207418
	10-15	120993	120.99	328411
	15-25	258627	258.63	587038
	25-30	77710	77.71	664748
	30-40	78378	78.38	743126
	40-50	21082	21.08	764208
	>50	14628	14.63	778836
Replicate #3	2-5	64117	64.12	64117
	5-10	132117	132.12	196234
	10-15	119265	119.27	315499
	15-25	251499	251.50	566998
	25-30	75094	75.09	642092
	30-40	77378	77.38	719470
	40-50	20762	20.76	740232
	>50	14966	14.97	755198
Average of 3	2-5	66867	66.87	66867
	5-10	133263	133.26	200130
	10-15	119858	119.86	319988
	15-25	254760	254.76	574748
	25-30	76450	76.45	651198
	30-40	77867	77.87	729065
	40-50	21007	21.01	750072
	>50	14765	14.77	764837

App. A-10: Inf. Size Distribution for Apr, 08				
	Size Range (μm)	Particle Count /mL	($\times 10^3$ /mL)	Cum. Count /mL
Replicate #1	2-5	65041	65.04	65041
	5-10	159413	159.41	224454
	10-15	153760	153.76	378214
	15-25	312450	312.45	690664
	25-30	77835	77.84	768499
	30-40	66623	66.62	835122
	40-50	16427	16.43	851549
	>50	10564	10.56	862113
Replicate #2	2-5	78629	78.63	78629
	5-10	188860	188.86	267489
	10-15	172743	172.74	440232
	15-25	317543	317.54	757775
	25-30	69736	69.74	827511
	30-40	56528	56.53	884039
	40-50	13567	13.57	897606
	>50	8615	8.61	906221
Replicate #3	2-5	66877	66.88	66877
	5-10	168599	168.60	235476
	10-15	160044	160.04	395520
	15-25	328534	328.53	724054
	25-30	82724	82.72	806778
	30-40	70886	70.89	877664
	40-50	17000	17.00	894664
	>50	10818	10.82	905482
Average of 3	2-5	70182	70.18	70182
	5-10	172291	172.29	242473
	10-15	162182	162.18	404655
	15-25	319509	319.51	724164
	25-30	76765	76.77	800929
	30-40	64679	64.68	865608
	40-50	15665	15.66	881273
	>50	9999	10.00	891272

App. A-11: Eff. Size Distribution for Oct, 07				
	Size range (μm)	Particle Count /mL	($\times 10^3$ /mL)	Cum. Count /mL
Replicate #1	2-5	8192	8.19	8192
	5-8	1728	1.73	9920
	8-10	198	0.20	10118
	10-15	160	0.16	10278
	15-20	73	0.07	10352
	20-25	40	0.04	10392
	25-30	21	0.02	10412
	>30	47	0.05	10460
Replicate #2	2-5	8172	8.17	8172
	5-8	1661	1.66	9833
	8-10	191.4	0.19	10025
	10-15	156	0.16	10180
	15-20	65	0.07	10246
	20-25	38	0.04	10283
	25-30	21	0.02	10305
	>30	44	0.04	10348
Replicate #3	2-5	8036	8.04	8036
	5-8	1714	1.71	9750
	8-10	190	0.19	9941
	10-15	157	0.16	10097
	15-20	69	0.07	10167
	20-25	37	0.04	10203
	25-30	21	0.02	10225
	>30	46	0.05	10271
Average of 3	2-5	8133	8.13	8133
	5-8	1701	1.70	9835
	8-10	193	0.19	10028
	10-15	157	0.16	10185
	15-20	69	0.07	10255
	20-25	38	0.04	10293
	25-30	21	0.02	10314
	>30	46	0.05	10360

App. A-12: Eff. Size Distribution for Feb, 08				
	Size Range (μm)	Particle Count /mL	($\times 10^3$ /mL)	Cum. Count /mL
Replicate #1	2-5	7200	7.20	7200
	5-8	1898	1.90	9098
	8-10	335	0.34	9433
	10-15	468	0.47	9901
	15-20	295	0.30	10196
	20-25	160	0.16	10356
	25-30	104	0.10	10460
	>30	254	0.25	10715
Replicate #2	2-5	7243	7.24	7243
	5-8	1915	1.91	9157
	8-10	340.4	0.34	9498
	10-15	457	0.46	9955
	15-20	298	0.30	10253
	20-25	167	0.17	10420
	25-30	104	0.10	10523
	>30	256	0.26	10779
Replicate #3	2-5	7130	7.13	7130
	5-8	1975	1.98	9105
	8-10	324	0.32	9429
	10-15	448	0.45	9877
	15-20	282	0.28	10159
	20-25	154	0.15	10314
	25-30	102	0.10	10416
	>30	241	0.24	10657
Average of 3	2-5	7191	7.19	7191
	5-8	1929	1.93	9120
	8-10	333	0.33	9454
	10-15	458	0.46	9911
	15-20	292	0.29	10203
	20-25	160	0.16	10363
	25-30	103	0.10	10466
	>30	250	0.25	10717

App. A-13: Eff. Size Distribution for Apr, 08				
	Size Range (μm)	Particle Count/ mL	($\times 10^3$ /mL)	Cum. Count /mL
Replicate #1	2-5	4245	4.24	4245
	5-8	3015	3.02	7260
	8-10	1587	1.59	8848
	10-15	326	0.33	9174
	15-20	320	0.32	9494
	20-25	234	0.23	9728
	25-30	165	0.17	9893
	>30	365	0.37	10258
Replicate #2	2-5	4864	4.86	4864
	5-8	3471	3.47	8334
	8-10	1636	1.64	9970
	10-15	338	0.34	10308
	15-20	337	0.34	10645
	20-25	249	0.25	10894
	25-30	175	0.18	11069
	>30	407	0.41	11476
Replicate #3	2-5	4889	4.89	4889
	5-8	3334	3.33	8223
	8-10	1621	1.62	9844
	10-15	328	0.33	10172
	15-20	325	0.33	10497
	20-25	243	0.24	10740
	25-30	174	0.17	10914
	>30	407	0.41	11321
Average of 3	2-5	4666	4.67	4666
	5-8	3273	3.27	7939
	8-10	1615	1.61	9554
	10-15	331	0.33	9885
	15-20	327	0.33	10212
	20-25	242	0.24	10454
	25-30	171	0.17	10625
	>30	393	0.39	11018

App. A-14: RAS Particle Size Distribution for April, 2008				
	Size range (μm)	Particle Count/mL	($\times 10^3$/mL)	Cumulative Count/mL
Replicate #1	2-5	30849	30.85	30849
	5-10	88943	88.94	119792
	10-15	90065	90.07	209857
	15-25	244999	245.00	454856
	25-30	105725	105.73	560581
	30-40	141961	141.96	702542
	40-50	46413	46.41	748955
	>50	29393	29.39	778348
Replicate #2	2-5	36340	36.34	36340
	5-10	90564	90.56	126904
	10-15	91346	91.35	218250
	15-25	246362	246.36	464612
	25-30	107470	107.47	572082
	30-40	148362	148.36	720444
	40-50	50432	50.43	770876
	>50	34698	34.70	805574
Replicate #3	2-5	36438	36.44	36438
	5-10	90446	90.45	126884
	10-15	89694	89.69	216578
	15-25	244382	244.38	460960
	25-30	107458	107.46	568418
	30-40	148462	148.46	716880
	40-50	50178	50.18	767058
	>50	34090	34.09	801148
Average of 3	2-5	34542	34.54	34542
	5-10	89984	89.98	124527
	10-15	90368	90.37	214895
	15-25	245248	245.25	460143
	25-30	106884	106.88	567027
	30-40	146262	146.26	713289
	40-50	49008	49.01	762296
	>50	32727	32.73	795023

Appendix B: Data for Chapter 4

Appendix B-1: TSS and Percent Removal Data of Clarifier Effluent for Type II Settling Test

Depth (m)	Initial wt. (g)	Final wt. (g)	vol. (ml)	TSS (mg/L)	Corrected TSS (kg/m^3)	% Solids Removal
Control	14.8269	14.8270	100	1.00		
Initial Effluent	16.0626	16.0721	500	18.90	17.90	
Final Sludge	16.3576	16.3790	500	42.80	41.80	
			5 min			
0.4	16.0823	16.0867	500	8.80	7.80	56.42
0.8	17.3077	17.3126	500	9.80	8.80	50.84
1.2	16.3237	16.3294	500	11.40	10.40	41.90
1.6	15.4557	15.4616	500	11.80	10.80	39.66
2	16.4559	16.4626	500	13.40	12.40	30.73
			10 min			
0.4	15.2064	15.2101	500	7.40	6.40	64.25
0.8	15.7109	15.7151	500	8.40	7.40	58.66
1.2	16.3885	16.3932	500	9.30	8.30	53.63
1.6	16.1251	16.1304	500	10.50	9.50	46.93
2	15.6486	15.6543	500	11.40	10.40	41.90
			15 min			
0.4	14.9640	14.9667	500	5.40	4.40	75.42
0.8	15.9016	15.9050	500	6.80	5.80	67.60
1.2	16.2287	16.2324	500	7.40	6.40	64.25
1.6	15.8783	15.8830	500	9.40	8.40	53.07
2	15.3139	15.3192	500	10.60	9.60	46.37
			20 min			
0.4	16.6830	16.6851	500	4.10	3.10	82.68
0.8	16.3367	16.3394	500	5.40	4.40	75.42
1.2	16.3419	16.3453	500	6.80	5.80	67.60
1.6	16.3813	16.3853	500	8.00	7.00	60.89
2	16.9752	16.9794	500	8.40	7.40	58.66
			30 min			
0.4	15.6133	15.6149	500	3.10	2.10	88.27
0.8	16.5975	16.6000	500	5.00	4.00	77.65
1.2	16.4351	16.4380	500	5.80	4.80	73.18
1.6	16.3949	16.3984	500	7.00	6.00	66.48
2	16.6183	16.6222	500	7.80	6.80	62.01
			45 min			
0.4	16.2495	16.2502	500	1.30	0.30	98.32
0.8	14.7664	14.7681	500	3.40	2.40	86.59
1.2	14.9689	14.9710	500	4.10	3.10	82.68
1.6	14.6768	14.6794	500	5.20	4.20	76.54
2	16.1544	16.1574	500	6.00	5.00	72.07

Appendix B-2: Time to Achieve Iso-removal at Different Depth for Type II Settling Test

% Removal	10	20	30	40	50	60	70	80	90
Depth (m)	Time (min)								
0	0	0	0	0	0	0	0	0	0
0.4	0.89	1.77	2.66	3.54	4.43	8.1	12.58	18.15	32.58
0.8	0.98	1.97	2.95	3.93	4.92	10.75	16.54	30.25	50.72
1.2	1.19	2.39	3.58	4.77	5.97	13	24.3	40.76	56.56
1.6	1.26	2.52	3.78	5.04	6.3	19.43	35.25	50.17	65.08
2	1.63	3.25	4.88	6.51	8.14	24	41.92	56.83	71.75

Appendix B-3: Overflow Rate at Different Iso-removal for Type II Settling Test

% Removal	10	20	30	40	50	60	70	80	90
Depth (m)	Overflow Rate (m^3/m^2.min)								
0.4	0.451	0.226	0.15	0.113	0.09	0.049	0.032	0.022	0.012
0.8	0.813	0.407	0.271	0.203	0.163	0.074	0.048	0.026	0.016
1.2	1.006	0.503	0.335	0.251	0.201	0.092	0.049	0.029	0.021
1.6	1.269	0.635	0.423	0.317	0.254	0.082	0.045	0.032	0.025
2	1.229	0.615	0.41	0.307	0.246	0.083	0.048	0.035	0.028

Appendix B-4: Sludge Volume Index (SVI) Data for Clarifier Influent

	time (min)	Settled Sludge Volume (mL/L)	Sludge Interface (mm)	SVI (mL/g)
October 16, 2007	0	1000	460	321
	5	870	400	279
	10	760	350	244
	15	650	299	209
	20	565	260	181
	30	435	200	140
	45	370	170	119
February 28, 2008	0	1000	460	273
	5	880	405	240
	10	785	361	214
	15	705	324	193
	20	640	294	174
	30	525	241	144
	45	435	200	119
April 28, 2008	0	1000	460	257
	5	860	396	221
	10	660	304	170
	15	560	258	144
	20	500	230	129
	30	440	202	113
	45	400	184	103

Appendix B-5: Batch Settling Test Data @ 5°C

Time (min)	5°C-1	5°C-2	5°C-3	5°C-4	5°C-5	5°C-6
	Depth of Interface (mm)					
0	12.5	15.0	15.0	12.5	16.0	13.0
5	450.0	400.0	350.0	135.0	85.0	25.0
10	472.5	455.0	435.0	267.5	210.0	45.0
15	475.5	463.0	450.0	327.5	280.0	77.5
20	477.5	465.5	451.5	356.5	317.5	114.0
25	480.0	468.5	454.0	374.5	340.0	141.0
30	481.0	470.0	455.0	385.0	355.0	168.5
40	482.5	473.5	457.5	400.0	375.0	205.0
50	484.0	475.0	460.0	405.0	385.0	230.0
60	485.0	475.5	460.5	410.0	390.0	250.0
70	485.0	476.0	462.0	410.5	395.0	265.0
80	485.0	476.5	462.5	413.0	398.0	275.0
90	485.0	477.0	463.0	415.0	400.0	285.0
100	485.0	477.5	464.5	415.0	401.0	290.0
110	485.0	477.5	465.0	415.0	401.5	295.0
120	485.0	477.5	465.0	415.0	402.0	301.0
Volume Reduction (%)	96.92	95.36	92.78	82.56	79.75	59.14

Appendix B-6: Batch Settling Test Data @ 15°C

Time (min)	15°C-1	15°C-2	15°C-3	15°C-4	15°C-5	15°C-6
	Depth of Interface (mm)					
0	15.0	15.0	17.5	15.0	12.0	10.0
5	275.0	190.0	125.0	122.5	62.5	22.0
10	385.0	332.5	250.0	230.0	137.5	50.0
15	415.0	375.0	315.0	302.5	194.0	90.0
20	430.0	395.0	347.5	335.0	232.5	127.5
25	437.0	408.0	365.0	355.0	260.0	157.5
30	440.0	415.0	377.5	368.0	280.0	180.0
40	441.0	422.5	392.5	385.0	310.0	217.5
50	444.0	424.5	400.0	394.0	327.5	240.0
60	444.5	425.0	404.5	400.0	340.0	255.0
70	445.0	427.5	408.0	404.5	350.0	262.0
80	445.5	428.5	409.5	405.0	355.0	271.0
90	446.0	429.5	410.0	405.5	360.0	277.0
100	447.5	430.0	411.0	408.5	365.0	283.0
110	447.5	430.0	412.0	409.0	369.0	288.5
120	448.5	430.0	412.5	409.0	370.0	292.5
Volume Reduction (%)	89.38	85.57	81.87	81.24	73.36	57.65

Appendix B-7: Batch Settling Test Data @ 27°C

Time (min)	27°C-1	27°C-2	27°C-3	27°C-4	27°C-5	27°C-6
	Depth of Interface (mm)					
0	10.0	17.5	12.5	15.0	11.5	14.0
5	375.0	300.0	225.0	165.0	100.0	30.0
10	425.0	384.0	330.0	280.0	190.0	70.0
15	438.5	405.0	370.0	327.0	240.0	120.0
20	440.5	415.0	390.0	353.5	270.0	162.5
25	441.0	420.0	400.0	370.0	296.0	195.0
30	442.5	424.0	405.0	380.0	315.0	217.5
40	444.0	425.0	410.0	391.0	337.5	250.0
50	444.5	426.0	410.5	395.0	351.0	269.0
60	445.0	427.5	412.5	399.0	360.0	280.0
70	445.0	430.0	414.0	405.0	365.0	290.0
80	445.0	430.0	414.0	405.0	369.0	300.0
90	445.0	430.0	414.0	405.0	370.0	305.0
100	445.0	430.0	414.0	405.0	371.5	310.0
110	445.0	430.0	414.0	405.0	373.0	314.0
120	445.0	430.0	414.0	405.0	374.0	317.5
Volume Reduction (%)	88.78	85.49	82.36	80.41	74.21	62.45

Appendix B-8: Zone Settling Velocity & Solids Flux Data for Clarifier Influent

Sample no.	Initial Sludge TSS (mg/L)	Initial Sludge TSS (kg/m^3)	Settling Velocity from Plot (mm/min)	Settling Velocity (m/day)	Calculated Solids Flux (kg/m^2-day)
		5°C			
5°C-1	710	0.710	87.50	126.00	89.46
5°C-2	1860	1.860	77.00	110.88	206.24
5°C-3	2200	2.200	67.00	96.48	212.26
5°C-4	2980	2.980	25.50	36.72	109.43
5°C-5	3940	3.940	15.96	22.98	90.55
5°C-6	6980	6.980	6.00	8.64	60.31
		15°C			
15°C-1	1680	1.680	52.00	74.88	125.80
15°C-2	2260	2.260	31.75	45.72	103.33
15°C-3	3140	3.140	20.35	29.30	92.01
15°C-4	4120	4.120	14.20	20.45	84.25
15°C-5	4690	4.690	11.45	16.49	77.33
15°C-6	6470	6.470	7.13	10.27	66.43
		27°C			
27°C-1	1460	1.460	73.00	105.12	153.48
27°C-2	2220	2.220	56.50	81.36	180.62
27°C-3	2640	2.640	31.75	45.72	120.70
27°C-4	3400	3.400	21.02	30.27	102.91
27°C-5	4310	4.310	15.51	22.33	96.26
27°C-6	6760	6.760	7.36	10.60	71.65

Appendix B-9: TS Analysis Data of Initial Sludge for Batch Settling Test					
Initial Sludge Sample	Initial wt. (g)	Final wt. (g)	vol. (ml)	TS (mg/L)	Average TS (kg/m^3)
		5°C			
5°C-1	30.5295	30.5496	25	804	0.798
5°C-1	31.2119	31.2317	25	792	
5°C-2	30.2919	30.3467	25	2192	2.192
5°C-3	32.7831	32.8481	25	2600	2.600
5°C-4	31.5131	31.6030	25	3596	3.596
5°C-5	29.8230	29.9386	25	4624	4.624
5°C-6	30.8264	31.0337	25	8292	8.312
5°C-6	30.4666	30.6749	25	8332	
		15°C			
15°C-1	30.2369	30.2855	25	1944	1.944
15°C-2	31.0359	31.1047	25	2752	2.752
15°C-3	31.3774	31.4695	25	3684	3.684
15°C-4	33.6674	33.7873	25	4796	4.796
15°C-5	31.3251	31.4659	25	5632	5.630
15°C-5	30.7386	30.8793	25	5628	
15°C-6	31.9677	32.1587	25	7640	7.676
15°C-6	32.1106	32.3034	25	7712	
		27°C			
27°C-1	32.5616	32.6047	25	1724	1.724
27°C-2	31.7546	31.8175	25	2516	2.516
27°C-3	30.8795	30.9608	25	3252	3.252
27°C-4	30.3733	30.4761	25	4112	4.112
27°C-5	31.5839	31.7115	25	5104	5.082
27°C-5	29.9485	30.0750	25	5060	
27°C-6	30.9596	31.1628	25	8128	8.126
27°C-6	29.1477	29.3508	25	8124	

Appendix B-10: TSS Analysis Data of Initial Sludge for Batch Settling Test					
Initial Sludge Sample	Initial wt. (g)	Final wt. (g)	vol. (ml)	TS (mg/L)	Average TSS (kg/m^3)
		5°C			
5°C-1	16.0635	16.067	5	700	0.710
5°C-1	15.8796	15.8832	5	720	
5°C-2	15.2078	15.2171	5	1860	1.860
5°C-3	15.6163	15.6273	5	2200	2.200
5°C-4	16.1087	16.1236	5	2980	2.980
5°C-5	15.5922	15.6119	5	3940	3.940
5°C-6	15.8992	15.934	5	6960	6.980
5°C-6	15.6368	15.6718	5	7000	
		15°C			
15°C-1	16.7628	16.7712	5	1680	1.680
15°C-2	17.3066	17.3179	5	2260	2.260
15°C-3	15.3832	15.3989	5	3140	3.140
15°C-4	16.2769	16.2975	5	4120	4.120
15°C-5	16.0802	16.1036	5	4680	4.690
15°C-5	15.4964	15.5199	5	4700	
15°C-6	15.7114	15.7438	5	6480	6.470
15°C-6	16.6185	16.6508	5	6460	
		27°C			
27°C-1	16.3885	16.3958	5	1460	1.460
27°C-2	15.8492	15.8603	5	2220	2.220
27°C-3	16.1249	16.1381	5	2640	2.640
27°C-4	16.1065	16.1235	5	3400	3.400
27°C-5	15.6510	15.6730	5	4400	4.310
27°C-5	16.4063	16.4274	5	4220	
27°C-6	15.2062	15.2400	5	6760	6.760
27°C-6	15.5908	15.6246	5	6760	

Appendix B-11: TS Analysis Data of Settled Sludge for Batch Settling Test

Settled Sludge Sample	Initial wt. (g)	Final wt. (g)	vol. (ml)	TS (mg/L)	Average TS (kg/m^3)
		5°C			
5°C-1	31.2894	31.5416	25	10088	10.018
5°C-1	31.1228	31.3715	25	9948	
5°C-2	32.4204	32.7694	25	13960	13.960
5°C-3	30.5795	30.9582	25	15148	15.148
5°C-4	30.1521	30.5690	25	16676	16.676
5°C-5	31.1254	31.5789	25	18140	18.140
5°C-6	30.0556	30.5148	25	18368	18.296
5°C-6	32.8368	33.2924	25	18224	
		15°C			
15°C-1	30.9578	31.3257	25	14716	14.716
15°C-2	32.8081	33.2309	25	16912	16.912
15°C-3	30.3128	30.7468	25	17360	17.360
15°C-4	32.7910	33.2263	25	17412	17.412
15°C-5	32.1028	32.5569	25	18164	18.090
15°C-5	28.7949	29.2453	25	18016	
15°C-6	33.2680	33.6962	25	17128	17.092
15°C-6	32.6922	33.1186	25	17056	
		27°C			
27°C-1	31.6108	31.9088	25	11920	11.920
27°C-2	32.1475	32.5043	25	14272	14.272
27°C-3	31.7968	32.1969	25	16004	16.004
27°C-4	31.7966	32.2345	25	17516	17.516
27°C-5	31.6712	32.1196	25	17936	17.862
27°C-5	31.7800	32.2247	25	17788	
27°C-6	31.5007	31.9967	25	19840	19.684
27°C-6	32.6293	33.1175	25	19528	

Appendix B-12: TSS & Turbidity Analysis Data of Supernatant for Batch Settling Test

Supernatant Sample	Initial wt. (g)	Final wt. (g)	vol. (ml)	TSS (mg/L)	Average TSS (kg/m^3)	Average Turbidity (NTU)
			5°C			
5°C-1	15.5206	15.5233	100	27	0.028	23.60
5°C-1	15.4581	15.461	100	29		
5°C-2	16.3230	16.3254	100	24	0.024	22.30
5°C-3	16.1282	16.1304	100	22	0.022	20.80
5°C-4	16.4584	16.4599	100	15	0.015	16.00
5°C-5	16.8110	16.8122	100	12	0.012	14.00
5°C-6	16.5983	16.6020	100	37	0.036	25.50
5°C-6	16.6345	16.638	100	35		
			15°C			
15°C-1	16.6820	16.6883	100	63	0.063	43.00
15°C-2	15.2195	15.2234	100	39	0.039	29.00
15°C-3	16.1271	16.1304	100	33	0.033	23.20
15°C-4	16.3563	16.3604	100	41	0.041	31.00
15°C-5	14.9620	14.9697	100	77	0.074	47.00
15°C-5	15.0537	15.0572	50	70		
15°C-6	16.9775	16.9849	50	148	0.144	91.25
15°C-6	16.6212	16.6351	100	139		
			27°C			
27°C-1	16.1560	16.1623	100	63	0.063	51.20
27°C-2	15.2022	15.2079	100	57	0.057	40.00
27°C-3	17.1280	17.1322	100	42	0.042	28.00
27°C-4	15.7412	15.7477	100	65	0.065	42.50
27°C-5	16.4373	16.4405	50	64	0.063	39.30
27°C-5	16.6194	16.6225	50	62		
27°C-6	15.3168	15.3188	20	100	0.108	62.80
27°C-6	16.3436	16.3459	20	115		

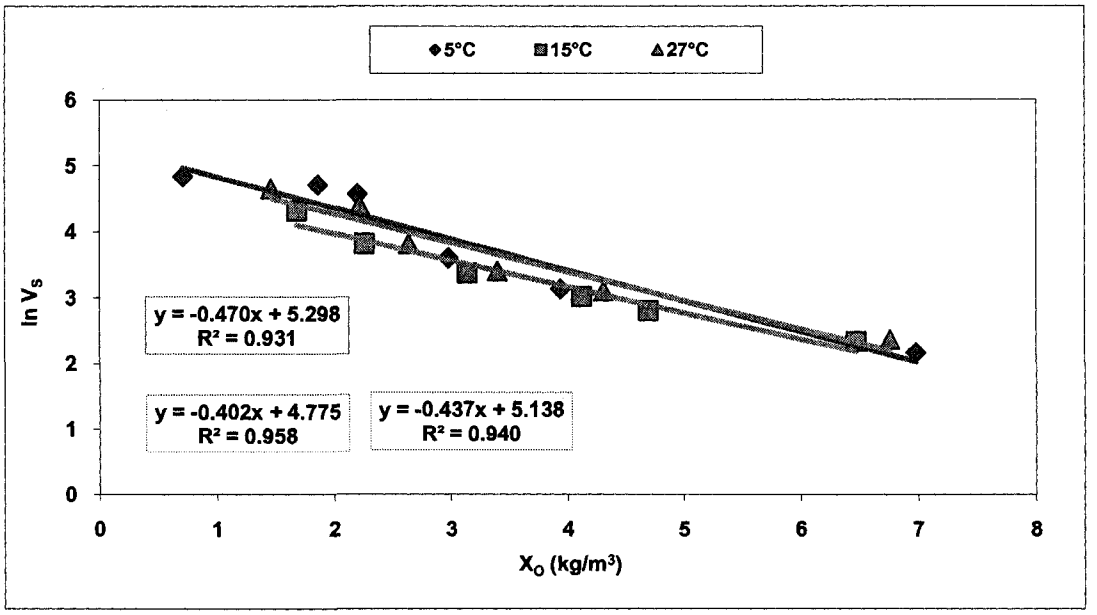

Appendix B-13: Model Fit for Vesilind Settling Velocity Model

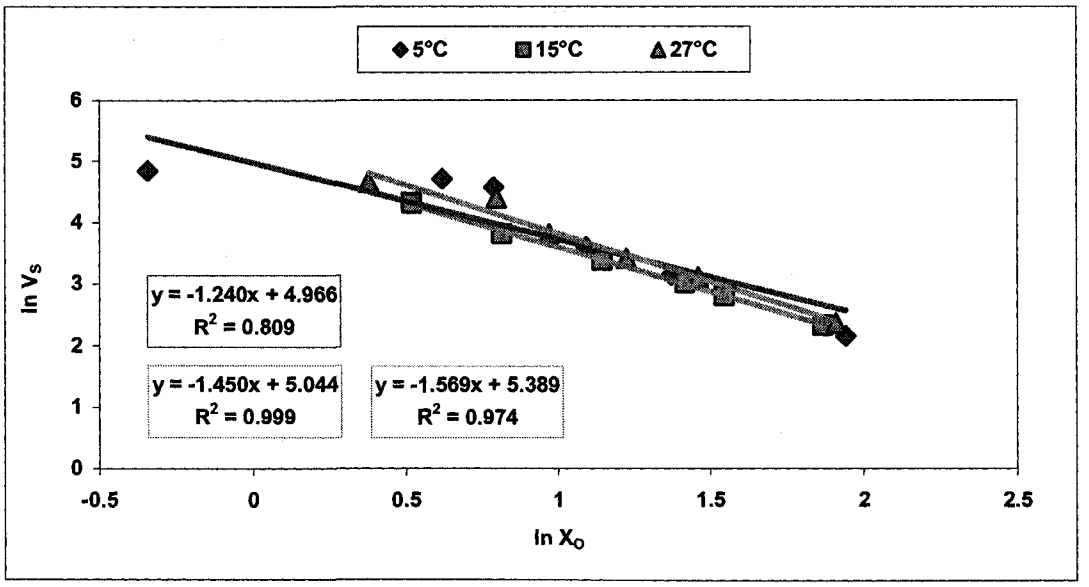

Appendix B-14: Model Fit for Dick and Young Settling Velocity Model

Appendix B-15: Responses generated by Settling Velocity Models

Sample no.	Initial Sludge TSS, X_o (kg/m^3)	ln X_O	Settling Velocity, V_s (m/day)	ln V_s	V_s (m/day) from Vesilind model	V_s (m/day) from Dick & Young Model
			5°C			
5°C-1	0.710	-0.34	126.00	4.84	143.21	219.35
5°C-2	1.860	0.62	110.88	4.71	83.41	66.45
5°C-3	2.200	0.79	96.48	4.57	71.09	53.96
5°C-4	2.980	1.09	36.72	3.60	49.27	37.04
5°C-5	3.940	1.37	22.98	3.13	31.38	26.20
5°C-6	6.980	1.94	8.64	2.16	7.52	12.89
			15°C			
15°C-1	1.680	0.52	74.88	4.32	60.52	73.09
15°C-2	2.260	0.82	45.72	3.82	47.99	47.55
15°C-3	3.140	1.14	29.30	3.38	33.75	29.51
15°C-4	4.120	1.42	20.45	3.02	22.81	19.91
15°C-5	4.690	1.55	16.49	2.80	18.16	16.50
15°C-6	6.470	1.87	10.27	2.33	8.91	10.35
			27°C			
27°C-1	1.460	0.38	105.12	4.66	89.62	120.88
27°C-2	2.220	0.80	81.36	4.40	64.15	62.61
27°C-3	2.640	0.97	45.72	3.82	53.32	47.70
27°C-4	3.400	1.22	30.27	3.41	38.17	32.06
27°C-5	4.310	1.46	22.33	3.11	25.57	22.09
27°C-6	6.760	1.91	10.60	2.36	8.70	10.90

Appendix C: Data for Chapter 5

Appendix C-1: Design Data for Full-Scale and Pilot-Scale System		
Dimension	Original Tank	Pilot-Scale Model
Overall Clarifier		
Total Length	76.192 m	3.048 m
Total Width	25.835 m	1.036 m
Side-water Depth	3.963 m	0.158 m
Depth at Hopper	4.115 m	0.165 m
Tank Inlet		
Total No. of Inlets	10	10
Width (each)	0.419 m	ø = 1.25"
Depth (each)	1.168 m	
Depth of Inlet Baffle	1.905 m	0.076 m
Distance of Baffle from Inlet	0.508 m	0.020 m
Hopper		
Distance of Hopper from Inlet	46.634 m	1.865 m
Distance of Hopper from Outlet	25.900 m	1.036 m
Total Hopper Width	3.658 m	0.146 m
Total Hopper Depth	1.524 m	0.061 m
Troughs or Launders		
No. of Troughs on Each Side	5	5
Length (each)	12.317 m	0.448 m
Width (each)	0.510 m	0.020 m
Depth (each)	0.710 m	0.028 m
Distance Between Troughs	2.640 m	0.106 m
Total Weir Length	246.34 m	8.96 m
Weir System	V-notched Weir Plates	Vertical Channels
Central Outlet Channel		
Length	17.455 m	0.698 m
Width	1.200 m	0.140 m
Depth at the beginning	0.762 m	0.030 m
Depth at end	2.300 m	0.092 m
Tank Outlet		
Total No. of Outlets	1	2
Width (each)	1.200 m	ø = 2.00"
Depth (each)	1.790 m	

Appendix C-2: Calibration Data for Conductivity meter

KCl Concentration (M)	KCl Concentration (mg/L)	Conductivity (μS/cm)	Adjusted Conductivity (μS/cm)
0	0	372	0
0.0001	9	388	16
0.0005	37	441	69
0.001	75	477	105
0.005	339	922	550
0.01	746	1550	1178
0.05	3728	6200	5828
0.15	11183	17090	16718

Appendix C-3: Raw and Calculated Data for Tracer Study

Time, t (min)	Temp. & Control Adjusted Conductivity (μs)	Conc. of KCl, C (mg/L)	Area/curve (mg.min/L)	E_t (min^{-1})	θ	Experimental E_θ	Tanks-in-Series E_θ
0.00	0.00	0.00		0.0000	0.00	0.00	0.00
1.00	0.00	0.00	0.00	0.0000	0.03	0.00	0.00
2.00	0.00	0.00	0.00	0.0000	0.05	0.00	0.00
3.00	0.00	0.00	0.00	0.0000	0.08	0.00	0.00
4.00	0.00	0.00	0.00	0.0000	0.10	0.00	0.00
5.00	0.00	0.00	0.00	0.0000	0.13	0.00	0.00
5.42	1.10	0.73	0.30	0.0008	0.14	0.03	0.00
5.85	2.20	1.46	0.63	0.0017	0.15	0.07	0.00
6.25	3.30	2.19	0.88	0.0025	0.16	0.10	0.01
6.90	3.30	2.19	1.43	0.0025	0.18	0.10	0.01
7.23	4.40	2.93	0.98	0.0034	0.18	0.13	0.01
7.85	4.40	2.93	1.80	0.0034	0.20	0.13	0.02
8.53	5.50	3.66	2.50	0.0042	0.22	0.17	0.03
9.08	5.50	3.66	2.01	0.0042	0.23	0.17	0.04
10.15	6.60	4.39	4.68	0.0051	0.26	0.20	0.06
10.95	6.60	4.39	3.51	0.0051	0.28	0.20	0.08
11.38	7.70	5.12	2.22	0.0059	0.29	0.23	0.09
11.68	7.70	5.12	1.54	0.0059	0.30	0.23	0.10
11.90	8.80	5.85	1.27	0.0068	0.30	0.27	0.11
12.18	8.80	5.85	1.66	0.0068	0.31	0.27	0.12
12.93	9.90	6.58	4.94	0.0076	0.33	0.30	0.15
13.83	11.00	7.32	6.58	0.0085	0.35	0.33	0.19
14.30	12.10	8.05	3.76	0.0093	0.37	0.36	0.21
14.75	13.20	8.78	3.95	0.0102	0.38	0.40	0.23
15.15	14.30	9.51	3.80	0.0110	0.39	0.43	0.26
15.33	15.40	10.24	1.88	0.0119	0.39	0.46	0.27
15.43	16.50	10.97	1.10	0.0127	0.39	0.50	0.27
15.57	17.60	11.70	1.56	0.0135	0.40	0.53	0.28
15.73	18.70	12.44	2.07	0.0144	0.40	0.56	0.29
15.95	19.80	13.17	2.85	0.0152	0.41	0.60	0.30
16.03	20.90	13.90	1.16	0.0161	0.41	0.63	0.31
16.15	22.00	14.63	1.71	0.0169	0.41	0.66	0.31
16.27	23.10	15.36	1.79	0.0178	0.42	0.70	0.32
16.68	24.20	16.09	6.71	0.0186	0.43	0.73	0.35
16.93	25.30	16.82	4.21	0.0195	0.43	0.76	0.36
17.13	26.40	17.56	3.51	0.0203	0.44	0.80	0.38
17.33	25.30	16.82	3.36	0.0195	0.44	0.76	0.39
17.75	26.40	17.56	7.32	0.0203	0.45	0.80	0.42
18.20	27.50	18.29	8.23	0.0212	0.46	0.83	0.45
18.38	28.60	19.02	3.49	0.0220	0.47	0.86	0.46
18.52	29.70	19.75	2.63	0.0229	0.47	0.90	0.47
18.67	28.60	19.02	2.85	0.0220	0.48	0.86	0.48
19.30	29.70	19.75	12.51	0.0229	0.49	0.90	0.52
19.40	30.80	20.48	2.05	0.0237	0.50	0.93	0.53

19.60	31.90	21.21	4.24	0.0246	0.50	0.96	0.54
19.90	33.00	21.95	6.58	0.0254	0.51	0.99	0.56
20.33	34.10	22.68	9.83	0.0262	0.52	1.03	0.59
20.75	35.20	23.41	9.75	0.0271	0.53	1.06	0.62
21.20	36.30	24.14	10.86	0.0279	0.54	1.09	0.65
22.30	37.40	24.87	27.36	0.0288	0.57	1.13	0.72
22.87	36.30	24.14	13.68	0.0279	0.58	1.09	0.76
23.07	37.40	24.87	4.97	0.0288	0.59	1.13	0.77
26.20	36.30	24.14	75.64	0.0279	0.67	1.09	0.95
26.97	37.40	24.87	19.07	0.0288	0.69	1.13	0.98
27.50	36.30	24.14	12.87	0.0279	0.70	1.09	1.01
28.92	35.20	23.41	33.16	0.0271	0.74	1.06	1.06
29.45	34.10	22.68	12.09	0.0262	0.75	1.03	1.07
29.98	33.00	21.95	11.70	0.0254	0.77	0.99	1.08
30.43	31.90	21.21	9.55	0.0246	0.78	0.96	1.09
31.02	30.80	20.48	11.95	0.0237	0.79	0.93	1.10
31.60	29.70	19.75	11.52	0.0229	0.81	0.90	1.11
32.27	28.60	19.02	12.68	0.0220	0.82	0.86	1.12
32.80	27.50	18.29	9.75	0.0212	0.84	0.83	1.12
33.65	26.40	17.56	14.92	0.0203	0.86	0.80	1.12
34.55	25.30	16.82	15.14	0.0195	0.88	0.76	1.12
35.42	24.20	16.09	13.95	0.0186	0.90	0.73	1.11
36.30	23.10	15.36	13.57	0.0178	0.93	0.70	1.10
37.17	22.00	14.63	12.68	0.0169	0.95	0.66	1.09
38.20	20.90	13.90	14.36	0.0161	0.98	0.63	1.07
39.27	19.80	13.17	14.04	0.0152	1.00	0.60	1.04
40.47	18.70	12.44	14.92	0.0144	1.03	0.56	1.01
41.07	17.60	11.70	7.02	0.0135	1.05	0.53	0.99
41.83	16.50	10.97	8.41	0.0127	1.07	0.50	0.96
42.93	15.40	10.24	11.27	0.0119	1.10	0.46	0.92
44.80	14.30	9.51	17.75	0.0110	1.14	0.43	0.85
46.73	13.20	8.78	16.97	0.0102	1.19	0.40	0.78
48.45	12.10	8.05	13.81	0.0093	1.24	0.36	0.71
50.07	11.00	7.32	11.83	0.0085	1.28	0.33	0.65
52.25	9.90	6.58	14.37	0.0076	1.33	0.30	0.57
52.95	11.00	7.32	5.12	0.0085	1.35	0.33	0.54
53.33	9.90	6.58	2.52	0.0076	1.36	0.30	0.53
54.63	11.00	7.32	9.51	0.0085	1.40	0.33	0.48
54.83	9.90	6.58	1.32	0.0076	1.40	0.30	0.48
57.28	11.00	7.32	17.92	0.0085	1.46	0.33	0.40
59.33	9.90	6.58	13.50	0.0076	1.52	0.30	0.34
63.85	8.80	5.85	26.43	0.0068	1.63	0.27	0.24
69.40	7.70	5.12	28.42	0.0059	1.77	0.23	0.14
73.17	6.60	4.39	16.53	0.0051	1.87	0.20	0.10
76.53	5.50	3.66	12.31	0.0042	1.95	0.17	0.07
83.17	5.50	3.66	24.26	0.0042	2.12	0.17	0.04
95.00	5.50	3.66	43.28	0.0042	2.43	0.17	0.01

Appendix D: Images of Pilot-Scale Model

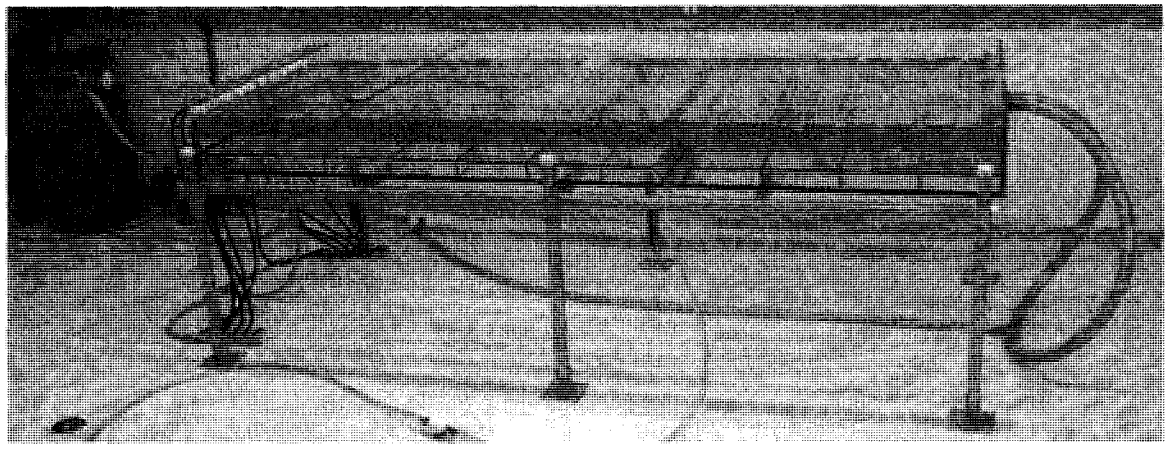

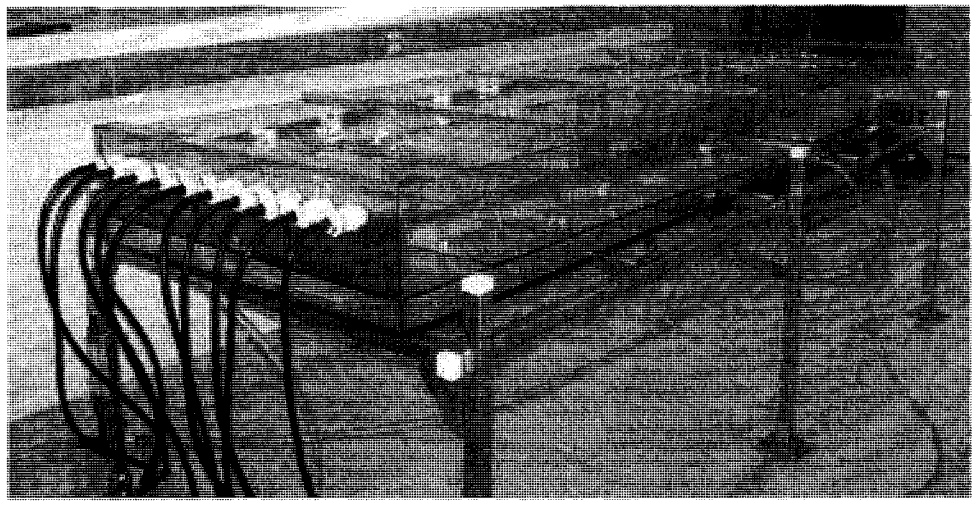

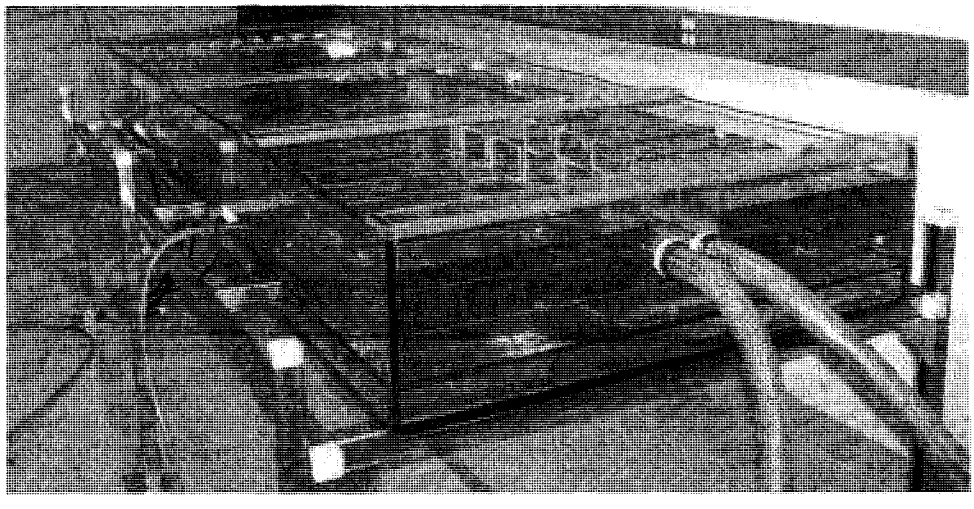

Appendix D-1: Different Views of the Pilot-Scale Model and Related Plumbing Arrangement

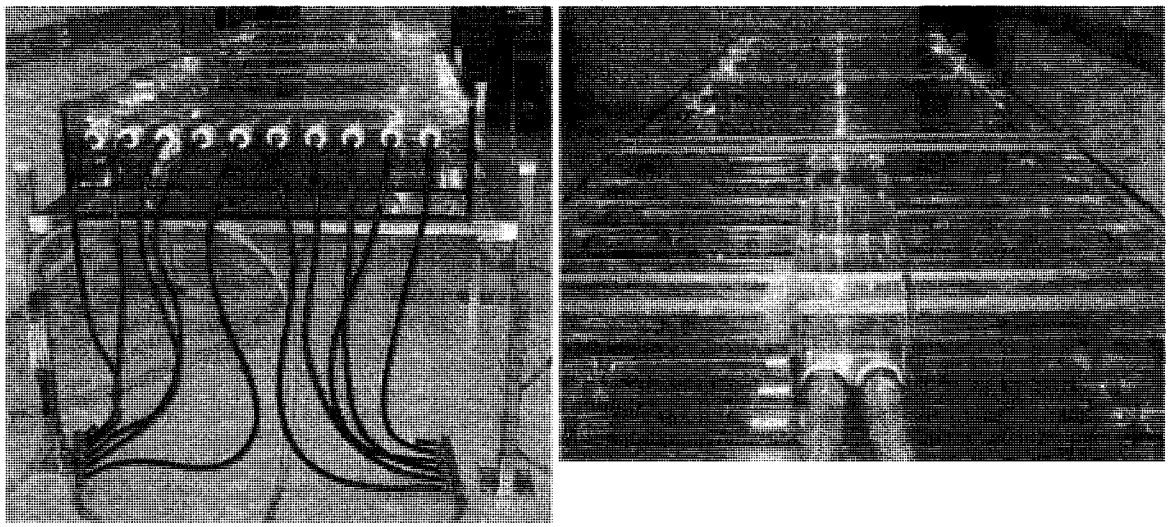

Appendix D-2: Inlet end (left) and Outlet end (right) of the Pilot-Scale Model

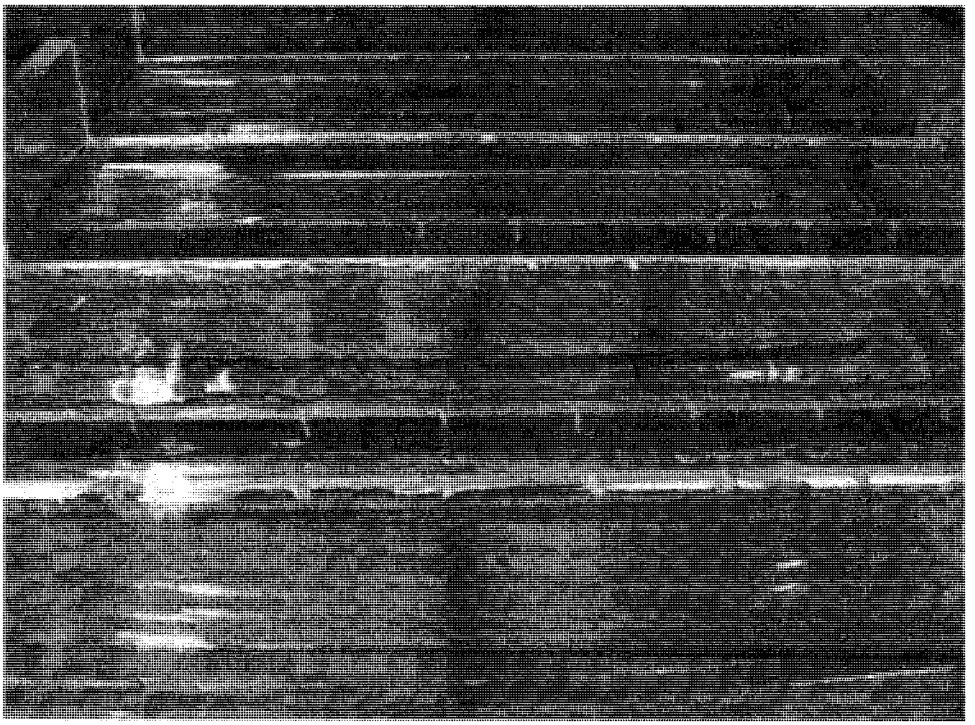

Appendix D-3: Operation of the Weir System in the Pilot-Scale Model